Role of Urotensin II during Zebrafish (*Danio rerio*) Embryogenesis

LI, Jun

A Thesis Submitted in Partial Fulfillment

of the Requirements for the Degree of

Doctor of Philosophy

in

Public Health

The Chinese University of Hong Kong

August 2010

UMI Number: 3483882

Thesis/Assessment Committee

Professor Hsiang-fu KUNG (Chair)

Professor Christopher H.K. CHENG (Thesis Supervisor)
Prof. Mingliang HE (Co-supervisor)
Professor King Ming CHAN (Committee Member)
Professor Woody Wood-Yee CHAN (Committee Member)
Professor Anderson On-Lam WONG (External Examiner)

尾加压素 II 在斑马鱼胚胎发育期间的功能研究

李 军

公共卫生课程

哲学博士论文

香港中文大学

2010 年 **8** 月

论文评审委员会

孔祥復 教授 (主席)
郑汉其 教授 (论文导师）
何明亮 教授 （联合导师）
陈竟明 教授 （委员会成员）
陳活彝 教授 （委员会成员）
黃安林 教授 （校外委员会成员）

Urotensin II (UII) is the most potent vasoconstrictor identified so far. This cyclic peptide stimulates its G protein-coupled receptor (GPR) to modulate cardiovascular system function in humans and in other animal species.

In the present study using zebrafish as the model organism, we have investigated the function of UII/UII-receptor (UIIR) signaling pathway during early embryogenesis. Herein we presented five lines of evidence supporting the hypothesis that UII/ UIIR signaling pathway is required for normal determination of asymmetric axis during early embryogenesis. First, function-loss of UII results in a concordant randomization of viscus asymmetries in embryos, including abnormalities in cardiac looping and positioning of visceral organs. Second, knockdown of UII randomizes the left-sided expression of asymmetrical genes including *lefty2, spaw* and *pitx2c* in the lateral plate mesoderm (LPM) and *bmp4* in the developing heart domain and the LPM. Third, reduced UII levels interfere with the normal organogenesis of Kupffer's vesicle (KV), an organ implicated in the early steps of left-right (L-R) patterning of embryos. Fourth, repression of UII function perturbs the asymmetrical distribution of free Ca^{2+} (intracellular Ca^{2+}) at the region surrounding embryo KV during early somitogenesis, which is one of the signaling mechanisms that propagandize and amplify the early clue of left-right (L-R) asymmetry. Fifth, depressing UII levels alters the normal pattern of Bmp and Nodal signaling, which modulate the establishment of L-R axis of developmental embryo. Collectively, these observations support a model in which

UII/UIIR signal system takes part in the early molecular events of L-R asymmetry patterning of embryo by modulating Bmp and Nodal signaling, regulating KV normal morphogenesis, so then, maintaining the asymmetrical distribution of free intracellular Ca^{2+} at the peripheral region surrounding embryo KV. This study documents a role of UII/UIIR signaling pathway in the establishment of L-R axis of embryos which promises to reveal the molecular mechanisms responsible for human congenital diseases with heterotaxy.

摘要

尾加压素 II（UII）是一种环形肽。它是目前已鉴定出能引起血管收缩效应最强的激素。它通过激活自身的 G 蛋白偶联受体（GPR）以调节人体和其他动物种的心血管功能。本研究使用斑马鱼作为模式动物研究了 UII 信号系统在胚胎发育方面的作用。

在这里，我们提供了五层证据来支持这一结论：在胚胎发育早期 UII 为胚胎左右模式化的确立所要求。首先，UII 功能抑制将随机化胚胎内脏器官的不对称性，其中包括心脏管弯曲异常和内脏器官定位异常。 第二，UII 功能下调随机化侧向性基因正常的偏左表达，包括 *lefty2*，*spaw* 和 *pitx2c* 在左侧板中胚层中的表达， 以及 *bmp4* 在发育中的心脏原基区的偏左表达。 第三，UII 功能下调导致 KV 这一涉及胚胎左右模式化的极早期步骤的器官发育异常。 第四，UII 下调扰乱围绕 Kupffer's vesicle (KV) 区自由的细胞质钙离子正常的偏左向分布，事实上，KV 区胞质钙离子偏左向分布是一个传播、放大上游早期不对称信号线索从而介导左右不对称的形态发生的关键因素之一； 最后， UII 功能的抑制修改了介导胚胎不对称发育的正常的 BMP 和 NODAL 信号转导模式。总的来说，这些研究结果支持这样一个结论：UII 通过调控 BMP 和 NODAL 信号转导，调节 KV 的正常的形态发生，进而，维持围绕 KV 区细胞中的胞质钙离子水平的方式来介导胚胎左右不对称模式化早期的分子事件。 这相应证明了 UII 及其 G 蛋白偶联受体系统为胚胎侧向性模式化发育的建立所要求。这有望为揭示先天性内脏异位方面的人类疾病发生的分子机制提供一丝线索。

Acknowledgement

I sincerely thank my supervisors Prof. Christopher HK Cheng and Prof. Mingliang He, for their great support, encouragement, friendship, and insight throughout the course of my studies at the Chinese University of Hong Kong. Without their thoughtful arrangements, instructions and help, it would be impossible for me to complete this study.

Sincere thanks are extended to the following from the Faculty of Medicine: Prof. Hsiangfu Kung, Prof. KingMing Chan, and Prof. Yangchao Chen for their guidance and suggestions concerning my graduate studies and research.

I would also like to thank Dr. Xigui Huang, Dr. Baowei Jiao and Mr. Guo Li for their illuminating discussions, Miss Josie Lai for her help in preparing the experimental materials and instrument, Mr. Jianzhen Li in preparing the zebrafish embryos, Mr. MingLiang Chen and Miss Yan Ma for their helpful discussion and assistance, and all my BMSB 513 lab buddies for their friendship.

Finally, I want to thank my wife and parents for their love and encouragement during my study.

Abstract of thesis entitled:

Role of urotensin II during zebrafish (*Danio rerio*) embryogenesis

Submitted by LI Jun

for the degree of Doctor of Philosophy

at The Chinese University of Hong Kong in Jan 2010

Urotensin II (UII) is the most potent vasoconstrictor identified so far. This cyclic peptide stimulates its G protein-coupled receptor (GPR) to modulate cardiovascular system function in humans and in other animal species. UII has diverse actions on the cardiovascular system such as modulation of cardiac contractility, vascular tone, vascular smooth muscle cell proliferation and cell growth. UII also has behavioral actions of stimulating locomotor activity, stimulating food consumption, inducing anxiogenic-like and depressant-like effects, and increasing the rapid eye movement sleep duration. It was found that the plasma levels of UII are higher in patients with atherosclerosis, heart failure, hypertension, preeclampsia, diabetes, renal disease and liver disease. Currently there is a dilemma about the role of UII on cardiovascular pathophysiology. Some evidence suggested the contributory role of UII in these diseases; while some other evidence uncovered high concentrations of circulating UII were protective on the cardiovascular system. Moreover, not all reports indicated a positive correlation between blood pressure and UII concentrations in patients, and a negative correlation had also been reported.

In the present study using zebrafish as the model organism, we have investigated the function of UII/UII-receptor (UIIR) signaling pathway during early embryogenesis. Before characterizing the function of zebrafish UII/UIIR signaling pathway *in vivo,* we first demonstrated the existence of the UII/UIIR system in zebrafish organism and the expression of UII/UIIR system during zebrafish

embryogenesis with three line evidence: (1) the bioinformatics analysis unraveled that there are two orthologous genes of human *UII* in zebrafish genome, which is consistent with the reports previously and five orthologous genes of human *UIIR* in zebrafish genome. (2) *In vitro* transactivation assays between ligands and receptors suggested that the activation of zebrafish UIIRs by synthetic zebrafish or human UII inhibits the formation of intracellular cAMP, same as the signaling pathway of human UII/UIIR system. (3) Reverse transcription polymerase chain reaction (RT-PCR) results implied that the zebrafish *UIIs and UIIRs* have transcript activity during embryogenesis.

Further, *in vivo* the functional characterization of zebrafish UII/UIIR system during embryogenesis was performed. Herein we presented five lines of evidence supporting the hypothesis that UII/ UIIR signaling pathway is required for normal determination of asymmetric axis during early embryogenesis. First, function-loss of UII results in a concordant randomization of viscus asymmetries in embryos, including abnormalities in cardiac looping and positioning of visceral organs. Second, knockdown of UII randomizes the left-sided expression of asymmetrical genes including *lefty2, spaw* and *pitx2c* in the lateral plate mesoderm (LPM) and *bmp4* in the developing heart domain and the LPM. Third, reduced UII levels interferes with the normal organogenesis of Kupffer's vesicle (KV), an organ implicated in the early steps of left-right (L-R) patterning of embryos. Fourth, repression of UII function perturbs the asymmetrical distribution of free Ca^{2+} (intracellular Ca^{2+}) at the region surrounding embryo KV during early somitogenesis, which is one of the signaling mechanisms that propagandize and amplify the early clue of left-right (L-R) asymmetry. Fifth, depressing UII levels alters the normal pattern of Bmp and Nodal signaling, which modulate the establishment of L-R axis of developmental embryo. Collectively, these observations support a model in which UII/UIIR signal system

takes part in the early molecular events of L-R asymmetry patterning of embryo by modulating Bmp and Nodal signaling, regulating KV normal morphogenesis, so then, maintaining the asymmetrical distribution of free intracellular Ca^{2+} at the peripheral region surrounding embryo KV. This study documents a role of UII/UIIR signaling pathway in the establishment of L-R axis of embryos which promises to reveal the molecular mechanisms responsible for human congenital diseases with heterotaxy.

摘要

尾加压素Ⅱ（UII）是一种环形肽。它是目前已鉴定出能引起血管收缩效应最强的激素。它通过激活自身的G蛋白偶联受体（GPR）以调节人体和其他动物种的心血管功能。尾加压素Ⅱ具有多效性，有证据表明它能引起心肌收缩、血管舒张、血管平滑肌细胞增殖、细胞生长；同时能调控动物行为方面的活动，例如刺激运动性活动、诱导类焦虑和类抑郁效应、刺激提高采食量和增加快速眼动睡眠期。另一方面，人们发现在动脉粥样硬化、心力衰竭、高血压、子痫前期、糖尿病、肾脏病及肝脏疾病患者的血浆中UII水平升高。关于UII在心血管中的角色研究，目前处于一个两难的窘境中；一些证据表明是UII上调引起了疾病发生，然而另有其它一些证据表明血液中UII浓度的升高对心血管系统有保护作用。此外，并非所有研究都显示血压升高与血浆中UII浓度呈正相关，一些负相关的临床病例也被观察到。

本研究使用斑马鱼作为模式动物研究了UII信号系统在胚胎发育方面的作用。首先，我们提供了三层证据证明斑马鱼有机体内存在UII信号系统，其基因在斑马鱼胚胎发育期间有转录活性。证据（1）生物信息学分析揭示斑马鱼基因组中存在两个与人 *UII* 直系同源的基因和五个与人 *UIIR* 直系同源的基因；证据（2）配体和受体间的体外相互作用试验结果说明人工合成的人的或斑马鱼的UII能够激活斑马鱼的这五个受体抑制细胞内第二信使环腺苷酸的合成，该结果与人UII信号系统类似；证据（3）逆转录聚合酶链反应检测结果表明斑马鱼UII信号系统在胚胎发育早期有转录活性。

然后，我们进行了UII信号系统在斑马鱼体内的功能研究。我们首次探查了UII在早期胚胎发育中可能起的作用。在这里，我们提供了五层证据来支持这一结论：在胚胎发育早期UII为胚胎左右模式化的确立所要求。首先，UII功能抑制将随机化胚胎内脏器官的不对称性，其中包括心脏管弯曲异常和内脏器官定位异常。 第二，UII功能下调随机化侧向性基因正常的偏左表达，包括 *lefty2*，*spaw* 和 *pitx2c* 在左侧板中胚层的表达， 以及 *bmp4* 在发育中的心脏原基

区的偏左表达。 第三，UII 功能下调导致 KV 这一涉及胚胎左右模式化的极早期步骤的器官发育异常。 第四，UII 下调扰乱围绕 Kupffer's vesicle (KV) 区自由的细胞质钙离子正常的偏左向分布，事实上，KV 区胞质钙离子偏左向分布是一个传播、放大上游早期不对称信号线索从而介导左右不对称的形态发生的关键因素之一；最后，UII 功能的抑制修改了介导胚胎不对称发育的正常的 BMP 和 NODAL 信号转导模式。总的来说，这些研究结果支持这样一个结论：UII 通过调控 BMP 和 NODAL 信号转导，调节 KV 的正常的形态发生，进而，维持围绕 KV 区细胞中的胞质钙离子水平的方式来介导胚胎左右不对称模式化早期的分子事件。 这相应证明了 UII 及其 G 蛋白偶联受体系统为胚胎侧向性模式化发育的建立所要求。这有望为揭示先天性内脏异位方面的人类疾病发生的分子机制提供一丝线索。

Table of Contents

x

List of figures and tables

List of abbreviations

AP-1	Activator protein-1 transcription factor complex regulatory element
BMP4	Bone morphogenetic protein 4
cAMP	The cyclic adenosine monophosphate
CHO cells	Chinese hamster ovary cells
CK1	Casein kinase 1
CPI-17	Protein kinase C-potentiated inhibitor protein of 17 kDa
CRE	cAMP response element
DAG	Diacylglycerol
DFCs	The dorsal forerunner cells
DIG	Digoxigenin
DMEM	Dulbecco's modified Eagle's medium
dpf	Day post-fertilization
EDHF	Endothelium-derived hyperpolarizing factor
EDTA	Ethylenediamine tetraacetic acid
ERE	Estrogen-responsive elements
ERK	Extracellular signal-regulated kinase
ETS	*cis*-element binding winged helix-turn-helix domain
FBS	Fetal bovine serum
GPR	G protein-coupled receptor
GSK3	Glycogen synthase kinase 3
GTP	Guanosine triphosphate
HEK293	Human embryonic kidney cells
hpf	Hour post-fertilization
IP_3	Inositol 3,4,5-trisphosphate
KV	Kupffer's vesicle
L-R	Left-right
LSF	*cis*-element binding HeLa transcription factor
Mef	Myocyte-specific enhancer
MLC-2	Myosin light chain 2
MLCP	Myosin light chain phosphatase
MO	Morpholino phosphorodiamidate oligonucleotides
Myc	*cis*-element binding avian myelocytomatosis viral-like factor
Myf	*cis*-element binding myogenic factor
NJ	Neighbor-joining method
NO	Nitric oxide
p38MAPK	p38 mitogen-activated protein kinase
PIP_2	Phosphatidylinositol (4,5)-bisphosphate
PKA/C	Protein kinase A/C
PKC	Protein kinase C
PLC	Phospholipase C
RACE	Rapid Amplification of cDNA Ends

RELT	The receptor expressed in lymphoid tissues
REM	The rapid eye movement sleep duration
Shh	Sonic hedgehog homolog
siRNAs	Short inhibitory RNAs
Smad3-Smad4 BE	Smad3-Smad4 binding element
Smad4 BE	Smad4 binding element
SRF	C-fos serum response element
TATA	TATA box
TEF	*cis*-element binding thyrotroph embryonic factor
UII	Urotensin II
UIIR	Urotensin II receptor
URP	UII-related peptide
VMSC	Vascular smooth muscle cell
7TMD	Seven transmembrane-spanning domain

List of amino acid code

1-Letter code	3-Letter code	Amino acid name
A	Ala	Alanine
B	Asx	Asparagine or aspartic acid
C	Cys	Cysteine
D	Asp	Aspartic acid
E	Glu	Glutamic acid
F	Phe	Phenylalanine
G	Gly	Glycine
H	His	Histidine
I	Ile	Isoleucine
J	Xle	Leucine or Isoleucine
K	Lys	Lysine
L	Leu	Leucine
M	Met	Methionine
N	Asn	Asparagine
P	Pro	Proline
Q	Gln	Glutamine
R	Arg	Arginine

S	Ser	Serine
T	Thr	Threonine
V	Val	Valine
W	Trp	Tryptophan
X	Xaa	Unspecified or unknown amino acid
Y	Tyr	Tyrosine
Z	Glx	Glutamine or glutamic acid

Chapter 1 General Introduction

1.1 Introduction to urotensin II (UII)

1.1.1 Cloning and tissue distribution of UII from different species

Urotensin II (UII) was first isolated from the urophysis of goby (Pearson et al., 1980) and subsequently from the brain of other fishes (Waugh et al., 1995) and also of *R. ridibunda* (Conlon et al., 1992). The cDNA encoding the precursor of UII has now been cloned from various mammalian species including rat and mouse (Coulouarn et al., 1999), pig (Mori et al., 1999), monkey (Elshourbagy et al., 2002) and human (Coulouarn et al., 1998). Moreover, an analogue of UII, termed as UII-related peptide (URP) has been isolated from the rat brain and the cDNA encoding its precursor has also been cloned in mouse, rat and human (Sugo et al., 2003). The sequences of UII and URP contain a cyclic hexapeptide (-Cys-Phe-Trp-Lys-Tyr-Cys-) that is fully conserved across whole vertebrate species. This cyclic motif is the minimal sequence retaining full biological activity (Chatenet et al., 2004; Flohr et al., 2002). Comparative genomic studies uncovered that the UII-URP genes and the somatostatin-cortistatin genes stem from a common ancestral gene. Within their cyclic core region all this four peptides share the common -Phe-Trp-Lys- sequence that is functionally vital (Tostivint et al., 2006).

It had been popularly accepted that UII is confined to the urophysis of fish (Conlon et al., 1997). However, immunohistochemical and biochemical studies indicated that UIIs also present in other tissues or organs. In particular, UII has been

isolated from whole brain extracts of trout, skate, lamprey and river lamprey (Waugh et al., 1993, 1995). Moreover, the occurrence of UII-like immunoreactivity has been reported in the cerebral ganglia of the gastropod *Aplysia californica* (Gonzalez et al., 1992). In the central nervous system, the UII and URP genes are primarily expressed in the motoneurons of the brain stem and spinal cord (Pelletier et al., 2002; Pelletier et al., 2005). UII and URP mRNAs have also been detected in various peripheral tissues including the pituitary, heart, smooth muscle, endothelial cells, leukocytes, spleen, thymus, pancreas, kidney, small intestine, colon, adrenal gland, placenta and prostate (Bousette et al., 2004; Coulouarn et al., 1998; Matsushita et al., 2001; Onan et al., 2004; Shenouda et al., 2002; Sugo et al., 2003; Totsune et al., 2001; Totsune et al., 2003).

1.1. 2 Post-translational processing of prepro-UII

Based on the bioinformatics method, the primary structure of almost all prepro-UIIs could be deduced from their cDNAs (the nucleotide sequence of cloned DNA complementary to prepro-UII mRNA). The deduced UII precursors from different species possess approximately 120 amino acids residues. For example, the frog, human and carp prepro-UII are 127, 124 and 125 amino acids long, respectively. The organization of both frog and human UII precursors is similar to that of the carp UII precursors. All precursors are composed of a consensus N-terminal signal peptide sequence, an N-terminal flanking peptide, a conserved proteolytic processing site (Lys-Arg-Lys-Arg), and a C-terminal extremity of the precursor, at which the UII sequence is located. Human mature UII is composed of only 11 amino acid residues, whereas frog and carp UII possess 13 and 12 residues, respectively. So, the prepro-UIIs need to be further processed to the mature peptides. Conlon et al., (1990) investigated the post-translational processing mechanism of the prepro-UII. They

2

isolated four peptides from an extract of flounder urophysis that are derived from prepro-UII by proteolytic cleavage. The comparison of action amino acid sequences between the mature peptides and the prepro-UIIs demonstrated that flounder prepro-UII is cleaved at two monobasic processing sites (single arginine residues) to generate peptides with limited homology to carp prepro-UII. Cleavage at a tribasic residue processing site generates an UII with the structure: Ala-Gly-Thr-Thr-Glu-Cys-Phe-Trp-Lys-Tyr-Cys-Val. The putative processing site for the prepro-UII is shown in Fig.1-1. In addition, Coulouarn et al., (1998) also drew similar conclusion (Fig.1-2) when characterizing the UIIs of human and frog.

1.1.3 Structure–activity relationship of UII and URP

Studies of Leprince et al., (2008) suggested that the minimal sequence required for retaining the full biological activity of UII and URP is the conserved UII $_{(4-11)}$ motif; in particular the Cys^5 and Cys^{10} residues involved in the disulfide bridge, and the Phe^6, Lys^8 and Tyr^9 residues. Instead, free α-amino group and C-terminal COOH group are not essential for the biological activity, and even though modifications of these residues may enhance the stability of these analogues.

1.2 Introduction to UIIR

1.2.1 Cloning and tissue distribution of *UIIR* from different species

By *in vitrol* experiments, Ames et al., (1999) first identified a human GPR, GPR14, which functions as a UIIR. Now many UIIR genes from different species have been cloned, such as in rat (Cheng et al., 1995; Tal et al., 1995), cat (Aiyar et al., 2005), mouse and monkey (Elshourbagy et al., 2002). UIIR shows a high degree of sequence identity to somatostatin receptors (Marchese et al., 1995). In fact, UIIR

and the somatostatin receptor sst3 are located in the same chromosomal region at 17q25 (Tostivint et al., 2006) suggesting that the two receptors arose by tandem duplication. RT-PCR analysis and *in situ* hybridization studies indicated that UIIR mRNA is widely distributed in the brain and in peripheral organs (Ames et al., 1999; Marchese et al., 1995; Clark et al., 2001; Je´gou et al., 2006; Liu et al., 1999; Matsushita et al., 2001; Tal et al., 1995). In the central nervous system, the UIIR gene is expressed in the olfactory system, hippocampus, amygdala, hypothalamus, locus coeruleus, motor nuclei and ventral horn of the spinal cord (Je´gou et al., 2006).

1.2.2 UIIR is a G protein-coupled receptor (GPR)

UIIR belongs to the subfamily A5 of GPRs, which are homologous with the rhodopsin receptor. So, UIIR possesses many features of this family including the 7 transmembrane-spanning domain (TMD), the D/ERY (Asp/ Glu-Arg-Tyr) motif at the junction of the third TMD and the second intracellular loop, the NPxxY (Asn–Pro-x-x-Tyr) motif in the seventh TMD, and the potential serine/threonine phosphorylation sites in the cytoplasmic tail. UIIR also has two potential N-glycosylation sites in the N-terminal domain and two cysteine residues in the first and second extracellular loops, which are thought to participate in disulfide bonding (Christophe et al., 2008; Boucard et al., 2003; Onan et al., 2004; Chung et al., 2002; Chung et al., 1988; Feng et al., 2003; Mhaouty-Kodja et al., 1999; Neve et al., 1991; Alewijnse et al., 2000; Ballesteros et al., 2001; Favre et al., 2005; Bihoreau et al., 1993) (Fig. 1-3).

1.2.3 UIIR signal transduction

The UIIR is coupled to the $G_{\alpha q/11}$ signal transduction pathway. When

4

extracellular UII molecule binds with it on the external cell surface, phospholipase C would be activated through coupling to $G_{q/11}$, which is bound to the guanosine triphosphate (GTP). The lipase hydrolyzes phosphatidylinositol (4, 5)-bisphosphate (PIP_2) into two second messengers: inositol 3, 4, 5-trisphosphate (IP_3) and diacylglycerol (DAG.). IP_3 binds with the receptor on the membrane of the smooth endoplasmic reticulum and mitochondria, which helps open the Ca^{2+} channel to increases cytosolic free calcium ion levels. DAG will help activate protein kinase C (PKC), which phosphorylates many other proteins, chang- ing their catalytic activities and leading to cellular responses (Saetrum et al., 2000; Tzanidis et al., 2003; Castel et al., 2006; Douglas et al., 2004; Ziltener et al., 2002; Sauzeau et al., 2001; Dutt et al., 2002; Sagi et al., 2001; Fromm et al., 1997; Gohla et al., 1998) (Fig.1-4).

In the GPR signaling system there are two principal signal transduction pathways: the cyclic adenosine monophosphate (cAMP) signal pathway and the phosphatidylinositol signal pathway (Gilman, 1987). Initiation of cAMP signal pathway requires the activation of Gi/s protein type linked to GPR. Therefore UII is not able to exert direct regulating effect on the cAMP levels. Observations from Song et al. (2006) indicated that human UII potently inhibits the forskolin-stimulated cAMP formation. However when experiments performed with Ca^{2+}-free buffer the observed inhibition of cAMP formation is completely abolished, indicating some cross-talk between Ca^{2+} mobilisation (Gq-mediated) and adenylyl cyclase inhibition (Gi/s-medaited).

1.3 Functions of UII

1.3.1 Cardiovascular actions of UII

UII has diverse actions on the cardiovascular system, with evidences for

modulation of cardiac contractility, vascular relaxation, vascular smooth muscle cell proliferation, and cell growth, while other evidences implicate UII as a harmful mediator. Observations suggested that there is some extensive variations for one of these cardiovascular system responses to the UII challenge, for example, the contractile response, in human, like other species, the condition of the vascular endothelium is a key determinant in deciding how the cardiovascular system responds to UII stimulation (Camarda et al., 2002; Douglas et al., 2000; McMaster et al., 1988; Douglas et al., 2004). About this, a report from MacLean et al., (2000) shows us a good example: in small pulmonary arteries, only 30% of vessels tested responded to UII with consist efficacy and of those the efficacy varied from 14% to 220% (relative to the contraction caused by 50 mM KCl).

Moreover, UII-mediated relaxation is also endothelium dependent, which has been demonstrated in isolated aorta from rabbits and rats (Ishihata et al., 2006; Bottrill et al., 2000). Vasodilation is generated by UII-mediated increases in intracellular calcium levels in endothelial cells, which results in the release of the endothelial derived relaxing factors, nitrogen monoxide (NO) and endothelium-derived hyper- polarizing factor (EDHF). UII-mediated release of NO and its resultant dilatory action attenuate UII-mediated contraction in the rat aorta (Ishihata et al., 2006). Endothelial factors might modulate the actions of UII in humans, thus contributing to contractile variability. In addition to endothelial factors, variations in both the vasodilatory and constrictor responses to UII might reflect the differentiation of the expression levels of UIIR in different organs, tissues or cellular types, which will depend on the size and location of the vessel (Onan et al., 2004).

1.3.2 Behavioral actions of UII

The widespread distribution of UIIR in the brain of mammals implies that the

UII/UIIR system might be implicated in diverse behavioral processes. For example, UII stimulates locomotor activity (Lancien et al., 2004), induces anxiogenic-like and depressant-like effects (Rego et al., 2005; Matsumoto et al., 2004), stimulates food consumption (Rego et al., 2005) and increases the rapid eye movement sleep duration (Huitron-Resendiz et al., 2005).

1.4 The role of UII in cardiovascular pathphysiology

It was found that UII levels are higher in the plasma of these patients with atherosclerosis, heart failure, hypertension, preeclampsia, diabetes, renal disease and liver disease (Bousette et al., 2006; Cheung et al., 2004). However, the cause relationship between the UII and these diseases remains unclear so far. Some evidence suggested it is the elevated plasma UII levels to cause these diseases. But, recently other observations have questioned this contributory role of UII in such diseases, and have postulated a protective effect on the cardiovascular system. For example, the high concentrations of plasma UII correlated with improved clinical outcomes in patients with renal disease or myocardial infarction circumstances (Mallamaci et al 2005, 2006; Zoccali et al 2006; Khan et al 2007).

Alike, the increase of plasma UII levels with increased pressure load raises the possibility that blood pressure is a stimulus for UII release. Evidence for this point is that plasma UII levels correlated positively with increased systolic and diastolic blood pressure in patients (Suguro et al., 2007; Cheung et al., 2004; Balat et al., 2005). However, a negative correlation had been observed between the plasma UII concentrations and the mean arterial pressure in patients with acute coronary syndrome and stable coronary artery disease (Joyal et al., 2006). Dschietzig et al (2001) also uncovered that the blood pressure were not the stimuli for UII production in cultures of bovine pulmonary artery endothelial cells. Currently there is still a

dilemma about the role of UII in cardiovascular pathophysiology.

1.5 The developmental biology of zebrafish

1.5.1 Advantages of zebrafish model for the study of vertebrate developmental biology.

An understanding of the functions of genes implicated in development requires us to identify as many of the genes involved in development as possible. The classical vertebrate for genetic analysis is the mouse. However, due to the embryonic lethality caused by the function-loss of many vital genes, consequently, discovery of mutations that interfere with the early steps in development has been very rare.

George Streisinger (1981) of the University of Oregon recognized that the zebrafish, a small tropical teleost, has many of the advantages of *C. elegans* and *Drosophila*; such as, short generation time (3 months), short embryogenesis (only 3 days), large number of progeny, and translucent embryos which enables the investigators to examine its development readily with the dissecting microscope. Moreover, what the most vital is that the embryonic lethality might be avoided at some extent when using the zebrafish model. For example, the embryo might still survive for longer than would be possible in mammals even in the absence of a functional cardiovascular system (Veldman et al., 2008).

1.5.2 Stages of embryonic development of the zebrafish.

Normal development has been described in considerable detail (Kimmel et al., 1995). Figure 1-5A gives an overview of zebrafish development during the first 24 hours (Haffter *et al.*, 1996), while development from 1 to 5 days is shown in Figure 1-5B. About the stages of embryonic development of the zebrafish Kimmel et al

(1995) defined seven broad periods of embryogenesis: the zygote, cleavage, blastula, gastrula, segmentation, pharyngula, and hatching periods. These divisions highlight the changing spectrum of major developmental processes that occur during the first **3** days after fertilization, the detail of stages has been shown in the Table 1-1. This table gives a simple system to describe the developmental stages of embryos, which has been extensively adopted by researchers. For example, using "x x ss" to describe embryos from segmentation period, while when describing embryos from the pharyngula period, the format "x x hpf" often is adopted by researchers.

1.5.3 The strategies and experimental techniques applied for the study of embryonic development of the zebrafish.

In 1980, Streisinger and his colleagues in Oregon continued to exploit zebrafish for developmental genetics and strive to establish the common laboratory techniques for zebrafish husbandry and embryological observation (Streisinger et al., 1981). In 1996, the large-scale chemical mutagenesis screens were performed by the Driever and Fishman laboratories and Nusslein-Volhard laboratory (Driever et al., 1996; Haffter et al., 1996). In these experiments, adult male fish were treated with the mutagen *N*-ethyl-*N*-nitrosurea (ENU), which efficiently creates point mutations in the germline (Grunwald et al., 1992; Solnica-Krezel et al., 1994). Then these zebrafish lines harbored the mutations are inbreeded within a stock to obtain the incrosses and recessive phenotypes can be appeared. These studies were the first systematic, large-scale genetic screens in a vertebrate species. Recently, retroviral and transposable element insertion mutagenesis techniques and targeted mutagenesis technique in zebrafish using customized zinc-finger nucleases have been developed for zebrafish (Allende et al., 1996; Wang et al., 2007; Nagayoshi et al., 2008; Foley et al., 2009). Moreover, there are other some techniques, such as, gene mapping,

9

transgenesis, protein overexpression or knockdown and cell transplantation, etc. With successful application of these methods our understanding of vertebrate development under normal and pathologic conditions would largely be improved.

1.6 Objectives of the present study

On the one hand, the increasing evidence suggests the possible role and importance of UII in human cardiovascular pathophysiology; however, the most basic cause relationship between UII and related human diseases remains far away from clear and the accumulating data from different Labs are filled with widely discrepant statements.

On the other hand, previous studies have suggested that UII mediates diverse biological processes in healthy organisms; however, to date there is still no report on the implication of UII in embryogenesis. Perhaps one of the reasons is that from lamprey, the representative of the basal group of jawless vertebrates to date, and elephant shark, the representative of the basal group of jawed vertebrates to date, to human, their UIIs share the completely identical biologically active sequence (CFWKYCV), suggesting that evolutionary pressure has acted to conserve the biologically active sequence of UII, indicating that the peptide may exert important physiological functions in vertebrates. Once deleted, that will result in early embryo lethality.

In this present study, zebrafish is used as the model organism because of the many advantages of this vertebrate (Veldman et al., 2008), which enables the achievement of the following objectives:

1. Demonstration of the existence of the UII/UIIR genes in zebrafish genome and of their expressing activity during zebrafish embryogenesis.

2.   Characterization of the role of UII during early embryogenesis.

The present study will not only contribute to our current knowledge about the functions of UII during embryogenesis but also shed light on the relationship between UII and human congenital cardiovascular diseases, particular with heterotaxy.

```
Carp        MMCNLLLSFS VLLLSCTHLV AHPVTDTADM TYSGPDSVEE AGGVSPDDFA
Flounder    MKCNHLLSWA FLLAASGPAL GHPITESAEM PYPGPASLEE RGVGSLDDLS


            VSDLNDLLQR AAVVEYSPLL  S----RENIK VPGQIPKEAL RELLLEKPYR
            LSEQNYPPQD GAGL-RYATLI SGEINRDGVR TTGLFPRGMK REVLLEKQSL


            LIPPSGLWGS RRQFRKRGGG AD CFWKYCV
            LNPFSHVFGI RKQFRKRAGT TE CFWKYCV
```

Fig.1-1. A comparison of amino acid sequence of flounder prepro-UII with that of carp. Amino acid residues highlighted in red represent the putative sites of post-translational processing of prepro-UII and the conservative motif high lighted in purple.

```
Carp_alpha MMCNLLLSFS VLLLSCTHLV AHPVTDTADM TYSGPDSVEE  AGGVSPDDFA
Carp_gamma MMCNLLLSCS VLLLSCSHLL AHPVTDTADM TYSGPDSVEE  AGGVNPDDFS
Frog       -MSKLFFCCL ILAGSFCSFR SLPIIVPSKG SL-RLSESALD  FGDLKSWDDE
Human      -MYKLASCCL LFIGFLNPLL SLPLLDSREI SFQLSAPHED  ARLTPEELER


           VSDLN---DL LQRAAVVEYS PLLSRENIKV PGQIPKEAL-R ELLLEKPYRL
           VSDLN---EH LQRAAVAGYS PLFSQENIKV PGQIPKEAL-R ELLLEKPYRL
           TRLL-RNLPMF VDKEAERDAE DIFSKEGFGL DAYN-MDDKE  ELFDKHPRIS
           ASLLQILPEM LG--AERGDI L-RKADSSTNI FNPRGNL-RKF QDFSGQDPNI


           IPPSGLWGSR RQFR
           IPPRGLWGSR RQFR
           LLSRLQSKDR  QF
           LLSHLLARIW  PY
```

Fig. 1-2. Alignment of deduced amino acid sequences of human, frog and carp prepro-UII. The deduced mature UIIs are highlighted in green. Prohormone convertase cleavage sites are highlighted in red.
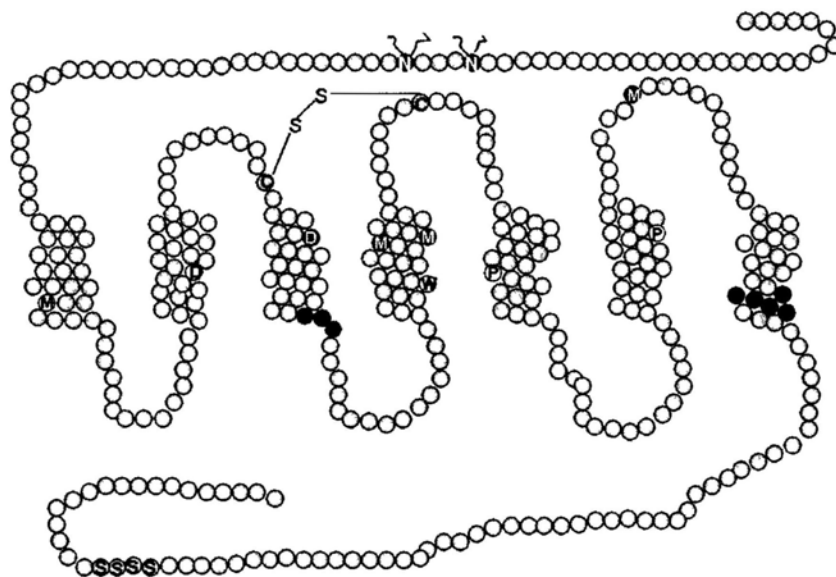
Fig.1-3. Schematic representation of the rat UIIR.

Residues circled in red represent the most conserved residue of each TMD. Motifs are highlighted in green. Residues of UIIR that have been shown to be important for UII binding in blue. Putative N (Asn)-glycosylation sites (N^{29}, N^{33}) and the conserved disulfide bridge are depicted. Figure modified from Proulx et al., (2008).
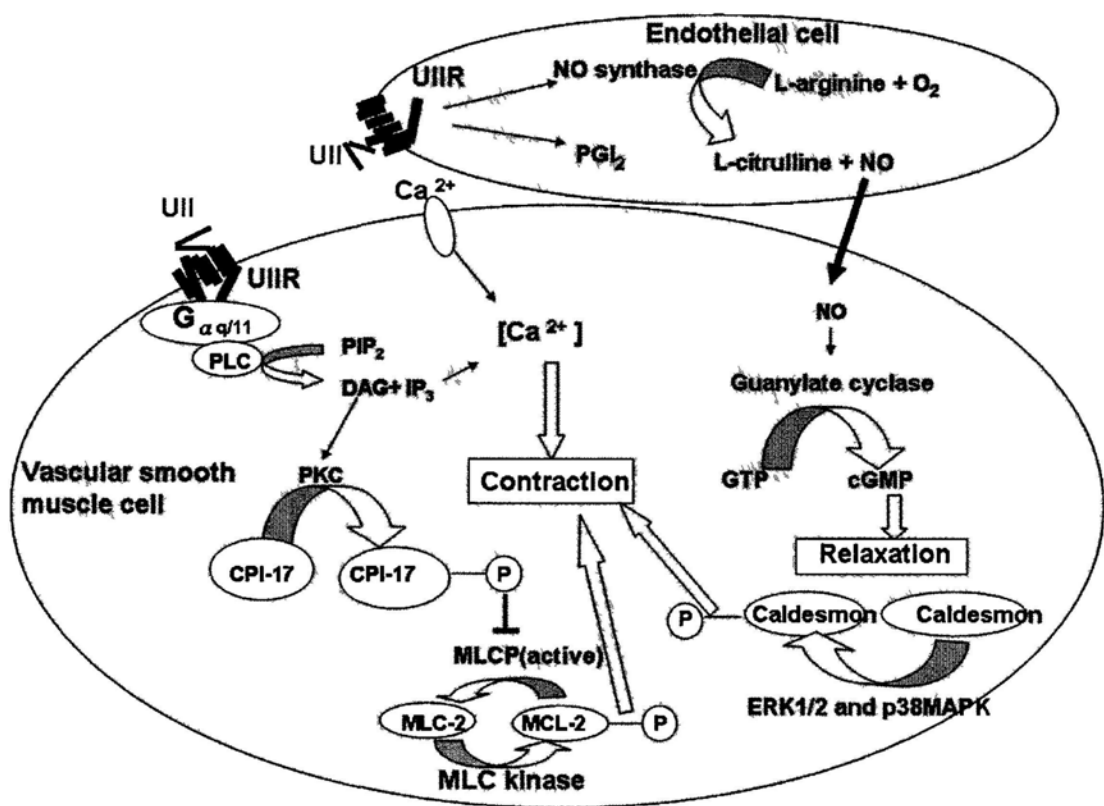
Fig.1-4. The signal transduction pathways involved in vasoconstriction and vasodilatation caused by UII

Fig.1-4. The signal transduction pathways involved in vasoconstriction and vasodilatation caused by UII

In vascular smooth muscle cell (VMSC), UII binds to a UIIR, leading to hydrolysis of phosphatidylinositol 4,5-bisphosphate (PIP_2) into two second messengers: inositol 1,4,5-triphosphate (IP_3) and Diacylglycerol (DAG) by phospholipase C (PLC). IP_3 increases the release of Ca^{2+} from the sarcoplasmic reticulum or endoplasmic reticulum. UII also mediates Ca^{2+} influx through activation of a voltage-gated Ca^{2+} channel. DAG stimulates protein kinase C (PKC) which phosphorylates CPI-17 (protein kinase C-potentiated inhibitor protein of 17 kDa), leading to inhibition of myosin light chain phosphatase (MLCP) which catalyses the dephosphorylation of phosphorylated regulatory myosin light chain (MLC-2). The increases in phosphorylated MLC-2, intracellular Ca^{2+} and phosphorylation of the actin-binding protein, caldesmon, by extracellular signal-regulated kinase (ERK) or p38 mitogen-activated protein kinase (p38MAPK) lead to contraction of VMSC. In endothelial cells, U-II stimulates the production of prostacyclin and nitric oxide (NO) which then diffuses into VMSC, leading to increase in cGMP and relaxation of VMSC. Figure modified from Ong et al., (2005).
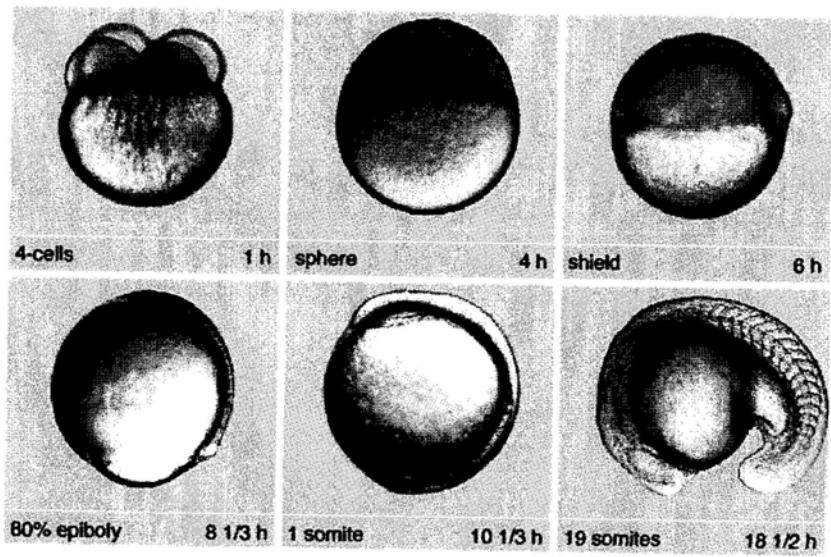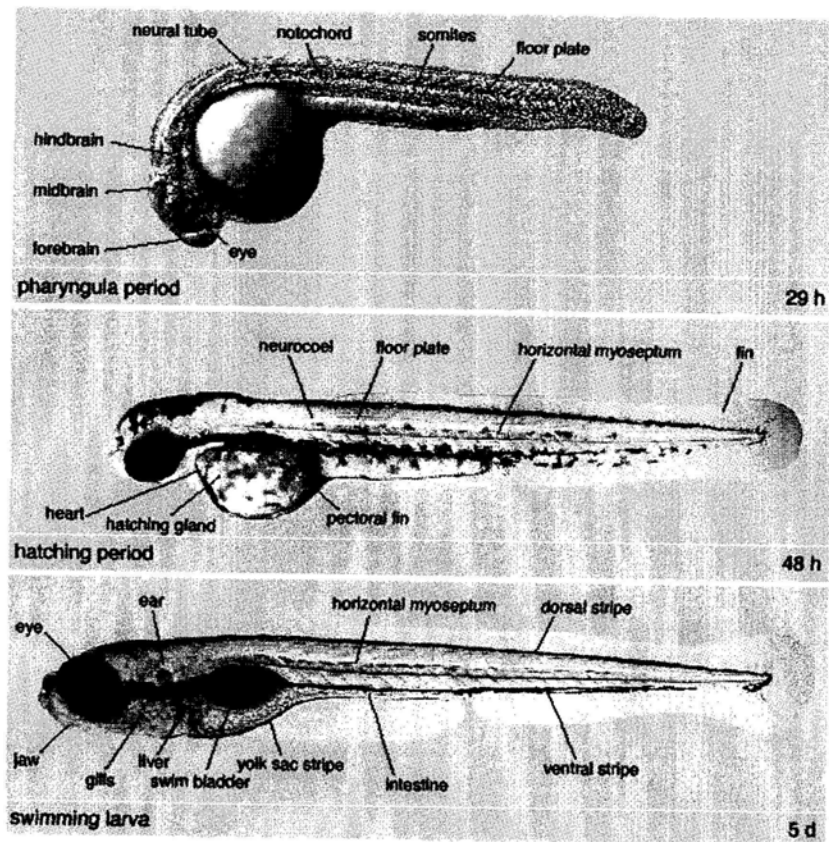
15

Fig.1-5A

4-cells 1 h   sphere 4 h   shield 6 h

80% epiboly 8 1/3 h   1 somite 10 1/3 h   19 somites 18 1/2 h

Fig.1-5B

neural tube   notochord   somites   floor plate

hindbrain

midbrain

forebrain   eye

pharyngula period   29 h

neurocoel   floor plate   horizontal myoseptum   fin

heart

hatching gland   pectoral fin

hatching period   48 h

ear   horizontal myoseptum   dorsal stripe

eye

jaw

gills   liver   yolk sac stripe   intestine   ventral stripe

swim bladder

swimming larva   5 d

Fig.1-5. Development stages of zebrafish embryo.

16

Fig.1-5. Development stages of zebrafish embryo. (A) The first 24 hours of development. (B) Embryos at 29 hours, 48 hours and 5 days of development. All embryos: lateral view. (This picture comes from Haffter *et al.*, 1996)

Table 1-1. Stages of embryonic development of zebrafish

Stage	hpf	Description
Zygote period		
1-cell	0	Cytoplasm streams toward animal pole to form the blastodisc
Cleavage period		
2-cel	3/4	Partial cleavage
64-cell	2	3 regular tiers of blastomeres
Blastula period		
128-cell	2+1/4	5 blastomere tiers, cleavage planes irregular
Sphere	4	Spherical shape, flat border between blastodisc and yolk
30%-epiboly	4+2/3	Blastoderm an inverted cup of uniform thickness, margin reaches 30% of distance between the animal and vegetal poles
Gastrula period		
50%-epiboly	5+1/4	Blastoderm remains uniform in thickness
Shield	6	Embryonic shield visible from animal pole, 50%-epiboly
75%-epiboly	8	Dorsal side distinctly thicker, epiblast, hypoblast, evacuation zone visible
Bud		Tail bud prominent, notochord rudiment distinct from neural keel, early polster, midsagittal groove in anterior neural keel, 100%-epiboly
Segmentation period		
1-somite	10+1/3	First somite furrow
5-somite	11+2/3	Polster prominent, optic vesicle, Kupffer's vesicle
26-somite		EL = 1 6 mm, HTA = 125", side-to-side flexures, otoliths, Prim-3
Pharyngula period		
Prim-5	24	EL = 1 9 mm, HTA = 120", OVL = 5, YE/YB = 1, early pigmentation in retina and skin, median fin fold, red blood cells on yolk, heartbeat
High-pec	42	EL = 2 9 mm, HTA = 55", OVL < 1 and > % YE/YB = 1 5, YB/HD < 1 3, PF(H/W) = 1 dechorionated embryos rest on side after swimming, YE remaining cylindrical, PF apical ridge prominent, early lateral stripe, complete dorsal stripe, xanthophores in head only, iridophores in retina only, pericardium prominent, NO heart chambers, segmental blood vessels, mandibular and hyoid arches, foregut developments, olfactory cilia, thickened otic vesicle walls
Hatching period		
Long-pec	48	EL = 3 1 mm, HTA = 45", OVL = PF(H/W) = 2, resting dorsal up, YE beginning to taper, PF pointed, dorsal and ventral stripes meet at tail, ca 6 melanophores in lateral stripe,

iridophores plentiful on retina, distinct yellow cast to head, NO circulation in 2-4 aortic

arches and in segmental vessels, olfactory cilia beating, semicircular canals, neuromasts

Note: EL, embryo length; PF, pectoral fin; h, hours of development at 28.5"C; HD, head diameter in dorsal view; NO, Nomarski optics; H/W, height/ width; Prim, Prim stages refer to the no. of the myotome to which the leading end of the posterior lateral line primordium has advanced; YB, yolk ball; YE, yolk extension; YSL, yolk syncytial layer; HTA, head-trunk angle; OVL, otic vesicle length. This table is modified from Kimmel et al (1996).

Chapter 2 Bioinformatics Analysis, Cloning and *in vitro* Characterization of UII/UIIR System in Zebrafish

2.1 Introduction

Since UII was first isolated from the caudal neurosecretory system of goby fish in 1969, functional studies about the cyclic peptide have been continued for more than 40 years. A major reason for the continued interest and investment in the mammalian UII research is the potential association of altered UII/UIIR system activity with human diseases. However, to date, it remains to be established the exact role of UII plays in human diseases.

In this present study, we use zebrafish as the model to investigate the role of UII in embryogenesis, particularly in cardiogenesis. In fact, the zebrafish model possesses many advantages for cardiovascular and developmental biology research:

- The development of the primitive vascular system has been finished at 24 h

- The embryo might still survive for longer than would be possible in mammals; even in the absence of a functional cardiovascular system.

- Until over a week old, the embryos are nearly transparent, allowing *in vivo* visualization of any tissue or organ during development

Considering that UIIR belongs to the subfamily A5 of GPRs sup-family and is coupled to the $G\alpha q_{/11}$ signal transduction pathway, the activation of which leads to the increase in mobilization of intracellular Ca^{2+} (Saetrum et al., 2000; Tzanidis et al., 2003) and inhibition of intracellular cAMP levelss (Song et al., 2006). Thus when performing the *in vitro* functional studies of zebrafish UII/UIIRs, we adopted the assay method of inhibition of cAMP formation.

In this present study, we revealed that the zebrafish genome harbors orthologs of the human UII/UIIR genes, including three ligands (UIIβ, UIIα and URP) and five receptors. Moreover we have cloned these orthologs (UIIβ and UIIα) from zebrafish and further demonstrated their expression during zebrafish embryogenesis. Third, by *in vitro* functional studies of zebrafish UIIRs, we have found that:

- The zebrafish UIIRs belong to the GPR family.

- The zebrafish UIIβ and UIIα may activate at least 4 of the 5 receptors and activation of these receptors inhibits cAMP formation. This finding is similar to that of the human UII/UIIR system.

- Activity of zebrafish UIIR3 is detected only by 10^{-5}M of human UII stimulation.

2.2 Materials and methods

2.2.1 Chemicals and reagents

The following reagents with their suppliers are listed below: restriction endonucleases (New England BioLabs), TRIzol (Invitrogen), RNase-free DNase I (Invitrogen), Oligo dT primers and ImProm-II Reverse Transcription System (Promega), Expand High Fidelity Taq polymerase (Roche), GOTaq (Promega), RACE System for rapid amplification of cDNA ends (Invitrogen), Dual Luciferase Kit (Promega), Pfu DNA polymerase (Stratagene), pCRII (Invitrogen), pcDNA3.1TOPT/A vector (Invitrogen).

2.2.2 Experimental animals and cell culture

Zebrafish (*Danio rerio*) were maintained at 28 °C with a 14:10 h light:dark cycle and fed twice daily. Embryos were generated by natural crosses. Fertilized eggs

were raised in embryo medium at 28.5°C. For *in situ* hybridization analysis, embryo medium was supplemented with 0.003% (w/v) 2-phenylthiourea to inhibit embryo pigment formation. All experiments were conducted in accordance with guidelines established by the University Committee on the use and care of laboratory animals at The Chinese University of Hong Kong.

The HEK293 cells were maintained in DMEM containing 10% fetal bovine serum (FBS) and 100 μg/ml penicillin and streptomycin in 5% CO_2 at 37°C. The cultures were diluted with 0.025% trypsin with 0.01% EDTA and re-plated when they have reached 90% confluency to maintain them in an asynchronous and exponential phase of growth.

2.2.3 Data mining and phylogenetic analysis

To identify UII and UIIR in different species, TBLASTN tool was used to search the genome database of species in these web sites:

- ensembl genome browser: http://www.ensembl.org/index.html

- NCBI database: http://www.ncbi.nlm.nih.gov/

- Elephant shark: http://esharkgenome.imcb.a-star.edu.sg

Multi-alignment of putative UII and UIIR from different species was performed with CLUSTALX. Phylogenetic analysis was performed using domain sequences of UII and UIIR from different species by the neighbor-joining method of the MEGA4 program. The reliability of the estimated tree was evaluated by the bootstrap method with 1000 pseudo-replications. Synteny mapping was carried out based on *Danio rerio* Zv7 and *Homo sapiens* Build 36.3 (www.ensembl.org/Homo_sapiens/index. synteny map html). Genomic structure was determined by searching the zebrafish genome at: www.ensembl. org/Danio_rerio/index.html.

2.2.4 RNA extraction and RT-PCR

Total RNAs were prepared from different zebrafish adult organs or embryos at different developmental stages using the Trizol, treated with RNase-free DNase I to avoid possible contamination from genomic DNA and then reverse transcribed using the ImProm-II Reverse Transcription System and Oligo dT primers or Random primers. The cDNAs were then subjected to PCR amplification using specific primers (see Table 2-1) using Expand High Fidelity Taq polymerase or GOTaq following the manufacturer's instructions. When possible, all primer pairs have been designed on different exons to avoid amplification of any contaminating genomic DNA which might be present in the cDNA preparations. Control PCR experiments with samples prepared without reverse transcriptase was performed to ensure that genomic DNA contamination did not contribute to the PCR amplification.

2.2.5 Molecular cloning and plasmid construction

Total RNA was digested with the RNase-free DNase I and was reverse transcribed into cDNA using the ImProm-II Reverse Transcription System and Oligo dT primers or Random primers. When performing the comparative genomic studies, Tostivint et al., (2006) had cloned the two zebrafish UII genes (*UIIα*, NM_212848; *UIIβ*, NM_205591.1). However, they had no done the functional characterization on the two genes. Herein, we directly used the sequence information of the two genes from their reports. As for the 5 zebrafish *UIIRs*, we used RACE (Rapid Amplification of cDNA Ends) kit to obtain the ends of the cDNA following the manufacturer's instructions. Based on the results of the bioinformatics analysis and the RACE experiments, primers (Table 2-1) were designed for cloning the open reading frame of *UIIRs* from zebrafish. The open reading frame of each zebrafish *UIIRs* was amplified by RT-PCR using Pfu DNA polymerase. The resulting cDNA was cloned

23

into the pCRII. To generate the receptor expression constructs, the above PCR product was also cloned into pcDNA3.1TOPT/A vector to produce the eukaryotic expression vector pcDNA3.1TOPT/A-*UIIR*s and was sequenced to confirm the direction and correctness of the sequences.

2.2.6 *In vitro* functional studies of zebrafish UIIRs

HEK293 cells were transiently co-transfected with the following plasmids: (1) 50 ng pcDNA3.1TOPT/A-*UIIRn*(n:1, 2, 3, 4, 5) carrying the entire coding region of each of the zebrafish UIIRs; (2) 500 ng experimental luciferase reporter plasmid controlled under a promoter containing CRE (cAMP response element); (3) 20 ng control luciferase reporter plasmid as an internal control. In this experiment, the pcDNA3.1TOPT/A plasmid was used as mock vector. Using RT-PCR, the transfection efficiency and expression levels of these receptor constructs were evaluated. After 6 h of transfection, synthetic zebrafish UIIβ, UIIα and human UII (as control) are diluted with free-serum DMEM. Then each kind of differently transfected HEK293 cell is incubated with DMEM containing different concentrations of different hormones for a further 20 h. Afterwards, luminescence was measured using a Lumat LB 9501 luminometer (EG&G, Berthold, Germany) and activities of both the firefly luciferase (experimental) and the *Renilla* luciferase (control) were measured sequentially from the same sample using the Dual Luciferase Kit. The zebrafish UIIβ, UIIα and human UII were synthesized by Sinoasis Pharmaceuticals, Inc. (Guangzhou, China).

2.2.7 Data analysis

All data which is from 3 times independent trials were expressed as mean values±S.E.M. Data were considered statistically significant at $P<0.05$ using either

one-way analysis of variance (ANOVA) or unpaired t-test. The statistical analysis was performed using the software GraphPad PRISM Version 5.0. (GraphPad, San Diego, CA)(www.graphpad.com).

2.3 Results

2.3.1 Zebrafish UII exhibits high sequence identity with that of other vertebrates.

In this study, we first searched for the presence of putative UII family members in genomes of different vertebrate species. The sequences of human UII were used as queries in TBLASTN searches. We found the orthologs of human UII in the genomes of the major vertebrate species. From lamprey, the representative of basal group of jawless vertebrates to date, and elephant shark, the representative of the basal group of jawed vertebrates to date, to human, their UIIs share the completely identical biologically active sequence: a cyclic hexapeptide (-Cys-Phe-Trp-Lys-Tyr-Cys-); which shows high conservation across different vertebrate species (Fig.   Fig.2-1 and Fig.2-2), suggesting that evolutionary pressure has acted to conserve the biologically active sequence of UII indicating that the peptide may exert important physiological functions in vertebrates. In the zebrafish genome there are three orthologs of human UII: UIIα UIIβ, and URP. To determine whether there is functional redundancy, divergence or differential regulation between UIIα and UIIβ, using the web promoter scan service we first performed the prediction of possible transcriptional factor binding to the promoters of UIIα and UIIβ at the following websites:

- http://bip.weizmann.ac.il/toolbox/seq_analysis/promoters.html
- http://www-bimas.cit.nih.gov/molbio/proscan/
- http://greengene.uml.edu/programs/promoter.html

- http://zlab.bu.edu/mfrith/cgi-bin/cister.cgi

All prediction results from these different websites are integrated to give the Figure 2-3, these results indicate that promoter of zebrafish UIIβ embodies more putative *cis*-elements than that of UIIα, suggesting that regulation of UIIβ is complex reflecting the potential widespread and diverse tissue distribution of UII and likely multiple functions.

2.3.2 Diversity of zebrafish *UIIRs*

Search results indicate that in zebrafish genome there are 5 different genes orthologous to the human *UIIR*, and they were distributed on different chromosomes of the zebrafish genome. According to Zebrafish Nomenclature Guidelines (www.zfin.org), we designed these new genes as: *UIIR1 (Chr.12), UIIR2 (Chr.3), UIIR3 (Chr.16), UIIR4 (Chr.6) and UIIR5 (Chr.12).*

2.3.2.1 Zebrafish UIIRs possess the structural characteristics of A class subfamily of GPR family

The multi-alignment of amino acid sequences of zebrafish and human UIIR shows that they possess some common features (Fig. 2-4). Similarly to human UIIR, the zebrafish UIIRs embody the 7TMD and encompass some conserved residues/motifs of the class A GPRs, such as, an (N/S)LxxxD motif in TMD2, a Glu/Asp-Arg-Tyr (E/DRY) motif at the junction of the TMD3, the second intracellular loop and the NPxxY motif. At the C-terminal region of zebrafish UIIR, putative phosphorylation sites could be found [Human, 8 sites; Zebrafish, 11 sites (UIIR1)]. The number of putative phosphorylation sites differs in zebrafish and human UIIR, which implies potential differences in the phosphorylation, internalization and desensitization of the receptors (Wyse et al. 2003). The zebrafish

UIIR also contains a putative caveolin-binding motif (FxFxxxxFxxF, where F is a hydrophobic residue and x is any amino acid) that is similar to that reported in the angiotensin AT1 receptor (Fig. 2-5).

2.3.2.2. Orthology relationship of UIIRs from different species

To establish the orthology relationships among UIIRs from different species we have performed a phylogenetic analysis. In Fig.2-6, we present a rooted neighbour-joining (NJ) tree obtained by aligning multiple protein sequences of the UIIR family from different vertebrate species. The topology of the tree is coherent with the known relationship between the different taxa and is supported by robust bootstrap values in almost all the nodes. The putative ortholog from lamprey, the basal group of vertebrates, is used as the outgroup which represents the root of the tree. In the phylogenetic tree we found that the five zebrafish UIIRs cluster into 4 different clades: UIIR2 clade, UIIR5 clade, UIIR1 clade and UIIR3/UIIR4 clade. UIIR3 and UIIR4 cluster into the same clade implying that the two loci are perhaps derived from a tandem duplication event of a common ancestral gene. However, the other receptors present only a single copy. The fact that there are four different types of zebrafish UIIRs suggests a probable functional diversification or functional redundancy of the UII/UIIR system in teleos.

Subsequently, to find evidence for the conservation of synteny, we compared genomic regions neighboring the zebrafish *UIIR* to the genes neighboring human and mouse *UIIR*. We used the Multi-Contig-View tool of ENSEMBL Genome Browser (www.ensembl.org) to analyze the neighboring genomic regions of each zebrafish *UIIR* with the human or mouse genome. Among the five zebrafish *UIIRs,* we only found the zebrafish *UIIR1* and *UIIR5* share good synteny with the orthologs. In the synteny region conserved genes, for example, a no-coding RNA gene and a *RELT*

27

(receptor expressed in lymphoid tissues) gene may be founded in genomic flanking regions around zebrafish *UIIR1* or *UIIR5* genes in the zebrafiish genome or in genomic flanking regions around their homolog in human genome. This strongly suggests that in zebrafish the two receptors UIIR1 and UIIR5 may have higher function conservation during vertebrate evolution. This point might be reflected by the homology between human UIIR and zebrafish UIIRs: The human UIIR is 74.68%, 42.21%, 37.66%, 36.54% and 45.59% identical to the zebrafish UIIR1, UIIR2, UIIR3, UIIR4 and UIIR5 homologues, respectively. On the contrary, as for UIIR2, UIIR3 and UIIR4, no syntenic gene is found in the flank around UIIR in the human and mouse genomes, indicating these *UIIRs* are specific to zebrafish, or are functionally redundant for zebrafish

2.3.2. Expression patterns of zebrafish *UII* and *UIIRs* during embryogenesis

The expression patterns of the 7 genes of the zebrafish *UII/UIIR* system, including 2 ligand genes and 5 receptor genes were examined. As shown in Fig. 2-7, *UIIα* mRNA is not detectable by RT-PCR in early embryogenesis until the hatching stage (48-72h). *UIIβ* mRNA is detectable throughout the different stages of embryogenesis, ranging from the 1-cell stage to 2 dpf. These data suggest that *UIIβ* transcripts not only are maternally deposited, but also are the products of the zygotic genes activated after the mid-blastula transition, since zebrafish embryonic genome is transcriptional activated only after 3 hpf (Alexander et al., 2007). In contrast, the mRNA of the five receptor genes is not detectable by RT-PCR in early embryogenesis. The mRNA of *UIIR1* and *UIIR2* became detectable at the Blastulation stage (around 30%-epiboly) *the levels of UIIR1* mRNA increased after 24 hpf and was maintained at relatively high levels thereafter. *UIIR2* mRNA was detected at 30%-epiboly and thereafter was maintained at relatively low but stable

levels across the other stages of embryo development. While transcripts of UIIR3, *UIIR4* and *UIIR5* were easily detectable only at 24hpf, thereafter were retained at same levels throughout the other development stages.

2.3.3. *In vitro* functional studies of zebrafish UIIRs

After bioinformatics characterization of putative zebrafish UII/UIIR system genes followed by their cDNA cloning, we further examined the biological activities of putative zebrafish UII/UIIR in cultured eukaryotic cells *in vitro*. In this study, the biological activities of the 5 zebrafish UIIRs were examined by a receptor transactivation assay using the Dual Luciferase Reporter Assay system. Results reveal that zebrafish UIIRs are biologically active and are able to respond to the stimulus of human UII. However, the activation of UIIR3 requires a much higher concentration of human UII to challenge than the other receptors. Ligand specificity of receptor interaction was ascertained by parallel studies in which the zebrafish UIIR-expressed cell lines were stimulated with synthetic zebrafish UIIβ, UIIα and human UII (as control) (Fig 2-8a, b, c).

2.4. Discussion

Originally, to establish the orthology relationships among UIIs from different species we performed a phylogenetic analysis. However, each of all UIIs identified so far is an extremely short peptide containing only 11 to 14 amino acid residues, when performing the phylogenetic analysis of all these UIIs using MEGA4 program, this program fails to run and some pair-wise distances cannot be estimated successfully by the program due to very short peptide chain. So, herein, we have not provided the phylogenetic tree of UIIs and only given the multi-alignment of amino acid sequences of UIIs (Fig. 2-2b), which shows extremely high conservation of UIIs

across different vertebrate species.

Based on *in vitro* ligand-receptor transactivation assay, we found UIIR 2, 4 and 5 have significantly response to the challenge from 10^{-8}M UIIa or 10^{-8}M UIIb (Fig.2-8 a, b), in comparison with them, UIIR1 shows variation, has significantly response to stimulation from10^{-8}M UIIa but has no significantly response to that from10^{-8}M UIIb, which seem means that UIIa is more physiological potent than UIIb and UIIR1 is specific for UIIa. On the other hand, UIIR2, 4, and5 have much more significantly response to stimulation from 10^{-8}M UIIb than 10^{-8}M UIIa (Fig.2-8 a, b) So, these receptors perhaps are specific for UIIb.

Expression profile of zebrafish *UIIs* and *UIIRs* uncovers transcripts of *UIIR1* and *UIIR2* are detected at approximately 30% epiboly stage (5hpf); transcripts of *UIIR3, UIIR4* and *UIIR5* become obviously detectable after 24hpf stage. Only after 48hpf *UIIa* begin to strongly express; instead, initially *UIIb* mRNA is maternal deposition and its zygotic transcriptional activity appears at approximately 60% epiboly stage (7hpf). In the light of that onset of circulation of zebrafish embryos occures after 24hpf and its development is completed at 48hpf (Isogai, et al., 2001), we hypothesize during embryogenesis UIIa mainly exerts its physiological effect on cardiovascular system, but UIIb contributes to early embryogenesis. The hypothesis perhaps gives a reasonable explain for the lag expression of *UIIa*, in fact which also is consistent with our previously conclusion: *UIIa* is more physiological potent than UIIb and

In *in vitro* experiments the HEK293 cells (human embryonic kidney cells) and the CHO cells (Chinese hamster ovary cells) are frequently used to study GPRs. These cell types possess a large repertoire of G proteins that are necessary for coupling to downstream effectors *in situ*. They also share a reliable history of positive functional coupling for a wide variety of known GPRs; particularly HEK293

cell line itself does not express the GPR14 and UII (Ames et al., 1999; Kitayama et al., 2003; Libert et al., 1991; Stadel et al., 1997; Zhao et al., 2009). In addition, previous reports (Song et al., 2006) suggest human UII stimulates CHO cells expressing the exogenous human UIIR inhibits the intracellular cAMP formation. Therefore when undertaking this *in vitro* assays of zebrafish UII/UIIR system we employ the pCRE-Luc plasmid construct (Stratagene) as the experimental luciferase reporter. The construct contains the luciferase reporter gene driven by a basic promoter element (TATA box) joined to tandem repeats of CRE,(cAMP response element) to sense the concentration change of intracellular cAMP levels and use HEK293 cells as the host expressing zebrafish UIIRs. Our results provide more convincing experimental evidence to demonstrate that: (1) UIIα and UIIβ may activate at least 4 of the 5 zebrafish receptors. (2) Activation of these receptors by synthetic zebrafish or human UII inhibits the formation of intracellular cAMP, similar to the signaling pathway of human UII/GPR14 system. (3) Bioactivity of UIIR3 could only be detected by 10^{-5}M of human UII stimulation.

In short, at this section, our observation demonstrates the existence of the UII/UIIR signal system in zebrafish and the expression of UII/UIIR system during zebrafish embryogenesis.

Table 2-1 List of PCR primers

Primer name	Sequence (from 5' to 3')	Purpose
UIIαF	ccggattcagtggaagagg	RT-PCR
UIIαR	ataacacacggctgttgctct	RT-PCR
UIIβF	tgtgtctgttggtgtcatcat	RT-PCR, *in situ* probe synthesis,
UIIβR	tctgcatgtttagtgcattgg	and ORF isolation
5'UIIR1	gagtggcacatgacaaccag	5'RACE
5'UIIR2	ggtcctgtgactgttggtga	5'RACE
5'UIIR3	atggggagagagagggtgat	5'RACE
5'UIIR4	atgatggcgagggtgtagag	5'RACE
5'UIIR5	gtcccgaaagtcgatgtgat	5'RACE
UIIR1f	atgaccactgtgtctgtggagc	RT-PCR, ORF isolation
UIIR1r	gaggctgctgttgttggt	RT-PCR, ORF isolation
UIIR3f	atggatatacctggttctacttcc	RT-PCR, ORF isolation
UIIR3r	ttgctcagagctgccctttttggc	RT-PCR, ORF isolation
UIIR4f	atgagtaacgcagctaatagcag	RT-PCR, ORF isolation
UIIR4r	tccaatttgatcgtggatcatg	RT-PCR, ORF isolation
UIIR5f	atgaattacaacaagtctagcggtcc	RT-PCR, ORF isolation
UIIR5r	ctgcatcacctttaactgcgcc	RT-PCR, ORF isolation
UIIR2f	atggaagcagatgatcatttttc	RT-PCR, ORF isolation
UIIR2r	cagtattacagaactgtttgccc	RT-PCR, ORF isolation
Pitx2cF	ggatgtgcacacggtttcagac	*in situ* probe synthesis
Pitx2cR	attggacgcgtttcagtggttt	*in situ* probe synthesis
lefty2F	cccggctcacattaagagcaag	*in situ* probe synthesis
lefty2R	tgtccatggagcatccacactt	*in situ* probe synthesis
lefty1F	aggggtttcacccacgaagac	*in situ* probe synthesis
lefty1R	cgtagccgtagttgcgctttg	*in situ* probe synthesis
NtlaF	gtcaccggtctcgaccctaatg	*in situ* probe synthesis
NtlaR	gagctctcgaactgggcatctc	*in situ* probe synthesis
SpawF	tgttgattgcgtgtggatcg	*in situ* probe synthesis
SpawR	cgctccggttggtagagctt	*in situ* probe synthesis

foxa3F	gcagtcacaaagcaagatgctca	*in situ* probe synthesis
foxa3R	agctccgtgttgaagatgtcctg	*in situ* probe synthesis
ngn-1F	ttcgcacacggatgatgaaga	*in situ* probe synthesis
ngn-1R	aagtggtgggaaagccgtcat	*in situ* probe synthesis
crestin-F	cacaccgggaacatcaccag	*in situ* probe synthesis
crestin-R	gcgcaagctagctgatgcaa	*in situ* probe synthesis
egr2b-F	tgtgcaccctcttgccgata	*in situ* probe synthesis
egr2b-R	gtgcgaatgtgggtcgtcag	*in situ* probe synthesis
pax2a-F	atgttcgcctgggagatcagag	*in situ* probe synthesis
pax2a-R	ggatttcggctccatgaaagtg	*in situ* probe synthesis
mab21L2-F	ggtgtcggatgtgctgaagg	*in situ* probe synthesis
mab21L2-R	ttacccggagagcagcatga	*in situ* probe synthesis
rx3-F	ggaaccgaaccacgttcacc	*in situ* probe synthesis
rx3-R	ggaaagtggccagctgcatt	*in situ* probe synthesis
barhl2-F	cagcctcatctgctcggtca	*in situ* probe synthesis
barhl2-R	tcacggtcacaggctcgact	*in situ* probe synthesis
Nkx2.5F	ctggagcagaatcaggaggaca	*in situ* probe synthesis
fgf8aF	tcctcaccttcatggacagctc	*in situ* probe synthesis
fgf8aR	ggtgcgtttagtccgtctgttg	*in situ* probe synthesis
chdF	cctgctgccatacaatggactg	*in situ* probe synthesis
chdR	cagtctgaagggttgcgtctga	*in situ* probe synthesis
flhF	ttgcatcaggactatgccacct	*in situ* probe synthesis
flhR	gagcaatggcgtgtgtaagtga	*in situ* probe synthesis
gscF	cgccgaacttacaatcggtga	*in situ* probe synthesis
gscR	cagcccattccagaacatcaga	*in situ* probe synthesis
iro3F	ccgacccatatactcgcaggac	*in situ* probe synthesis
iro3R	tgtctgaagttgtggcggtctc	*in situ* probe synthesis
eomeF	ttcaccgccatcaaactgaga	*in situ* probe synthesis
eomeR	cagcaggtcatcggtgtatgc	*in situ* probe synthesis
dhmF	acatactcacgcagcttttgg	*in situ* probe synthesis
dhmR	attcctgatgatcctccagagc	*in situ* probe synthesis

33
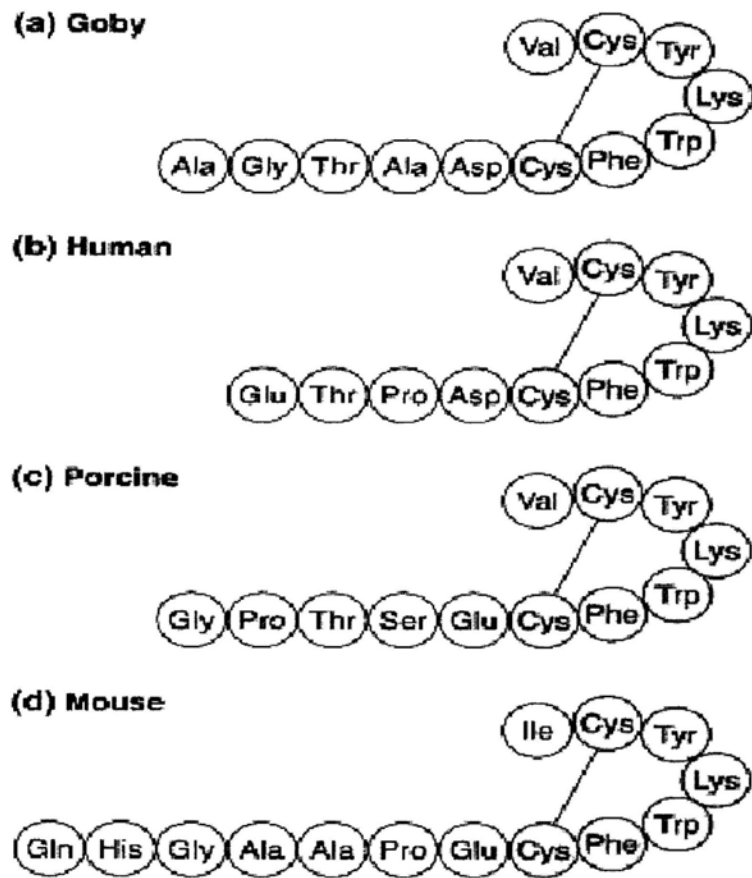
Fig. 2-1. Amino acid sequences of predicted UII from different species.

(a) goby, (b) human, (c) porcine, and (d) mouse. Shading indicates the C-terminal cyclic hexapeptide sequence, which is conserved across species. Figure was modified from Davenport et al., (2000).

34

```
Guttata_URP        EELEKLKDQLSAEDGSEVAYALESLSASQ--------------PKKRACFWKYCI--
Chicken_URP        EQLLKFKDQLSAEEGSEVADALESLTASQ--------------PKKRACFWKYCI--
Frog_URP           EQLEKLKEQLLEGKTADVTYAVEGMASSH--------------PNKRACFWKYCV--
Cattle_UII         NQLEKLKEQLMEAKDAEMSYAIDGLSSSH--------------PNKRACFWKYCV--
Horse_URP          NQLEKLKEQLMEANDAEISYTIDGLASSY--------------PNKRACFWKYCV--
Human_URP          NQLEKLKEQLVEEKDSETSYAVDGLFSSH--------------PSKRACFWKYCV--
Chimpanzee_UII     NQLEKLKEQLVEEKDSEASYAVDGLFSSH--------------PGKRACFWKYCV--
Monkey_URP         NQLEKLKEQLVE-KDSDMSYAIDGLFSSH--------------PSKRACFWKYCV--
Mouse_URP          RQVKKL-RDWIMEAKNTGLSNALDNLSSSH-------------TKKRACFWKYCV--
Rat_URP            RQLKKL-REWFMEAKSAEPSNALDKLSSSH-------------PIKRACFWKYCV--
Flounder_UII1      LEVLLEKQSLLNPFSRVFGI-RKQFAG----------------TTECFWKYCV--
Founder_UII2       REVLLEKQSLLNPFSHVFGI-RKQFRKR--------------AGTTECFWKYCV--
Grouper_UII        REVLLEKQSLLNPFSRVLGI-RKQL-RKR-------------AGNSECFWKYCV--
SticklebackUII     REVLLERQSLLNPFSRLFGI-RKQFRKR--------------AGNSECFWKYCV--
Medaka_UII         KDFFLEKQRLLNPFGHILGI-QKDFRKR--------------SGNTECFWKYCV--
Fugu_UII1          KEVLLEKQHLLDPFSQALGI-RKQL-RKR-------------TGNNECFWKYCV--
Tetraodon_UII      KEVLQEKQSLLNPFSHVLGI-RKQFRKR--------------HGNDECFWKYCV--
Carp_UII_beta      ----------------------------------------GGNTECFWKYCV--
Zebrafish_UIIbeta  KEALLEKP----LWSRFLGS-RKQYHKR-------------GSNTECFWKYCV--
Sucker_UII         ----------------------------------------GSNTECFWKYCV--
Guttata_UII        KETFHGNHPRNAFLGRFLIKDRKQYKKR--------------GNLSECFWKYCV--
Chicken_UII        KEAFYGNHPRIALLGRLLVKDRKQYKKR--------------GNLSECFWKYCV--
Trout_UII          ----------------------------------------GGNSECFWKYCV--
Mouse_UII2         GQNS------NTVLSRLLARTRKQHKQH--------------GAAPECFWKYCI--
Rat_UII            GQDS------NTVLSRLLARTRKQRKQH--------------GTAPECFWKYCI--
Pig_UII1           GQDP------NIFLSHLLARIKKPYKKR--------------GPPSECFWKYCV--
Pig_UII2           GQDP------NIFLSHLLARIKKPYKKR--------------GPPSECFWKYCV--
Paddlefish_UII     ----------------------------------------GSTSECFWKYCV--
Sturgeon_UII       ----------------------------------------GSTSECFWKYCV--
Catshark_UII       ----------------------------------------NNFSDCFWKYCV--
Lamprey_UII        ----------------------------------------NNFSDCFWKYCV--
Frog_UII           KEELFDKHPRISLLSRLQSKDRKQFKKRA-------------GNLSECFWKYCV--
Human_UII1         RKFQDFSGQDPNILLSHLLARIWKPYKK--------------RETPDCFWKYCV--
Human_UII2         RKFQDFSGQDPNILLSHLLARIWKPYKK--------------RETPDCFWKYCV--
Human_UII3         RKFQDFSGQDPNILLSHLLARIWKPYKK--------------RETPDCFWKYCV--
Monkey_UII         RKFQDFSGQDPDILLSHLLARIRKPYKK--------------RETPDCFWKYCV--
Sucker_UII1        ----------------------------------------AGTADCFWKYCV--
Carp_UII_alpha     RELLLEKPYR-LIPPSGLWGSRRQFRKR--------------GGGADCFWKYCV--
```

```
Carp_UII_gamma      RELLLEKPYR-LIPPRGLWGSRRQFRKR---------------GGGADCFWKYCI--
Zebrafish_UIIalpha  KEFLLEKPYR-LVPPSGLLGSRRQFRKR---------------GGGADCFWKYCV--
Sucker_UII2         -------------------------------------------GSGADCFWKYCV--
Tetraodon_URP       EMITALEELQRAVNSTLSSRITVMSRDSANPVVTGQNSKKSQTKKTKRVCFWKYCSQN
Zebrafish_URP       TIDSGGISPKASTDQMDPKLNGKSFKKSLP----------STKKTNKRVCFWKYCSQN
                                                                          ******
```

Fig. 2-2a. Alignment of pre-UII and pre-URP amino acid sequences.

The conserved residues are highlighted in red. The accession numbers of the sequences used in this alignment are listed as followed: Grouper UII, ACN65410.1; Guttata UII, XP_002195510.1; Cattle UII, XP_871317.2; Frog UII, NP_001120467.1; Flounder UII, P21857.1; Founder UII, CAD56907.1; Horse URP, XP_001500- 234.1; Human UII1, NP_068835.1; Human UII2, AAI26444.1; Human URP, NP_937795.2; Fugu UII, NP_001072085.1; MouseUII, NP_036040.1; Mouse URP, NP_937809.1; Chimpanzee URP, XP_001161544; Chimpanzee UII, XP_0011- 57678; Monkey UII, NP_001028067.1; Chicken URP, NP_996872.1; Chicken UII, NP_996873.1; Zebrafish UIIα, NP_998013.1; Zebrafish URP, NP_001076411.1; Rat URP, NP_937766.1; Rat UII, NP_062033.1; Zebrafish UIIβ, NP_991154.1; Sucker UII, P04559.1; Pig UII, NP_999308.1; Pig UII, BAB60889.1; Carp UIIα, 1007166A; Carp UIIβ, P04561.1; Carp UIIγ, 1007166C; Trout UII, 2003277A; Catshark UII, P35490.1; paddlefish UII, P81022.1; Sturgeon UII, AAB47079.1; Sucker UII, P01147.1; Sucker UII, P04558.1; Frog UII, P33715.2; *Taeniopygia guttata* URP, XP_002190569.1; Tetraodon URP, CAG04941.1; Tetraodon UII, ENSTNIP00000002161; Lamprey UII, P81022; Medaka UII; ENSORLP00000017414; Stickleback UII, EN-SGACP000000163-60.

```
Grouper_UII              --AGNSECFWKYCV--
Stickleback_UII          --AGNSECFWKYCV--
Trout_UII                --GGNSECFWKYCV--
Fugu_UII                 --TGNNECFWKYCV--
Tetraodon_UII            --HGNDECFWKYCV--
Zebrafish_UIIbeta        --GSNTECFWKYCV--
Sucker_UII               --GSNTECFWKYCV--
Carp_UII_beta            --GGNTECFWKYCV--
Medaka_UII               --SGNTECFWKYCV--
Flounder_UII1            -FAGTTECFWKYCV--
Founder_UII2             --AGTTECFWKYCV--
Frog_URP                 ------ACFWKYCV--
Chimpanzee_URP           ------ACFWKYCV--
Guttata_UII              --GNLSECFWKYCV--
Frog_UII                 -AGNLSECFWKYCV--
Chicken_UII              --GNLSECFWKYCV--
Pig_UII                  --GPPSECFWKYCV--
Paddlefish_UII           --GSTSECFWKYCV--
Sturgeon_UII             --GSTSECFWKYCV--
Mouse_URP                ------ACFWKYCV--
Monkey_URP               ------ACFWKYCV--
Catshark_UII             --NNFSDCFWKYCV--
Lamprey_UII              --NNFSDCFWKYCV--
Cattle_UII               ------ACFWKYCV--
Horse_URP                ------ACFWKYCV--
Rat_URP                  ------ACFWKYCV--
Human_URP                ------ACFWKYCV--
Human_UII                ---ETPDCFWKYCV--
Chimpanzee_UII           ---ETPDCFWKYCV--
Monkey_UII               ---ETPDCFWKYCV--
Sucker_UII1              --AGTADCFWKYCV--
Zebrafish_UII_alpha      --GGGADCFWKYCV--
Carp_UII_alpha           --GGGADCFWKYCV--
Carp_UII_gamma           --GGGADCFWKYCI--
Sucker_UII2              --GSGADCFWKYCV--
Mouse_UII                QHGAAPECFWKYCI--
Rat_UII                  QHGTAPECFWKYCI--
```

```
Guttata_URP        ------ACFWKYCI--
Chicken_URP        ------ACFWKYCI--
Zebrafish_URP      ------VCFWKYCSQN
Tetraodon_URP      ------VCFWKYCSQN
                         ******
```

Fig. 2-2b Alignment of putative mature UII and URP amino acid sequences.

The conserved residues are highlighted in red. The accession numbers of

These sequences used in this alignment are listed in the legends of Fig. 2-2a.

1) Possible functional *cis* elements in the zebrafish *UIIα* promoter.

CTCTACAAATGCGCTTTGTATCTTCAACTACATGTTGCATACTAGGGCTACTCGACCAAAAAGCCTCACTTCTCAT

AAGCTCATAGCTGAATTTGGCAGTGTCTCTGAACCAAACGCGAACTATAATTACGTAGTTTCAAAGTTTCCGACC

AGAAAGACAACGAAACAATGGCATGAAACTTCCACAGGGATGGTAAGCCTGAGCGGACAAACTTCTGCTC<u>CCTC</u>

<u>c-myc-PUR</u>   mTDT-site_B_(10)   EGFR-undefined-site-5

<u>CC</u>TCCACCAGCACGCCCATGACATCATCGCACCGGCTCACCCAATCATACCAAACATTAAAGACATTACTTGCTG

CTTATGTTCATAAACATGTTCATTTATTGTATTTTTTCATTTAATTATTCATTAAATACATAAACAATTCATTAAAT

            opaque-2-zein storage prot_(1)

TTCTTTTCAGATTTGTCCACGCGGAATGAACCGGGGACTTATCCAGGATAGGTTTTGCACAGCGTATGCCCTTCCA

            RAP1-LSR1/UAS(rpg) CS

GCTGCAACCCATCACTGGGAAACACCCATACACTCCCATTCACTCACATACACTACAGACAATTTAGCTTACCCA

ATTCACCTATAGCATGTCTTTGTACTTTTGGGGGAAACCGGAAACACGGGGAAACCATGCAAACTCCACATAAAA

ATGCCACCTGACCCAGTTGAGGCTTGAACCACCAACCTTCTTGCTGTGAGGCGACAGGGCTACCCATTGTGCCAC

            TBP-ARS domain A

CAGGCCCCCCTTATAATTATTAAATTATTATAAAAAATAAAAAAAAAATGTACTTTATAGAACATTGACTACGGTG

ATAAATATTTACAATAAATAAGTTACCATCATGTGGTGGAAAAATTCATTTTAACTATTACTAAAACATTGATTTC

                                GR-MSV-II

TAAAAAAACGTCTCATTCTTACTAGAAACACCAAATATTAGAAAACATATGCCTTCCTAAGAAAAGATGGTACA

                         Prl-1D

AAAACATATTACAAGAAGGGTCATTCAGAAGGGGGTCATCTGTTTTTTAAAATATGCATTCAATAAACACAAATC

CTGGGAGCCATGTCCTGATCCTCAGAAGAGGAACGCTCTAAGCAGAACTGGGTGTCATCTGTGACAGTGTGCCTT

    myc-PRF   <u>RVF</u>

GAAGAAGGGGAAAG<u>AAGATAAAACC</u>TGCTGGTTAGCCTATGTGCACTCTGCAGCAACCGGTGTTCCTGTATGAC

TGTCGGACCTATTCTTTGCAAAGAATAAAACCTTTTTGGAATTAAACCTTGTCTTTTGATCAGCAAGAGTCTCTTT

ATTGAAATGGCCATGACAATTATTTTAATAAATAAGCTATATATTTTTTCAATTATATTTTCCATCATTATACACC

ATTACATTAATTTATAAAAAATTTTAAAAACCTTGAAACATAATTAGGTGGGACTTAATGCACATTTTCTTAAATG

CTGTGAACAATATATTATATTATATTATATTATTCATTCATTTTCATTTCAGCTTCGTCCCTTAACTAAT<u>CTGGGGT</u>

  CreA-prn   **APF-alb4**   <u>**Myf**</u>   **Tcf**

<u>CGCCAC</u>AGCGCAATGAACCACCAGCTTATTCAGCTTATGTTTTAC<u>ACAGCAGATGCCC</u>TTCCAGCTACAACCCAT

CCCTGGGAAACACCCTTACAAGTGGAACACCCAGATGAAACCTATGTGAACATGGGAGAACATGCAAACTCCAC

        AP-1   **LSF**

ACAAAAATGCTAACTGACCCAGCC<u>GAGGCTCAAACCAGA</u>GACTTTCTTGCTGTGAGACAACAGTGTTACCCACTG

CyIIIa-P1.1   **LSF**

CTCCCCCACATTCATTTTCTTGTCGGCTTAGTCCCTTTATTAATC<u>CAGGGTCGCCACAGC</u>GGAATGATTTGCCAAC

                          <u>**LSF**</u>   **Sry-delta-genomic-1**

TTATCCATTAAGTTTTTACGCATTTATCCAGCAAGTTTTTACGCTCTTC<u>CAGCCGCAACCCATC</u>TCTAGGAAACAT

Tef   **CBF1-rRen**

TACACACACACTCATACACTACGGACAATTTAGCCTACCCAATTCACCTGTACCGCATGTCTTTGGACTGTGTGG

                        Myf   *Myc*   **CRE**   **LSF**

GAAACCGGAGCACCTGGAGGAAA*CCCACGCGAC*GCAGGGAGAACATGCAAACTTCACACAGAAACGCCAACTG

                LSF

AGCCGAGGATCGACCCAGCGACCTTTTTGCTGTTAGGCGACAGCACTACCTACTGCGCCACTGCATCGGCCTGCT

                                                                FoxA2-cdx-2 **M14b** SDI-A2

CCACCACATATTATACATTAAGTTATATTATATTATATATTGTAATAG*TTTGTTTGTTTT*TGTCCATAAAAAAAACA

TAAAAATCATAAAATGTAACCATAAAATAATCATCTTTTCACCATGTGCACATTTATCCAGTCCAACAAAAAAAT

ATAGCAATAAGATTAAATCACCATAGACGATTAATCAATGATTGTGGCAAATATTCCAGATCATCTTTTTGCTTTA

            HNF-4 CS

TCTTAGGCAAGGTTCACACTTCCATGTGTTCTACATGTACGGTGTATTGCACCAGACTAAATGACACACTCTAAA

                                                                        MIG1-SUC2_(1) **LUN**

AAATGTGTGTTGCTGTAAACCAACATTGGGTTTGTCCATATTTACCCTAATGTCAGAGTACAACAACCCAGCATTT

TTGGAGTGTGCCATTTAAGCTGGTGGACTACACTGTGAATGTAGGAGTGCTATTCACTGTTTTTTAGAGTGTGTCA

            MIG1-SUC2   **Ets**

TTTAACAACCCAGCATTTTTTCAGCGTCATCAGTTTTTTTTGTTTTTAATTAATAACGTAATTCAAGAACATAAATT

                                                                                HFH-2 CS2

GATCAGCTTCTTTTCTGAATATTGGGGGATAATATCTGATATTGAACAGCCTAGCATTGCAAATTGTTATTTTCTT

TTTTAAACTGTTTAATGCTGGGAGCAATACATGCAAATAAACGCCTCATGGGATCAATCTTTCATATATAGATCA

ACAAGTGCAGTAAAACTGAGTGACGCACAGTATAATGCGTCTGCTCTGTCTGATTTCACTCCAAGCTTTTATAAA

TGTCAAATGTGCATTGCTAATATGACTTCACCAATGGATGATAAACA

            TXS-nfe2-3

AATGTGTTGCTGATTCAAATGTGTTGAATCTCAAGTTTATATTCCTGATGCTCTCCACTTTTATCACCCCAATTGAT

ATAATGTTGACAGGATCAGTGTTGCAGCCAGAATCCCCAGTAAAACCTCTTTACCTATGCATCAGTTGTGAAATA

TACTTCCATCTTTTTCAGTATAAAAGGCCTACATAAAAGACAGCTGACACGTTCATAAAAATAGACTTTTATGCGTC

GTGGAGTTAATAGAAGGACATTTGCACACCTGTGTTCCCCGATTTACAAACTCAGTAAAACAAATGAGATTCAAA

            hPRL-Pitx-B1

GGTGATAAAGCCACTGCGATCCCGATTTATTCATGGATGCATTAATGCAATGGGATCTAAATGTGAAAATAAGAC

                                    Sp1-zeta-globin

GTTCAATAAAAACGTGGCATTCGGTATGATTGGTAGTGTGGGGTATATAAGATGAGAGAGTGTCTGTGGAGCTG

CCAAT box   **MyoD-acetylcholine receptor**

ATTGACCT*GACAGGAGCTGGAGCCGCTGTAGAGA*TG

2) Possible functional *cis* elements in the zebrafish *UIIβ* promoter

Tll-Kr (2)

AGTTGCTCTGGAAAATATAATTAAATTTTTCAATATAATGTTAACATATACTTTCTCTGTCAATTTATGTGTTGAGTTTT

BP1-beta-globin   H1TF1 RS (AC-box)

TACTGCAAATGTCACATCCATAACGCTGGAATTGCTCATATATGTATATATTCATATATATGTGTGTTTGTTTGTGTACA

hb1   Genesis-site-3

TGTATCATTTGTAATTTTTTATTTTTGTTTCATACTGTTATCAACCATGCTATACACATTGAACCAAGTCAATGTTGAG

ACATTCACTAATTTAAAACTGTTGAGAAATTCATTAAAAACACAATAAAGTTTAAGTAAAAAAAGAAAATAACATA

ACAAAAATGTTTTAAGTCTAAGAACTTGGTCTAATATTGTCCTCCAGAATGTCCTTCACAGTAAAACATGAATATCT

RZR/ROR RE

AGGTCAAACTTTTAGTGTTCGTGTTGGTTTCCAGACTCACAAACAACCACAGTGAACTTATTAAACAATTACACGG

TCTGCTTTTGAGTTGTGTTGTTGACTTGCACGTAAACAGACTTTATTGTACATCTATATAAAGTTTTATCGATGTAAA

CAATAGTTCAGAAAATAATGAAAACAAACTTACCCTCTTCTGTCACTCCAGACACGCGCAGACCCGTGAAAGTCG

AC-box   RAP1-mdscan-motif

CGTCTCATTCACGCACACACACACACAAACACATAGACGGTCAGGCGTGACACACGACAAAAGACACGCACACTCTC

GTGTTTTGTTGGACTGCAGTCAATCACAGCATCCTCTTCTCTCCGGTCTGAGCTCTGTGTCCGCTGTTCTTCATGTT

MET31/32 RS

TCCACAGTTTTTCTTCACTCAATGACAGTTTGACTTTGGCTGCTACTTTTGTTCTCAGTCAAAACAAAGAGAATGAT

C/EBP-HBV Box-beta

GTAGAGTTTCTCACGCGCCTCCATCGCCGTCTGCTGGTCATTCGGATTACTTCAAAGACTTTGCTCCTGTTTTTTGA

qa-1F-qa-2.2   Pit-1-CS-1 (2)

GCATTTCTACATGCTTATTATCGGTGATAGAATTGTTAAACACAATTAGGATTTTAATCAACCCCGCTGTTAGGATTTA

fAE2B/ CDRE

TGCATAGGCATATACATATTTAAGTCTATGATTTAAGATTTACTGCAGTGATTAATATGTTTATTTGTTTATGAAATTAT

TTTAATCCTTAACTGATGTACTGTCGTAGGCTACTCGTATGTAGCTTTTATTTTTTAACAATTGTGTTAAGCTAATGGT

FoxA2-cdx-2

CAAAAATGACCATGACCACTTGTAGACAGACAGACAGACTGACAAAAAACAAACAAACAGATGGATAGACAGAA

E1(IEF1-IEB) Nir_box

GGATGAACAGGCAGATGGCTAGACTGACAGACAGACAGATATATAGTCAGACAGACAGATTAATAGACAGAAAGA

CGGACAGTTATATAGAAAAACAGATAGACAGATAGAAGACAAGCAGATGACTAGATAGATAGAGTGACGAACAGA

GATAGACGAACAGACAGATAATTGATAGACAGACAGACGACAGACAGACAGACGAATAGGTAGACAGACAGTTG

GCTAGACAGACAGACGGACAGATAGACAGACAGAGAACAGATGGACAGACAGACAGAAAAAAATAGATAGATAA

AGACAGACAGACAAATGTTCAGACATACAGACAAACAAGATAGATAGATGAATAGACAGAGATGGATAGACAGAC

myc-CF1-c-myc (1)

AGACTCACAGAGAGAAAATGGACAGACAGACAGACAGACAGACAGACAGACAGACAGACAGACAGATAGATAG

ACAGACAGTTAGATAGACAGACAGTTAGATAGATAGATAGATAGATAGATAGATAGACAAATACACAGAAGATGGATCGA

41

CAGACTGACAGACAGACAGATAAATAGGTAGACAGATAGATGGCTAGATAGAAAGACAGACAGATGGACGGACA

GATAGACAGACAAACAGACGACTAGACAGATAGACAAACACAAATAGGCAGACAGAAAAACAGATAGAGAAACA

<u>HNF3</u>

AATAGACAGACAGACAGACAGACAAATAGACGAATAAAG<u>AGAACAAACAGA</u>TGACTAGATAGATAGACAGAAAG

ACAGATGTACGGATAAACAGACAGACAGACGGAAGGACAGATAGACAGATGGACAGACAGATTGATAGATGACA

CAGACAGACAGGAAGACAGACTGGTGGATATATGAACAGACTGACAGACAAACTGACGGACAAACAGACATAAA

TGGACAGACAGAAAAACAGATAGATAAATGAATAGACAGAGACGGATGGACAGACAGACCCACAGAAAGAAAC

GGATAGATAGAAGAACAGACAGACAGACAGACAGACAGACAGGCAGGCAGGCAGGCAGGCAGATAGATAAATAG

ATAGATAGATAGATAGACAGACAGACAGACAGACAGACAGACAGACAGACAGACAGACAGACAGACAGACAGA

CAGACAGACAGATAGATAGATAGATAGATAGATAGATAGATAGATAGATAGATAGATAGATAGATAGATAGATA

GATAGATAGATGAATAGACAGATAGACAGAAGAATAGGCAGAGAGATAGACGGATAGAAAGACAAACAAA<u>TGACT</u>

rPRL-FPI

<u>AGATATATAAA</u>CAGACAGACAAATAGACAGAAAGGCAGACAAACAGAAAGACAGAAGTATTGAAAAATAAATAG

ACAGACAAATGGACGGATGGACAGACAGATTAACAGATAGATAGACAAATAGACAGACGGATAGACAGAGGCTCA

CAGAGAGAAAAGGGACAGACAGACAGACAGACAGACAGACAGACAGACAGATAGATAGATAGATAGATAGATAG

ATAGATAGATAGACAGACAGACAGACAGACAGACAGATAGATAGATAGATAGATAGACAGACAGACAGACA

GACAGACAGACAGACAGACAGATTAGTAGGTAGGTAGACAGATAGACGGATAGAAAGACAAAGACAGACAGAGG

AATGGACAGACAGACAGACAGACAGACAGACAGACAGACAGACAGATAGACAGATAGATAGATAGATAGATAGAT

AGATAGATAGATAGAGACAGGCGGACGGACAGAGGAATGAACATATAGATAGGCAGACAGACAGACAGACA

<u>**ERE (GR-Mrib)**</u>   TATA Box   <u>E4BP4</u>

CTTGCAGAGGCAGCAGAAATAAATGAGAT<u>TGACACGCTGTCCT</u>GAGGCCAGAATAGCTCT<u>CACCTTTTACA</u>CCATT

       <u>**Myf**</u>   Ets   *LysHREVI*   SRF   <u>HNF3beta(3)</u>   Mef-2

GTCACACGTTCGCGT<u>CTGCACC</u>*TCCTGTCCGTCCC*GTTTTTGAGCGTC<u>TT</u>AAAATAGAAGACGTCAAGATGCAAG

<u>**Myf**</u>   <u>**Myf**</u>   , **TATA Box**   HAP-2/3/5-CYT1   <u>AP-1</u>

CGAGTAACTGCAGGAATAAATCT<u>CAGCGGCCTCTT</u>AAATAAATGAATGCGGGCAATTTGCCTG<u>GTGGAGTCATCC</u>

                Myf   LSF   <u>beta-RARE1</u>

CGCAGACTCTAACGCACAGAGCGCTT<u>CTCCACCTGCGTT</u>CAGCTGGATTTA<u>TGAACTCTGAACA</u>CTGGTAAAAAA

    <u>Tef</u>   <u>Ets</u>   GAGA-kruppel1.3   <u>**TATA Box**</u>   **Prl-4D**   <u>Tef</u>   Ets

AAGTGT<u>CCCGTTCCTGAC</u>GCGCTGT<u>CTCTCAGTTTTATGG</u>AGCCA<u>TTCATT</u>CATCCTCTGTCAATTTA CAAGCGC

         <u>**opaque-2-albumin b-32 (5)**</u>   TATA Box   <u>ICS (3)</u>   mu-E4

AGAATATGCAGAGGAGGGA<u>GATGACATGG</u>ACACTTCTGAAGCGTATAT<u>AAACCCAGG</u>AGGAGTTTCACTGAGGA<u>L</u>

<u>N4</u>   <u>Myf</u>   H1TF1 RS   <u>CRE</u>   AP-1

<u>GAAACTCCAGGCT</u>GAAGG<u>CTTCAGTTGTT</u>**TGTGTCT**<u>GTTGGTGTCATC</u> ATG

Fig.2-3 Possible functional *cis* elements in the zebrafish *UII* promoters

The blue region of DNA sequence represents a 25 times repeated *cis* Smad3-Smad4 binding elements region (CAGACAGACAGACA); c-myc-PUR, a *cis*-element binding Pur, Ref: Mol Cell Biol 12: 1257-1265 (1992); mTDT-site_B_(10) , a *cis*-element, Ref: Mol Cell Biol 11: 5229-5243 (1991); EGFR-undefined-site-, a *cis*-element, Ref: J Biol Chem 268: 16065-16073 (1993); opaque-2-zein storage prot_(1, a *cis*-element binding opaque-2, Ref: Plant Cell 4: 689-700 (1992); RAP1-LSR1 , a *cis*-element binding RAP1, Ref: Mol Cell Biol 8: 5086-5099 (1988); TBP-ARS domain A , a *cis*-element binding TBP, Ref: Proc Natl Acad Sci U S A 90: 8018-8022 (1993); GR-MSV-II , a *cis*-element binding GR, Ref: J Steroid Biochem 27: 9-14 (1987); Prl-1D , a *cis*-element binding Pit-1, Ref: J Biol Chem 269: 29335-8 (1994); myc-PRF , a *cis*-element, Ref: Nature 339: 718-21 (1989); RVF , a *cis*-element, Ref: Mol Cell Biol 11: 1875-82 (1991); CreA-prn , a *cis*-element binding CreA, Ref: Eukaryot Cell 3: 144-56 (2004); APF-alb4 , a *cis*-element binding APF, Ref: Genes Dev 2: 957-74 (1988); CyIIIa-P1.1 , a *cis*-element, Ref: Genes Dev 4: 1999-2010 (1990); Sry-delta-genomic-1 , a *cis*-element Sry-delta, Ref: EMBO J 10: 2533-2541 (1991); CBF1-rRen , a *cis*-element binding CBF1,Ref: J Biol Chem 280: 20860-6 (2005); FoxA2-cdx-2 , a *cis*-element binding FoxA2, Ref: Mol Cell Biol 17: 1626-41 (1997); M14b , a *cis*-element, Ref: Nature Genet 22: 281-5 (1999); SDI-A2 , a *cis*-element, Ref: Mol Cell Biol 15: 4158-66 (1995); HNF-4 CS , a *cis*-element binding HNF-4, Ref: Genes Dev 4: 2353-65 (1990); MIG1-SUC2_(1) , a *cis*-element binding MIG1, Ref: Mol Cell Biol 14: 1979-1985 (1994); LUN RS , a *cis*-element binding LUN,Ref: J Biol Chem 276: 14004-13 (2001); HFH-2 CS2 , a *cis*-element binding HFH-2, Ref: Mol Cell Biol 14: 2755-66 (1994); TXS-nfe2-3, , a *cis*-element binding NF-E2/p45,Ref: EMBO J 16: 5654-61 (1997); hPRL-Pitx-B1 , a *cis*-element binding Pitx-1,Ref: J Biol Chem 277: 44408-16 (2002); Sp1-zeta-globin_(1) , a *cis*-element binding Sp1, Ref: Mol Cell Biol 10: 282-294 (1990); MyoD-acetylcholine receptor , a *cis*-element binding MyoD, Ref: Nature 341: 716-720 (1989); Tll-Kr, *cis*-element binding Krüppel (Kr) and tailless (tll), Ref: Science 256: 94-97 (1992); BP1-beta-globin,

43

cis-element binding BP1,), Ref: Nucleic Acids Res 17: 8833- (1989); H1TF1 RS , *cis*-element

binding H1TF1,Ref: Mol Cell Biol 9: 1566-75 (1989); hb1, *cis*-element binding hunchback,), Ref:

Nature 341: 335-337 (1989); Genesis-site-3 *cis*-element binding,), Ref: J Biol Chem 271: 23126-33

(1996); RZR/ROR, *cis*-element binding RZR/RORalpha and RZR/RORbeta; RAP1-mdscan-motif, a

cis-element binding RAP1,Ref: Nat Biotechnol 20: 835-9 (2002); AC-box is a *cis*-element containing

sequential "CA", Ref: J Biol Chem 265: 2238-43 (1990); MET31/32 RS a *cis*-element binding

MET31/MET32,Ref: Mol Cell Biol 17: 3640-8 (1997); C/EBP-HBV_Box-beta a *cis*-element,Ref:

DNA Seq 1: 33- (1990); qa-1F-qa-2.2 a *cis*-element binding qa-1F,Ref: Mol Cell Biol 7: 1256-66

(1987); Pit-1-CS-1_(2), a *cis*-element binding Pit-1, Ref: J Biol Chem 266: 9805-9813 (1991);

fAE2B/ CDRE, a *cis*-element binding Cad, Ref: Genes Dev 5: 855-867 (1991); FoxA2-cdx-2), a

cis-element binding FoxA2, Ref: Mol Cell Biol 17: 1626-41 (1997); E1(IEF1-IEB), a multiple E-box

binding IEF1, Ref: DNA Cell Biol. 11:549-58 (1992); Nir_box_(2), a *cis*-element binding NF-InsE1,

Ref: Mol Cell Biol 8: 2620-7 (1988); myc-CF1-c-myc_(1), a *cis*-element binding myc-CF1, Ref: Mol

Cell Biol 11: 1765-1769 (1991); HNF3beta3, a *cis*-element binding HNF3beta, Ref: Eur J

Pharmacol. 464:87-94(2003); rPRL-FPI, a *cis*-element binding PREB/Pit-1,Ref: Science 234: 1552-7

(1986); GR-MRib, a *cis*-element binding, Ref: DNA 5: 383-91 (1986); E4BP4(NFIL3) , , a

cis-element binding E4BP4, Ref: Nucleic Acids Res, 22:59-65 (1994); Myf, a *cis*-element binding

myogenic factor, Ref: EMBO J. 8:4358 (1989). ETS, a *cis*-element binding winged helix-turn-helix

domain, Ref: Biochem. Biophys. Res. Commun. 264: 119-126(1999); LysHREVI a *cis*-element, Ref:

EMBO J 7: 2063-73 (1988); SRF, C-fos serum response element, Ref: J. Biol. Chem. 280:

11816-11828(2005); Mef-2, a Myocyte-specific enhancer,Ref: J. Biol. Chem. 275: 22563-22567

(2000); HAP-2/3/5-CYT1, a *cis*-element binding HAP-2/3/5, Ref: Mol Cell Biol 11: 4934-42 (1991);

LSF, a *cis*-element binding HeLa transcription factor, **Ref:** Hum. Molec. Genet. 9: 2275-2280 (2000);

beta-RARE1, a *cis*-element binding RAR-gamma,Ref: Cell 68: 377-395 (1992);TEF, a *cis*-element

binding thyrotroph embryonic factor, Ref: Genes Dev. 5: 1739-1753 (1991); GAGA-kruppel.3, a

cis-element binding GAGA, Ref: J Biol Chem 266: 574-82 (1991); Prl-4D, a *cis*-element binding

Pit-1, Ref: J Biol Chem 269: 29335-8 (1994); opaque-2-albumin b-32_(5) , a *cis*-element binding

opaque-2, Ref: EMBO J 10: 617-624 (1991); ICS_(3), a *cis*-element Ref: J Biol Chem 267:

25589-96 (1992); mu-E4 , a *cis*-element binding NF-uE4, Ref: In Transcriptional Control

Mechanisms: 83-101; LN4, a *cis*-element, Ref: EMBO J 5: 1791-7 (1986); H1TF1 RS, a *cis*-element

binding H1TF1, Ref: Mol Cell Biol 9: 1566-75 (1989);CRE, a cAMP response element, Ref:Molec.

Endocr. 6: 647-655 (1992); AP-1, a activator protein-1 transcription factor complex regulatory

element, Ref: Science 297: 1700-1703 (2002); Search parametrs: Expected Mean Number: 0.01;

Statistical Siginicance Levels: 0.9500000; Levels of homology between known RE and motif: 80%;

Variation of Distance between RE Blocks: 20%.
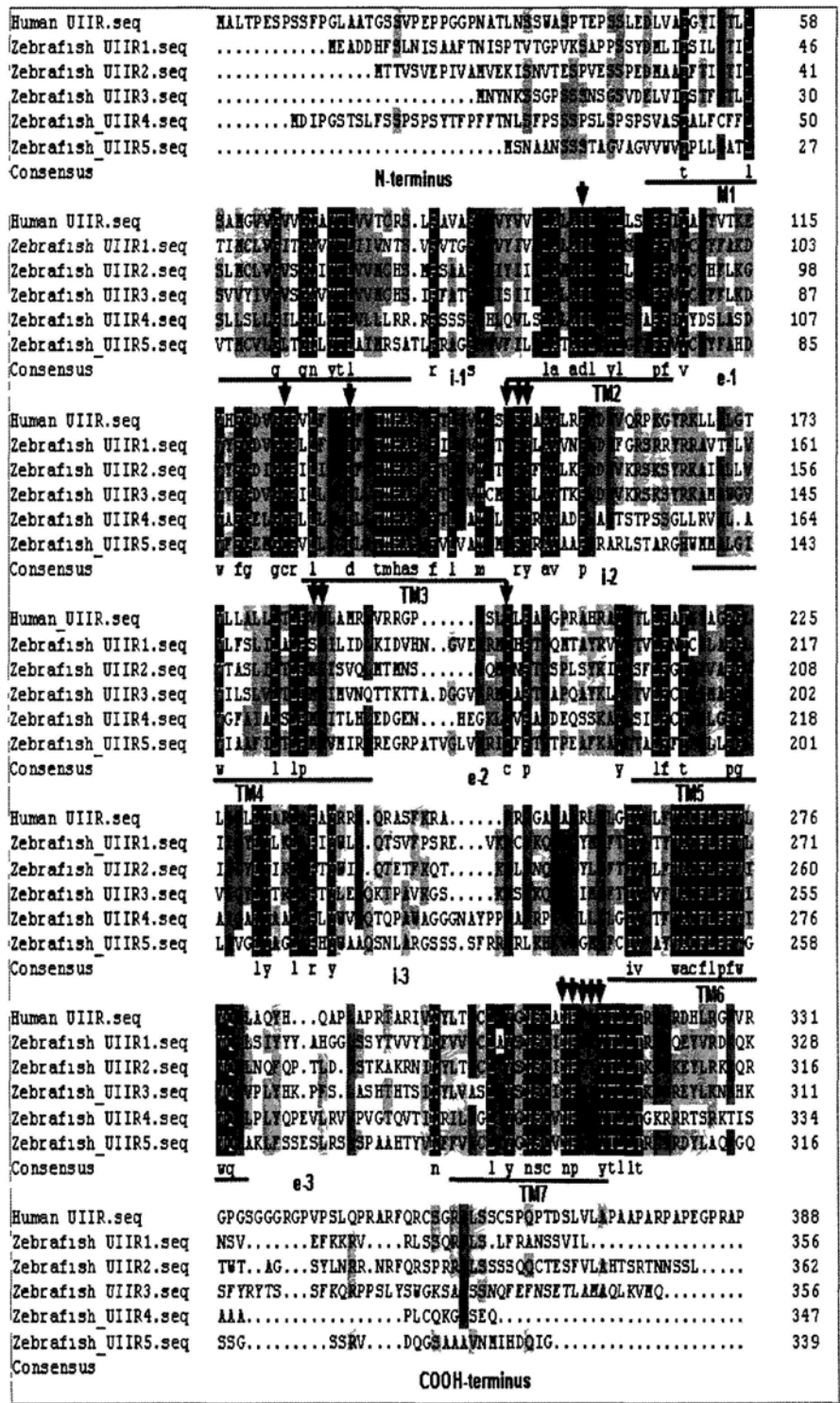
Fig. 2-4. Alignment of UIIR amino acid sequences from different species.

Fig. 2-4. Alignment of UIIR amino acid sequences from different species.

The UIIR consists of a 7TMD, an extracellular N-terminal region, three extracellular loops (e1–e3), three intracellular loops (i1–i3) and a long cytoplasmic C terminus. The human UIIR is 74.68%, 42.21%, 37.66%, 36.54% and 45.59% identical to zebrafish UIIR1, UIIR2, UIIR3, UIIR4 and UIIR5 homologues, respectively. It contains two cysteine residues (C_{123} and C_{199}), which are thought to form a conserved disulfide bridge that stabilizes the receptor structure, a conserved aspartic acid residue (D_{97}) in TM2 and other key signature residues of the rhodopsin family of GPRs, including the [E/D]RY motif at the beginning of i2 and a NPx2–3Y motif at the end of TM7(indicated with red arrowhead). F_6 and K_8 of UII contact M_{184}/M_{185} (TM4) and D_{130} (TM3), respectively, of the UIIR (indicated with blue arrowhead).

The putative phosphorylation sites (red) of COOH-terminal region of human UIIR

 PKA/C   CKI   PKA CKI
YTLLTRNYRDHLRGRVRGPGSGGGRGPVPSLQPRARFQRCSGRSLSSCSPQPTDSLVLAPAAPARPAPEGPRAPA

The putative phosphorylation sites (red) of COOH-terminal region of zebrafish UIIR

       PKC   PKA CKI   GSK3
YTLLTKNYKEYLRKRQRTWTAGSYLNRRNRFQRSPRRSLSSSSQQCTESFVLAHTSRTNNSSL
----
caveolin-binding motif

Fig. 2-5. An expanded view of the C-terminal region of human and zebrafish UIIR.

The C-terminal region of UIIRs reveals putative phosphorylation sites (red) and their potential kinases. (Upper panel: human; lower panel: zebrafish). The number of putative phosphorylation sites differs in zebrafish and human UIIR, which indicates potential differences in the phosphorylation, internalization and desensitization of the receptor (CK1, casein kinase 1; GSK3, glycogen synthase kinase 3; PKA/C, protein kinase A/C). The zebrafish UIIR contains a putative caveolin-binding motif (FxFxxxxFxxF, where F is a hydrophobic residue and x is any amino acid) that is similar to that reported in the angiotensin AT1 receptor (Wyse et al., 2003).

teleost and tetrapod (3, 4)

mammal

Human UIIR
Chimpanzee UIIR
Monkey UIIR
Rat UIIR
Mouse UIIR
Horse UIIR
Cattle UIIR
Dog UIIR
Cat UIIR

90
99
99
100
99
41
78
64
65

Fugu UIIR3
Zebrafish UIIR3 chr16
100

Tetraodon UIIR
Fugu UIIR4
Zebrafish UIIR4 chr6
98
100

Xenopus UIIR3
Stickleback UIIR2
Stickleback UIIR1
100

Flounder UIIR
Fugu UIIR2
Medaka UIIR2
Medaka UIIR3

42
37
52
28
33
100
95

teleost and tetrapod (1)

Guttata UIIR
Xenopus UIIR1
Fugu UIIR1
Zebrafish UIIR1 chr12
Medaka UIIR1
94
33
99
98

teleost and tetrapod (5)

Xenopus UIIR2
Grouper UIIR
Zebrafish UIIR5 chr12
99

cartilaginous fishes; Gnathostomata (2)

Elephant shark UIIR
Zebrafish UIIR2 chr3
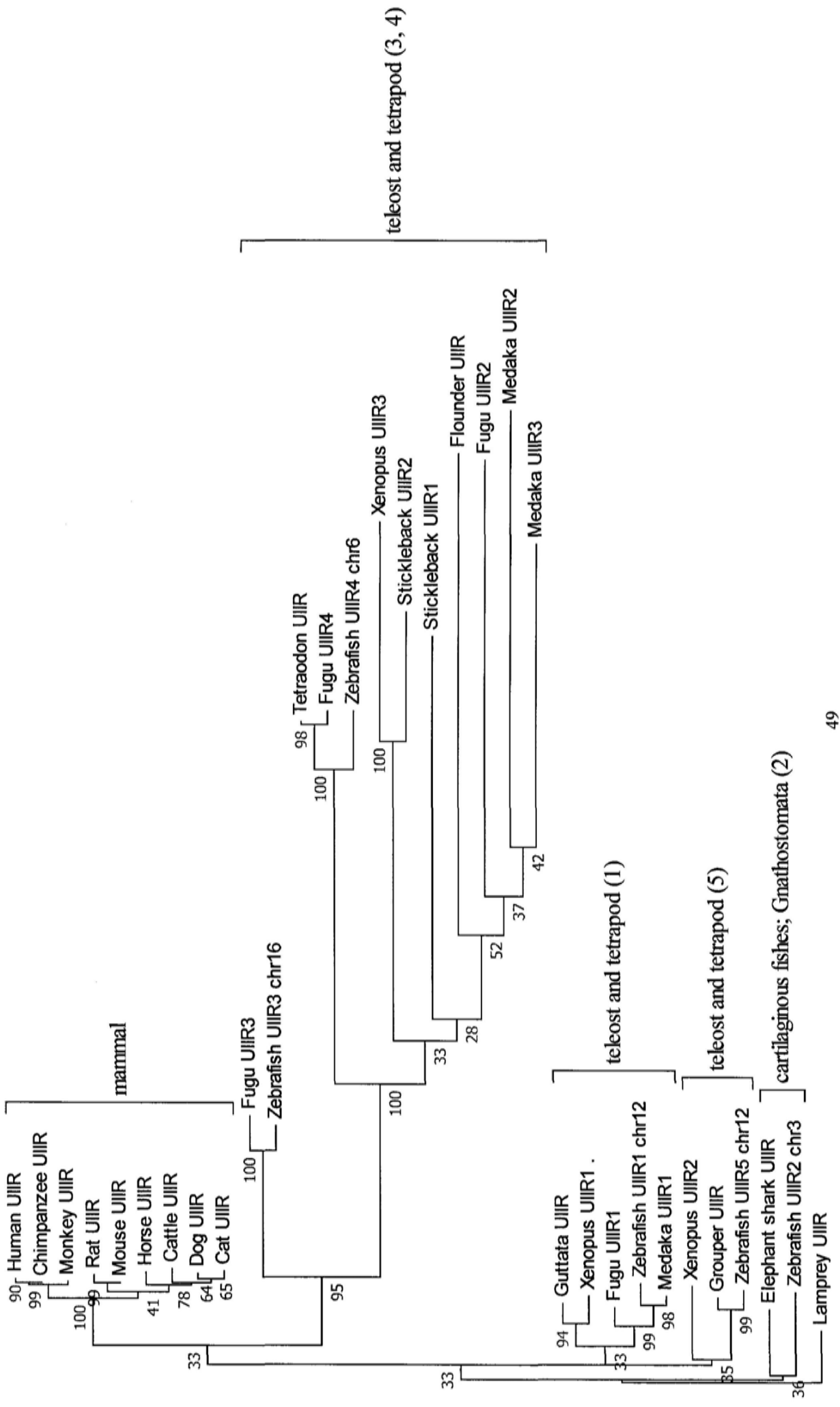35

Lamprey UIIR
36
33
33

49

0.1

Fig. 2-6. Phylogenetic relationship of UIIRs.

Evolutionary comparison of different members of UII receptor protein family represented in a phylogenetic rooted tree generated using MEGA 4.1 program with a Neighbor-Joining (NJ) method and 1,000 bootstrap replicates. Branch lengths are measured in terms of amino acid substitutions, with the scale indicated below the tree. Numbers at nodes indicate percent of bootstrap probabilities. The accession numbers of these genes or proteins are show as followed: Lamprey UIIR, GENSCAN00000111145; Elephone Shark UIIR, AAVX01039854.1; Cattle, UIIR, NP_001035574.1; Rat UIIR, NP_065412.1; Mouse UIIR, NP_663415.1;Human UIIR, NP_061822.1; Monkey UIIR, NP_0- 010028066.1; Flounder UIIR, CAI30311.1; Grouper UIIR, ACN65411.1; Dog UIIR, XP_548799.2; *Taeniopygia guttata* UIIR, XP_002188305.1; Zebrafish UIIR3; Zebrafish UIIR4; Zebrafish UIIR2; Zebrafish UIIR1; Horse UIIR , XP_001490494.1; Chimpanzee UIIR, XP_001167994.1; Cat UIIR, AAX39012.1; Fugu UIIR4, ENSTRUG00000011760; Fugu UIIR2, ENSTRUG00000008902; Fugu UIIR1, ENSTRUG00000002567; Fugu UIIR3, ENSTRUG00000000119; Tetraodon UIIR, ENSTNIG00000018- 816; Medaka UIIR3, ENSORLG00000018957; Medaka UIIR 2, ENS-stickleback UIIR 2, ENSGACG00000000119; Tetraodon UIIR, ENSTNIG00000018- 816; Medaka UIIR3, ENSORLG00000018957; Medaka UIIR 2, ENS-ORLG00000010691; Medaka UIIR1, ENSORLG00000020371; *Xenopus* UIIR2, ENSXETG00000019036; *Xenopus* UIIR3, ENSXETG00000015991; *Xenopus* UIIR1, ENSXETG00000012229.

Note: although having cloned the 5 zebrafish *UIIRs*, we have not registered at GeneBank for these genes; so, currently, these genes or correspondingly proteins have no the accession number. Clade 1 contains the zebrafish UIIR1; Clade 2 contains the zebrafish UIIR2; Clade 3, 4 contains the zebrafish UIIR3 and UIIR4; Clade 5 contains the zebrafish UIIR5
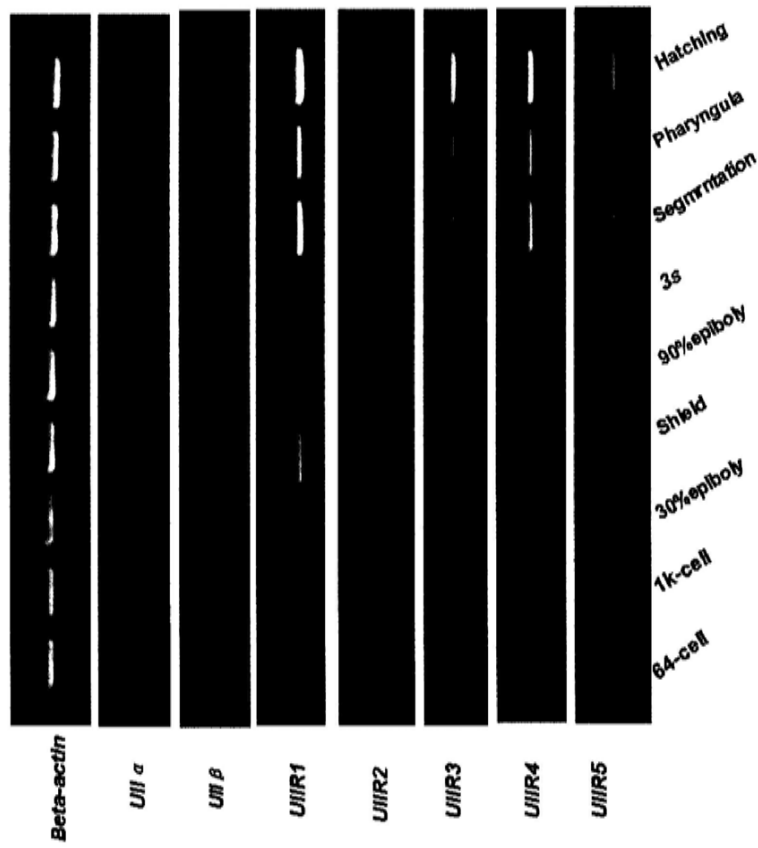
Fig. 2-7. Expression profile of zebrafish UII and UIIR during embryogenesis.

Zygote period (0-3/4 h); Cleavage period (0.7- 2.2 h); Blastula period (2 1/4 - 5 1/4 h); Gastrula period (5 1/4 - 10 h); Segmentation period (10-24 h); Pharyngula Period (24-48 h); Hatching period (48-72h).

51

Interaction of zebrafish UIIa with 5 zebrafish UIIR's

Fig. 2-8a UIIα-receptor interaction studies through receptor transactivation assay.

Transactivation of CRE promoter was conducted in transfected HEK293 cells. The cells were co-transfected with a pcDNA3.1 vector containing the entire coding region of either zebrafish UIIRs together with a luciferase reporter plasmid driven by the promoter containing CRE. The control was the empty pcDNA3.1 vector. The transfected cells were subsequently stimulated by synthesis zebrafish UIIα at different concentrations. Correction for transfection efficiency was performed by measurement of the *Renilla* luciferase activities. Results are mean values±S.E.M. (n=3; *P<0.05; **P<0.01; ***P<0.001 as compared with the respective controls by one-way ANOVA).Note: UIIα: UII alpha or UIIa. The statistical analysis is performed using the software GraphPad PRISM Version 5.0. (GraphPad, San Diego, CA)(www.graphpad.com).

52
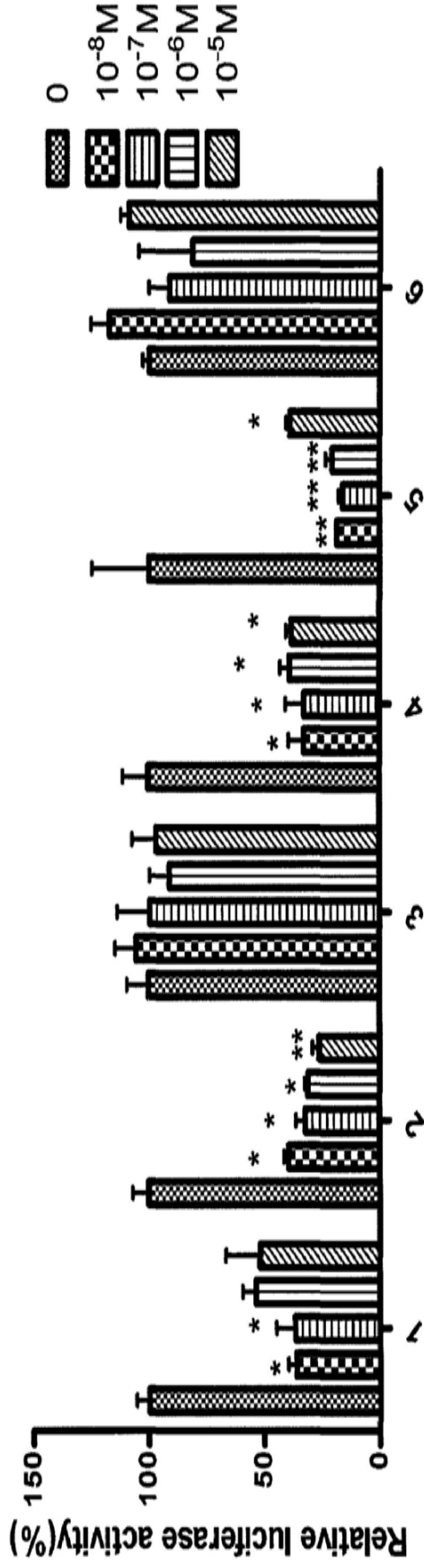
Interaction of zebrafish UIIb with 5 zebrafish UIIR's

Fig. 2-8b UIIβ-receptor interaction studies through receptor transactivation assay.

Transactivation of CRE promoter was conducted in transfected HEK293 cells. The cells were co-transfected with a pcDNA3.1 vector containing the entire coding region of either zebrafish UIIRs together with a luciferase reporter plasmid driven by the promoter containing CRE. The control was the empty pcDNA3.1 vector. The transfected cells were subsequently stimulated by synthesis zebrafish UIIβ at different concentrations. Correction for transfection efficiency was performed by measurement of the *Renilla* luciferase activities. Results are mean values±S.E.M. (n =3; *P<0.05; **P<0.01; ***P<0.001 as compared with the respective controls by one-way ANOVA). Note: UIIβ: UII beta or UIIb. The statistical analysis is performed using the software GraphPad PRISM Version 5.0. (GraphPad, San Diego, CA)(www.graphpad.com).

53

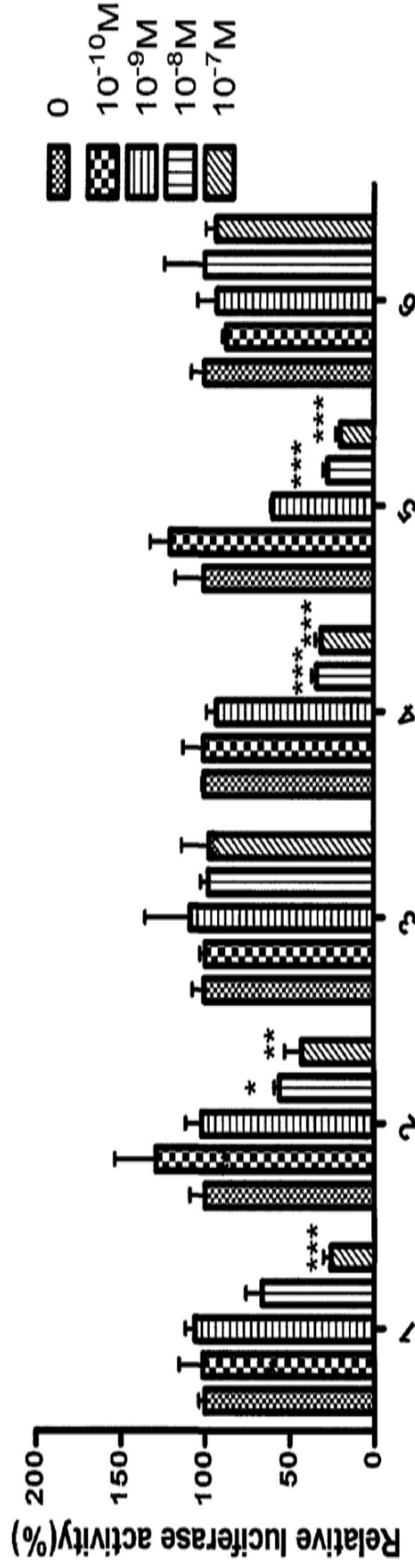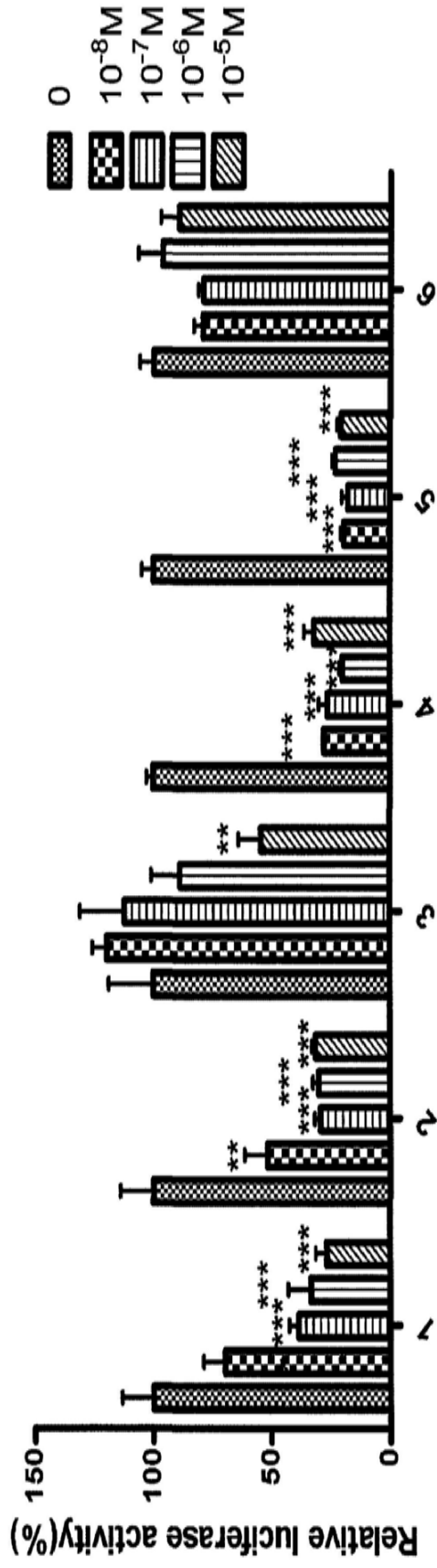**Fig. 2-8c Human UII-receptor interaction studies through receptor transactivation assay.**

Transactivation of CRE promoter was conducted in transfected HEK293 cells. The cells were co-transfected with a pcDNA3.1 vector containing the entire coding region of either zebrafish UIIRs together with a luciferase reporter plasmid driven by the promoter containing CRE. The control was the empty pcDNA3.1 vector. The transfected cells were subsequently stimulated by synthesis human UII at different concentrations. Correction for transfection efficiency was performed by measurement of the *Renilla* luciferase activities. Results are mean values±S.E.M. (n = 3; *P<0.05; **P<0.01; ***P<0.001 as compared with the respective controls by one-way ANOVA). The statistical analysis is performed using the software GraphPad PRISM Version 5.0. (GraphPad, San Diego, CA)(www.graphpad.com).

54

Chapter 3 Urotensin IIβ is required for the L-R patterning of zebrafish embryos

3.1 Introduction

While vertebrate external appearance exhibits bilaterally symmetry, the distribution of circulatory system, the structure of the brain, and the structure and placement of internal organs are neither identical nor symmetrical with respect to its left-right body axis. For example, in humans the most of the heart, the stomach, the pancreas and the spleen is positioned on the left side of body, whereas the most of the liver and the gall bladder is located on the right side of body. Moreover, the left lung has fewer lobes than the right lung, and the gut exhibits a coiling anticlockwise. L-R asymmetry is a common feature of all vertebrates (Levin et al., 2005; Raya et al., 2006). The failure of the L-R patterning during embryogenesis leads to severe medical conditions (Hackett et al., 2002; Bisgrove et al., 2003; Peeters et al., 2006).

In the last decade, a great deal of work has been done in this field. However there are still many un-answered questions on the molecular basis of L-R asymmetry (Aw et al., 2008). Observations from chick, *Xenopus laevis*, mouse and zebrafish embryos suggest that the development of L-R asymmetry can be conceptually divided into three main phases: (1)an initial-breaking of symmetry; (2) establishment of asymmetric gene expression; and (3) transfer of positional information to the developing organs (Levin et al., 1998a). This conceptual process has been showed in Figure 3-1. Brend et al (2009) suggested two very broad themes involved in the

55

molecular process of L-R patterning during early embryogenesis. The first is the critical role for cilia-dependent asymmetric fluid flow in all vertebrates and the second is the variation on the initial-breaking of symmetry, the timing and mechanism of early L-R specification, depending on species.

3.1.1 Two models on the initial-breaking of bilateral symmetry of the embryo

In the process of laterality determination of the embryo, a key question need to be solved is what kind of signals and mechanisms operate the initial-breaking of symmetric status of the embryo for orienting the L-R axis in the same direction across all individuals from same specie? Currently, there are two equally plausible models trying to deal with the problem:

1) Ion flux model.

Based on several observations from the early stages of sea urchin, ciona, chick, frog, and zebrafish embryonic development, Levin et al (2006) suggested that the higher membrane potential caused by L-R asymmetric distribution of maternal ion transporter (H^+/K^+-ATPase or H^+-V-ATPase) in midline right side of early embryo than that in left initiates the initial-breaking of symmetric status of early embryo. The detail of ion flux model has been showed in Fig.3-2.

2) Nodal flow model

Work in mouse and zebrafish model organisms has implied that the leftward fluid flow (termed as the nodal flow) generated by rotational movement of node cilia that protrude from cells located on the ventral side of the node breaks the L-R symmetry

by transport of the L-R determinant signal, for example, Ca^{2+} signal, Nodal signal and the so-called nodal vesicular parcels, which contain the sonic hedgehog homolog (Shh), retinoic acid and Ca^{2+} etc, towards the left side of embryo to induce the asymmetrical expression of *nodal* specifically in the left side of the early somite stage embryo (Sulik et al., 1994; Nonaka et al., 1998, 2002; Tabin et al., 2003; Tanaka et al., 2005; Hirokawa et al., 2006). A strong bolstering evidence for the model is that exogenously supplied directional flow is sufficient to reverse the L-R orientation of wild type embryos and to restore L-R asymmetry to randomized mutant embryos (Nonaka et al., 2002). The detail of nodal flow model has been showed in Fig. 3-3. (a, b, and c).

3.1.2 The asymmetrical genes

Tabin and colleagues in 1995 identified a regulatory cascade (the Nodal cascade) involving three TGF-b family member genes, *nodal, lefty1* and *lefty2*, and the homeobox transcription factor gene *pitx2*. This cascade is apparently conserved across all vertebrates analyzed so far. A single *nodal* gene has been identified in mammals and in chicken, whereas multiple *nodal*-related genes are present in frog and zebrafish (Table. 3-1).

At the early somite stage *nodal* and *lefty* from different species show common asymmetrical expression pattern on the left LPM (Table3-1). Several lines of evidence suggested that Nodal is a determinant of 'leftness' and it activates its own expression (Shiratori *et al.* 2001; Oh & Li 1997; Yan *et al.* 1999), while *lefty2* inhibits *nodal* overexpression on the left side of embryo. Thus *nodal* and *lefty2* form a feedback on the left LPM. The *lefty1* acts as the midline barrier to inhibit bleeding

57

of nodal signal to the right side of embryo. As for the *pitx2*, Yoshioka et al. (1998) uncovered that the mouse homolog of human *pitx2* is a bicoid-type homeobox gene, which expresses asymmetrically in the left LPM and is involved in determination of L-R asymmetry in both mouse and chick.

Mouse *pitx2* has a left side-specific enhancer (ASE) that contains 3 binding sites for the transcription factor Fast. The Fast-binding sites function as Nodal-responsive elements and by which the asymmetrical expression of *pitx2* is initiated indirectly. Subsequently the asymmetrical expression of *pitx2* is maintained by the binding of Nkx2 to the Nkx2.5-binding site within the ASE (Shiratori et al., 2001). This control strategy may represent a general mechanism for gene regulation during development.

3.1.3. Calcium ion and left–right patterning

Asymmetrical distribution of free Ca^{2+} (intracellular Ca^{2+}) across the region surrounding embryo node had been described in the mouse (McGrath et al 2003), chick and zebrafish embryo respectively (Raya et al., 2004; Sarmah et al., 2005). In all three species, the left-biased distribution of Ca^{2+} at the region surrounding node/KV (Fig.3-4) is transient, but also precedes the normal left-sided expression of *nodal* in the lateral plate mesoderm (LPM). Strikingly, during the gastrulation of chick embryo, using the low-affinity, cell-impermeant Ca^{2+} indicators and the two-photon excitation microscopy Raya et al., (2004) unveiled that the distribution of extracellular Ca^{2+} also appears a left bias pattern around the Hensen's node from HH4 to HH6 (HH, Hamburger Hamilton Stage, a standard system to describe the developmental stages of chick embryo). However, at HH8 the distribution of extracellular Ca^{2+} became symmetric. In zebrafish embryo, similar phenomenon had

also been observed. The transient of Ca^{2+} from symmetric distribution to asymmetrical distribution surrounding the KV happens at 4-5 somite stage, thereafter is maintained until 12 somite stage (based on our observation, Sarmah et al., 2005; and Francescatto et al., 2010). The asymmetrical calcium ion signal surrounding node is require for the proper L-R patterning of embryos (Sarmah et al., 2005; Leung et al., 2008). Alike, the similarity indicates it is a conserved biological phenomenon.

It needs to be noted that in experiments using mouse and zebrafish embryos the detected transient ion is free cytoplasmic Ca^{2+}, however, in the chick embryos, it is extracellular Ca^{2+} levels is evaluated. To date it is still unclear whether or no the two status of Ca^{2+} are directly related, although the alteration of asymmetrical distribution of this two type free Ca^{2+} across the region surrounding embryo node results in consistent defects of L-R patterning in three embryo species.

3.1.4. The laterality organ

During the establishment of left-right axis of the vertebrate a key step is that the early asymmetry clues are transferred to the left LPM of embryos by the leftward nodal flows, which are generated by the laterality organ : ventral node in mouse embryos (N. Hirokawa et al 2006), Kupffer's vesicle in zebrafish embryos (Essner, et al 2005), Hensen's node in chick embryos and gastrocoel roof plate in frog embryos (Qiu et al 2005). Current understanding of the node origin is obtained mainly from the observation to the KV development of zebrafish. The KV is a fluid-filled organ at the posterior end of the notochord at the early somite stages of teleosts (Essner et al., 2005). Several reports suggested KV, the laterality organ of zebrafish, derives from a

surface epithelium in dorsal organizer domain (the Spemann organizer domain). Thereafter these surface epithelial cells undergo Nodal signaling-dependent ingression and immigrate at the ahead of dorsal organizer margin to form dorsal forerunner cells (DFCs) at 60% epiboly stage. So, DFCs represent a spatially distinct cellular domain that is part of the zebrafish organizer region. During early somitogenesis, DFCs coalesce into a single rosette that differentiates into the KV with a ciliated lumen at its apical centre (Essner et al., 2005; Oiu et al., 2005 and Oteíza et al., 2008). The origin of KV has been showed in Fig. 3-5.

During the development of KV, DFCs are specified during the blastula period. While the T-box transcription factor no tail (*ntl*) and the Nodal signaling (*oep*) are necessary for the expression of *L-Rdr1* in DFCs and for DFCs organizing to form KV during early somitogenesis. But *spt* is only required for KV organogenesis but not for *L-Rdr1* expression in DFCs (Essner et al., 2005; Oteíza et al., 2008).

3.1.5. The Spemann organizer region

Spemann and Mangold firstly revealed that the organization of the vertebrate embryo depends on the activity of a dorsal regional named as the Spemann organizer (Spemann et al 1924). They defined the organizer activity as the ability to induce a secondary axis. The Spemann organizer regional have also been identified in other vertebrates. In teleosts, it is located at the dorsal gastrula margin and corresponds to the embryonic shield but much broader than the shield region (Fauny et al 2009).

Recently, using the zebrafish model, Fauny et al., (2009) and Agathon et al., (2003) found that during zebrafish embryogenesis there are two organizing centers, the dorsal and tail organizers, located at the dorsal and ventral gastrula margins,

respectively (Fig. 3-6, picture a) The dorsal organier margin contributes to axial structures and the ventral organizer margin contributes to non-axial tissues. The formation of different parts (tissues or organs) of the embryo along the anteroposterior (A/P) axis is controlled by the ratio of marginal BMP to Nodal activity. The dorsal Spemann organizer is a source of growth factor antagonists that participate in the creation of signaling gradients. The expressing molecules of dorsal and ventral centers are under opposite transcriptional control. For example, BMP2 and ADMP are expressed dorsally, while BMP4 and BMP7 are produced ventrally. The BMP antagonist Chording is secreted by dorsal Spemann's organizer, while another BMP antagonist Crossveinless-2 is produced in the ventral center. Similarly, in the dorsal side there is Crescent, while in the ventral center there is Sizzled (Pear et al., 2000; Ambrosia et al., 2008).

3.1.6 Signaling pathway involved in the L-R patterning of embryos

Accumulating evidence uncovered that the L-R patterning of vertebrate embryos requires the function of Nodal signaling and Bmp signaling (Bisgrove et al., 1999; Campione et al. 1999; Essner et al. 2000; Faucourt et al., 2001; Rebagliati et al., 1998a; Sampath et al., 1998). Bmp signaling acts as a 'right determinant' and Nodal signaling functions as a left determinant (Capdevila et al., 2000; Klingensmith 2000; Brennan et al., 2002). Between the two pathways there is a crosstalk, because involvement of Lefties in Bmp signaling has been proposed (Meno et al., 1997; Branford et al., 2000; Ulloa et al., 2001); although the significance of the crosstalk between Bmp and Lefty for L-R patterning remains unclear.

In the process of L-R patterning of vertebrate embryos, perhaps much more

attention should be paid on the asymmetrical Ca^{2+} signal, because studies in several vertebrate model organisms exclusively implicated a requirement for Ca^{2+} signals in L-R asymmetry, which mediates the transfer and propagation of initial asymmetrical determination from upstream to LPM (Brennan et al., 2002; McGrath et al., 2003; Shimeld et al ., 2004; Raya et al., 2004; Hashimoto et al., 2004; Marques et al., 2004; Sarmah et al., 2005; Tanaka et al., 2005; Hirokawa et al.,2006; Schottenfeld et al., 2007; Schneider et al., 2008). In fact, in wild-type zebrafish embryos, a transient flux of intracellular Ca^{2+} in cells around KV is consistently greater on the left side than in those on the right side. Reports from two different labs consistently proposed that the disruption of the asymmetrical distribution of intracellular Ca^{2+} by the elevation of intracellular Ca^{2+} level caused the concordant randomization of both molecular and anatomical asymmetries in zebrafish embryos (Sarmah et al., 2005; Leung et al., 2005).

Based on the above discussion and the calcium mobilization effect of UII/UIIR signaling system, we propose a hypothesis here: UII/UIIR signaling system mediates the laterality determination of the development embryos. In order to obtain some clues for the study on the zebrafish UII/UIIR system, we have analyzed the promoters of zebrafish UIIα and UIIβ. The results revealed that only the promoter of zebrafish UIIβ, no that of UIIα, embodies more different kinds of *cis*-elements than that of UIIα but also possesses a *cis* Smad4 binding element (GACAGACAGACAGACTGACAAA) between-2361 and -2339 and a 25 times repeated *cis* Smad3-Smad4 binding elements region (CAGACAGACAGACA) between -1636 and -521 (Table. 3-2). In fact, previous studies have been shown that Bmp and Nodal commonly belong to the TGF-β (transforming growth factor-beta)

superfamily. Smad4 is a common transduction factor for both Bmp and Nodal/activin/TGF-β pathways. It acts as comediator to merge the two signaling pathway altogether and mediates the crosstalk between them at the downstream of their signaling transduction by modulating the translocation of transcriptional complexes into nuclei and activation of target genes. Instead, Smad3 only acts at the downstream of Nodal Nodal/activin/TGF-β pathway and is specific for Nodal signaling (Wu et al., 2002; Davis et al., 2008; Kim et al., 2006; Inman et al., 2002; Chen et al., 2002; Zhou et al., 1998; Shioda et al., 1998; Kishigami et al., 2005). Smad5 is specific for Bmp signaling as suggested by *in vitro* biochemical analysis and *Xenopus laevis* explant assays (Massague et al., 1998). Chang et al (2000) demonstrated that *smad5* mutant embryos have defects in heart looping and embryonic turning which are the first signs of L-R asymmetry in mice. Moreover, our further analysis also indicates that one to two cAMP responsive elements are contained in the promoters of zebrafish *UIIα, bmp4, smad5, cyclops* and *spaw* respectively.

In the light of the effect on intracellular cAMP level from UII/UIIR system and based on the above analysis, we further refine the hypothesis: in zebrafish UIIβ mediates the earlier molecular events for initiating the L-R patterning of embryos by regulating Nodal signaling, Bmp signaling and Ca^{2+} signal.

Here we provide evidence that UIIβ is required for the establishment of L-R body plan of zebrafish embryos. This documents a role of UII/UIIR signaling pathway in asymmetry development of embryos which promises to reveal the molecular mechanisms responsible for human congenital heart diseases, especially those with heterotaxy.

3.2 Materials and methods

3.2.1 Animals

Zebrafish, *Danio rerio*, wildtype strain: AB and Tubingen; mutant line: tp53M214K, a p53(-/-) null zebrafish line. This Zebrafish lines harbors missense mutations in the tp53 DNA binding domain. Cells in the tp53M214K embryos failed to undergo apoptosis in response to radiation at both 28 and 37°C. Unlike wild-type control embryos, irradiated tp53M214K embryos also failed to up-regulate p21 and did not arrest at the G1_S checkpoint. Zebrafish were maintained at 28.5 °C in a recirculation aquaculture system of the fish facility.

The detail for all solutions and buffer used in the experiments mainly come from this book: Westerfield, M. (2007) THE ZEBRAFISH BOOK, 5th Edition, University of Oregon Press, and this website: www. zfin.org.

3.2.2 RNA overexpression

A zebrafish UIIβ overexpression construct was generated by RT-PCR using primers (see Table 2-1) and then subcloned into pCS2+ vector at XhoI/XbaI sites, respectively. Capped sense RNA was synthesized using the Mmessage or mMACHINE kit (Ambion).

3.2.3 Microinjection of morpholino oligonucleotides (MO) and mRNA

Two splicing MOs against two different splice sites of *UIIβ* were designed and synthesized by Gene Tools, LLC, who finished the design and synthesis of these MOs according to Targeting Guidelines (http://www.gene-tools.com/node/18). The basic mechanism on how to block the splice of pre-mRNA and disrupt the translation

of UII has been show in Fig. 3-2. The MO sequences used were:

MO1: 5'- GGCCTGAATGAGAAGTGGATGTTAA -3'

MO2: 5'- TGTCGCATTTAATCACTCACCTCTT-3'

Control MO: 5'-CCTCTTACCTCAGTTACAATTTATA-3'

The control MO is a standard control ordered from Gene Tools, LLC This oligo should have no target and no significant biological activity in zebrafish model and has been used extensively by researchers who use zebrafish as model to perform research. The oligos were dissolved in water as a 25 mg/ml stock solution and the RNA is dissolved in RNase free water, and then injected at different dosages (1-10 ng for MO, 10-200 pg for RNA) into 1- or 2-cell-stage embryos. Injected embryos were subsequently incubated in 0.3× Danieau's medium at 28.5 °C. Embryos were maintained in the above condition until they reached different developmental stages.

3.2.4 RNA whole-mount *in situ* hybridization

Details of the whole-mount *in situ* hybridization protocol and probes used in this study are given in the appendices and the table 2-1. All hybridization signals were detected via anti-digoxigenin-AP (Roche) and purple AP substrate (Promega).

3.2.5 RT-PCR

Total RNAs were prepared from different zebrafish adult organs or embryos at different developmental stages using Trizol reagent (Invitrogen), treated with RNase-free DNase I (Invitrogen) to avoid possible contamination from genomic DNA and then reverse transcribed using the ImProm-II Reverse Transcription System (Promega) and Random primers or Oligo dT primers. The cDNAs were then

subjected to PCR amplification using specific primers (see Table 2-1) using Expand High Fidelity Taq polymerase (Roche) or GOTaq (Promega) following the manufacturer's instructions. When possible, all primer pairs have been designed on different exons to avoid the amplification of genomic DNA contaminations present in the cDNA preparations. Control PCR experiments with samples prepared without reverse transcriptase was performed to ensure that genomic DNA contamination did not contribute to the PCR amplification.

3.2.6 Detection of intracellular Ca^{2+} in zebrafish embryos

Ca^{2+} green-dextran 10,000 MW (Molecular probe/Invitrogen) was used at 0.05% (w/v) for microinjection into zebrafish embryos at 1 cell stage with an injection volume of about 0.5 nl. Embryos were incubated in 0.3× Danieau's medium at 28.5 °C. Fluorescent image at 500 ms exposure of the KV at 3 to 6-somite stage was documented using the Axioimager Z1 fluorescence microscope (Zeiss) and the intensity of images is measured using ImagePro+ software (Media Cybernetics).

3.2.7 Image acquisition and analysis

For general examination, GFP-positive embryos or larvae were viewed under an Axioimager Z1 fluorescence microscope (Zeiss), equipped with 5×, 10× and 20× objectives. Images of *in situ* hybridization results were taken under a Zeiss Stemi 2000-C microscope or an Axioimager A1 microscope (Zeiss).

3.2.8 Data analysis

All data which is from 3 times independent trials were expressed as mean

values±S.E.M. Data were considered statistically significant at P<0.05 using either one-way analysis of variance (ANOVA) or unpaired t-test. The statistical analysis is performed using the software GraphPad PRISM Version 5.0. (GraphPad, San Diego, CA)(www.graphpad.com).

3.3 Results

3.3.1 Expression of UIIβ during zebrafish embryogenesis

To detect the transcripts of zebrafish UIIβ during early embryonic development, we first analyzed UIIβ mRNA levels in 0 to 3 days post fertilization (dpf) embryos using RT-PCR. Initially, UIIβ mRNA showed a maternal deposition until 4hpf. At 5hpf, these maternal transcripts became undetectable. Secondly the zygotic transcriptional activity of UIIβ firstly appears at approximately 60% epiboly stage (7hpf), thereafter, throughout the other stages of embryogenesis (Fig. 2-7 and Fig. 3-8). To further investigate the tissue-specific expression pattern of UIIβ, RNA whole-mount *in situ* hybridization was performed. Consistent with the RT-PCR result, UIIβ mRNA was present in cleavage-stage embryos, indicating maternal deposition, and was ubiquitously distributed throughout the blastula stages of embryogenesis (Fig. 3-8). At approximately 10s, UIIβ expression prevails at the anterior LPM, but a faint signal might be observed at the posterior LPM. At 24 hpf, UIIβ expression domains converged into the brain, LPM and tail regions (Fig. 3-8). At 48 hpf, weak expression is detected in brain region. However in the tail region there is no distinct signal. Instead, in the veins wall of the heart region, UIIβ expression is significantly high.

3.3.2 Phenotypes of UIIβ morphants

To investigate how zebrafish UIIβ may function in embryonic development, we performed UIIβ loss-of-function experiments by injecting cleavage-stage embryos of tp53M214K line with an antisense MO designed to block the pre-mRNA splicing. To confirm the sequence specificity of any observed defects, two MOs targeted against different regions of the zebrafish UIIβ prepro-mRNA were used (Fig. 3-7). The morphants from the two MO-injected embryos are consistent, the heart looping of two type MO-injected embryos showed consistent defect and no distinct differences can be observed between the two types of morphants, therefore, for the sake of convenience, we only use MO1. The blocking effect is monitored by RT-PCR (Fig.3-9). Phenotypes of UIIβ morphants are showed in Fig. 3-10.

3.3.2.1 UIIβ knockdown perturbs the laterality of heart

Stainier et al., (1992) firstly reported the normal cardiac morphogenesis during zebrafish embryogenesis. At the 14-somite stage the ventral-derived cardiac precursors migrate toward the animal axis and form bilateral heart primordia on either side of the embryo, flanking the prechordal plate and notochord. At about 19 hpf (the 20-somite stage) the bilateral heart tubes fuse to form a short cone-shape structure at the midline, which subsequently elongates in the anteroposterior direction. At 24 hpf, the prospective atrial end of the heart abruptly moves to the left with respect to the midline (Fig.3-11a, red arrow). This process is termed as cardiac jogging. By 36 hpf the ventricle firstly bends rightward (the D-loop) and the atrium bends leftward, which is termed as the heart looping. As showed in Fig.3-11a (Heart is labeled using *NKX2.5*), the cardiac jogging is randomized in

UIIβ-MO1-injected embryos, which display three-type cardiac jogging, rightward-jogging, no or reduced-jogging and leftward-jogging with 29.0%, 49.5% and 21.5% frequency respectively). At 42 hpf, in contrast to the control, although the UIIβ MO1 embryos appeared morphologically normal except for pericardial edema and slightly somite-fused tail (Fig.3-10). Closer examination showed alike randomization of heart laterality. As showed by *cmlc2* marker in Fig. 3-11a, at 42 hpf, in a population (n = 278) of embryos injected with 1.5 ng UIIβ MO1, 42.6% underwent the normal looping of heart tube (D-looping). Aberrant looping of the ventricle was observed in a significant portion of UIIβ knockdown embryos, which exhibited either no looping or abnormal looping of the ventricle to the left (L-looping), in contrast to 97% of the control embryos that underwent normal D-looping. To further confirm that randomization of heart-looping was due to knockdown of zebrafish UIIβ, we showed that the defect could be partially rescued by co-injection of UIIβ MO1 along with the zebrafish UIIβ mRNA (Fig.3-11b). Quantitative analysis showed that 69.5% of the rescued embryos displayed proper D-looping (Fig. 3-11a), compared to 42.6% injected with UIIβ MO1 alone. Collectively, these results indicate that zebrafish UIIβ mediates the process of cardiac looping.

3.3.2.2 UIIβ function is also essential for the establishment of normal visceral and diencephalic asymmetry

In addition to the asymmetry defects in the heart that were caused by UIIβ knockdown, we have further used *in situ* RNA hybridization to assess whether repression of UIIβ function also has affected on the asymmetric positioning of

visceral organs and brain. Because in normal zebrafish embryos between 20 and 36 hpf the gut primordium begins to loop, with the liver bud positioning to the left of gut and the pancreatic bud occupying an asymmetric position on the right side of the gut (Fig. 3-12, cartoon). However, as showed in Fig. 3- 12 using the pan-endodermal marker *foxA3*, which marks the developing gut primordium, the liver and pancreatic buds (Horne-Badovinac et al., 2003), we found that the visceral organs of majority UIIβ knockdown embryos fail to correct positioning. By contrast, the majority of UIIβ knockdown embryos did not show the normal L-R asymmetrical distribution of the visceral organs. In these embryos (80.6%), their livers and pancreas were located at the midlines.

Brain asymmetry was also assessed by marker *lefty1* (Thisse et al., 1999), which is normally expressed on the left side of the diencephalon at 22–24s. As the positioning defects of visceral organs and heart, UIIβ MO1 injection also rendered the randomization of *lefty1* expression in the diencephalon. 21.3% of UIIβ-MO1-injected embryos did not show any detectable expression of *lefty1*, 45.0% showed bilateral expression, 16.7% right expression and 16.9% left expression (Fig. 3-13) and Table 3-3).

3.3.3 UIIβ knockdown randomizes asymmetrical expression of L-R genes

Because the asymmetrical morphogenesis of organs is controlled directly by the Nodal cascade involving three TGF-b family member genes, *nodal, lefty1* and *lefty2,* and the home-box transcription factor gene *pitx2* (Tabin et al., 1995). At 22-24 somite stage, these genes asymmetrically express on the left LPM to specify LR identity of multi-cell field, further cause the asymmetrical morphogenesis.

To understand how UIIβ functions in the molecular cascade of asymmetrical morphogenesis, UIIβ MO1 embryos at 22-24 somite stage were examined for the expression patterns of *spaw, lefty1, lefty2* and *pitx2* regarding their roles in L-R determination. *lefty1* are expressed in midline precursor and margin cells, which might act as a midline barrier (Thisse et al., 1999), this gene also express at the left side of diencephalon at 22-24 somite stage. As for *lefty2*, this gene is left-biased expressed on the heart primordia at this stage. While *pitx2* is expressed in prechordal plate cells during late gastrulation and may function in morphogenesis at later stages (Essner et al., 2000). We found that the expression patterns of *lefty1, lefty2* and *pitx2* in UIIβ MO1 embryos were randomized and all kinds of expression patterns can be observed, including left-sided, right-sided, bilateral, or absent expression pattern (Fig.3-13). The frequency of randomized expression is shown in the Table 3-3. In order to investigate whether the Nodal signaling pathway was affected by UIIβ knockdown, we further examined *southpaw*, the earliest asymmetrically expressed molecular marker in zebrafish. This gene is expressed in the left LPM preceding asymmetric *lefty1, lefty2* or *pitx2* expression. Our observation suggested that the nodal related gene *spaw* was also alike affected in UIIβ MO1 embryos (Fig. 3-13 and Table 3-3). We conclude that UIIβ knockdown perturbs early asymmetric expression of *southpaw* and that UIIβ may function at the upstream of *southpaw* during establishment of L-R patterning of embryos.

3.3.4 Midline tissues are not affected by function-loss of UIIβ

Previous observations have shown that heart and visceral asymmetries are dependent on intact midline, which may serve as a boundary or barrier to maintain

left and right domains (Midline tissues, including notochord, floor plate, and hypochord, are still normal in UIIβ knockdown embryos as showed by the two markers *ntl* and *shh* (Fig.3-14) and in the UIIβ MO-injected embryos at 22-24 somite stage expression patterning of the two markers has no significant change in contrast to the control, which indicates that the role of UIIβ in L-R patterning of embryos is independent of midline development.

3.3.5 The reducing of UIIβ levels perturbs KV morphogenesis and stirs the asymmetrical distribution of intracellular Ca^{2+} flux around the KV region.

In zebrafish, KV morphogenesis and organization and function of ciliated cells are essential for generating nodal flow to transfer upstream LR information to LPM and induce the asymmetrical expression of nodal cascade (Amack et al, 2004; Essner et al., 2005). Our observation on randomized expression of nodal cascade in LPM caused by reduced expression of UIIβ promotes us to further check whether KV is affected by UIIβ knockdown. We compared the morphology of KV between UIIβ MO1-injected embryos and control embryos (Fig. 3-15a, b DIC picture). Some significant differences were observed, not only reduced KV size but also multi-KV indicating that repression of UIIβ function affects KV morphogenesis. This raises the possibility that UIIβ function is required prior to the role of ciliated KV cells to transfer the asymmetrical signaling to the LPM.

In zebrafish embryo, the transient of Ca^{2+} from symmetric distribution to asymmetrical distribution at periphery surrounding the KV occurs at 4-5 somite stage, thereafter is maintained until 12 somite stage (based on our observation, Sarmah et al., 2005; and Francescatto et al., 2010). The asymmetrical calcium ion signal

surrounding KV is require for the proper L-R patterning of embryos. Loss or elevation of asymmetric flux in cells surrounding the Kupffer's vesicle would result in the disruption of L-R patterning of embryos (Sarmah et al., 2005; Leung et al., 2008). However, the mechanism on how the asymmetrical distribution of free intracellular calcium ions in peripheral cells of node relays and modulates upstream L-R information still is undefined so far.

To investigate whether UIIβ function is required for the asymmetrical distribution of Ca^{2+} flux around KV, zebrafish embryos were injected with the Ca^{2+} green indicator at 1-cell stage as described previously (Leung et al., 2008). Using fluorescence microscopy, we detected the evident abnormal distribution of free intracellular calcium ions in peripheral cells of small multi-KV domain in UIIβ MO knockdown embryos from 3s to 6s stage (Fig. 3-15b). Apparently the normal distribution of Ca^{2+} flux around KV is stirred by the abnormal multi-KV structure.

3.3.6 UIIβ knockdown renders the defect of DFCs development

KV derives from a cluster of non-involuting cells termed the DFCs, which migrate ahead of the dorsal boundary during gastrulation (Cooper et al., 1996; Melby et al., 1996). The phenotype of multi-KV of UIIβ morphant embryos promotes us further trace the progress of DFC development. *ntl* is the zebrafish homologue of the mouse T (Brachyury) gene. At 85% epibody, *ntl* is expressed in midline precursor cells, blastoderm boundary cells, and DFCs (Schulte-Merker et al., 1994). As a T box transcription factor, *ntl* functions in DFCs to regulate KV morphogenesis and L-R determination. We visualized the DFC morphology at 80% epiboly stage embryos by using RNA in situ analysis of *ntl*. In the control embryos, DFCs form a single,

compact DFC cluster (Fig. 3-16); but in UIIβ morphant embryos the morphological defect of DFCs can be observed (B1, B2 and B3 in Fig. 3-16), the morphant embryos displays significantly smaller but multiple DFC clusters, which disperse at the ahead of dorsal organizer margin (B1-B3, arrow in Fig. 3-16). The fact that the early DFC marker *ntl* still normal expression at the DFC region implies that UIIβ down-regulation does not disrupt the specification of the DFCs. However the smaller but multiple DFC clusters suggests that either the migration or converging of DFC cells might be perturbed, or there were ectopic nodal signaling that is responsible for the initial specification of DFC identity.

In fact the phenotype is similar with the Li-treated embryos. The noninvoluting, highly endocytic marginal (NEM) cells, the precursor of DFCs, in Li-treated embryos form multiple clusters arranged in widely separated domains (Stachel et al. 1993; Klein et al., 1996). Li is currently thought to exert its hyperdorsalizing effects on vertebrate embryos by repressing GSK-3's inhibitory on β-catenin.

Interesting, using different experimental method Schneider et al., (2008) observed that treating embryos at 60% epiboly stage with thapsigargin, a membrane permeable Ca^{2+}-ATPase inhibitor that prevents the pumping of Ca^{2+} back into the endoplasmic reticulum, causing the transient cytoplasmic Ca^{2+} elevation but ultimately rendering depletion of internal Ca^{2+} stores, results in the suppression of the DFC-regional Ca^{2+} release. Consequently, migrating DFCs in thapsigargin-treated embryos show a dispersal pattern of individual cells, but this only occurs during somite stages and during early epiboly, DFC migration in thapsigargin-treated embryos is same as in the control. Instead, the morphological

defect of DFCs in UIIβ morphant embryos has occurred during epiboly. Whether is there a common mechanism underlying the three observations from different experiment treatments? It is worthy of paying more attention. Schneider et al., (2008) thought the un-coalescence of DFCs at later stage of KV development might result from that the suppression of the DFC-regional Ca^{2+} release increases the stability /activity of β-catenin.

3.3.7. UIIβ knockdown disrupts the correct orientation of L-R axis by altering Bmp signaling and then expanding dorsal Spemann organizer.

A series of observations from different model organisms strongly buttress that Bmp signaling plays a vital role in L-R patterning during vertebrate embryogenesis (Bisgrove et al. 1999; Campione et al. 1999; Essner et al. 2000; Faucourt et al. 2001; Rebagliati et al. 1998a; Sampath et al. 1998; Capdevila et al., 2000; Klingensmith 2000; Brennan et al., 2002; Meno et al., 1997; Branford et al., 2000; Ulloa et al., 2001; Chocron et al., 2007). Chocron et al., (2007) firstly unraveled that there are two distinct phases during LR patterning of zebrafish embryos in which BMP signaling is required. During early segmentation by inducing *lefty1* expression to repress southpaw expression in the right LPM, BMP signaling modulates both visceral and heart laterality and during late segmentation, BMP ligand left-biased expresses in heart field and LPM, functions at downstream of *spaw* to regulate left-sided gene expression and heart laterality. In addition, they found it is *Bmp4* ligand to be responsible for both phases of BMP signaling. However, whether is there a much more earlier phase before the segmentation period in which BMP4 exerts its effect on the L-R patterning of zebrafish embryos? In fact, reports from

Ellertsdottir et al., (2006) and Adams et al., (2006) had indicated that some early molecular events involving into the L-R patterning of embryos have occurred at least before zebrafish segmengenesis. Moreover, during gastrulation *bmp4* transcripts have presented and show a gradient distribution along ventral to dorsal axis. So, it is reasonable to hypothesize there is an earlier phase during gastrulation at which *bmp4* functions to affect the establishment of L-R axis.

In fact our observations demonstrated the existing of earlier phase at which *bmp4* expression regulates the LR patterning of embryos. Using RNA in situ hybridization we evaluated the expression pattern of *bmp4* in three sequential phases. At late segmentation stages (from 22ss to 24ss), the asymmetrical distribution of *bmp4* transcripts have been altered by reduced UIIβ levels. The UIIβ morphant embryos show a down-regulation of *bmp4* expression in the left side of heart field and LPM (Fig.3-17), In consequence, *bmp4* expression became even and weaker in the cardiac field and LPM (B, from 22s to 24s stage; E, 24hpf). Further, statistics analysis implied that at 22 somite stage, 88.0% of control embryos displayed the asymmetrical distribution of *bmp4* mRNAs on the cardiac field and LPM. In comparison, only 38.1% of UIIβ morphant embryos appear this pattern and the rest of which exhibits even distribution of *bmp4* transcripts on the heart field and LPM (Fig. 3-17). At 24hpf the difference of bmp4 expression pattern between the controls (Fig. 3-17,E) and UIIβ morphant embryos became much more distinct (Fig. 3-17, F).

At the early segmentation stage (10 somite stage) the *bmp4* expression in tailbud and periphery of KV is also significantly down-regulated by UIIβ knockdown (Fig.3-18 boxed area). On the contrary, it is striking that *bmp4* transcripts are

up-regulated by UIIβ knockdown in the polster region of UIIβ-knockdown embryos (Fig. 3-18).

The vertebrate body plan develops along three geometric axes: anterior-posterior, dorsal-ventral, and left-right. By diminishing dorsal-anterior development of embryos, Danos et al., (1995) evidenced L-R asymmetries are not random with respect to the dorsal-ventral and anterior-posterior axes, but there is a linkage of left-right and dorsal-anterior development; alteration in dorsal-anterior development perturbs the left-right orientation of heart looping. Current, a widely accepted model of dorsoventral patterning postulates that during gastrulation a BMP activity gradient patterns cell fates along the dorsoventral axis, which involving β-catenin, members of BMP family, and BMP antagonists. The dorsal Spemann organizer is a source of growth factor antagonists that take part in the establishment of signaling gradients and its genes are induced by low BMP levels (Heather et al., 2007; Pear et al., 2000; Ambrosia et al., 2008). Observations from zebrafish suggest that the BMPs are required for dorsoventral patterning during gastrulation. During zebrafish gastrulation, three bmp genes are expressed, bmp4, bmp2b, and bmp7, all of which show a degressive gradient distribution from ventral to dorsal; Heather et al., (2007) demonstrated that BMP4 is required during the later gastrulation for the specification of ventroposterior cell fates. Our work suggests that reduced gradient distribution of *bmp4 along* ventral-to-dorsal axis in UIIβ morphant embryos results in the dorsalization of embryos (Fig.3-19 and Fig.3-20). The dorsalization marker *gsc* is significantly up-regulated in UIIβ morphant embryos and the territory of dorsal Spemann organizer is distinctly enlarged to the ventral side as exhibited through organizer markers *flh* (Fig.3-20). It is worthy of noting that the BMP antagonist gene,

chordin, not only appears significantly up-regulated expression in dorsal Spemnna organizer region and margin along dorsal-ventral axis in UIIβ morphant embryos but also shows ectopic expression in the DFCs domain.

In addition affecting the L-R positioning of ventral organs, the dorsalization of embryos would also render function-loss impact on them. For example, using RT-PCR we evaluated the myocardial development. Results unravel that for 24hpf and 48hpf embryos, myocardial marker *cmlc2* and atrial marker *amhc* were down-regulated by the UIIβ knockdown, although ventricular marker *vmhc* had no distinct change. It appears that myocardium development suffered from some impact from the dorsalization which is induced by UIIβ knockdown (Fig. 3-21)

Recently an important evidence of involvement of Bmp signaling in mammals came from the study of *smad5* mutant embryos (Chang et al., 2000). The *smad5* mutants have defects in heart-looping. The null of *smad5* not only severely reduced *lefty1* expression, but also caused the abnormal bilateral expression of *nodal, lefty2* and *pitx2*. However, in zebrafish, to answer whether *smad5* is implicated into the L-R body plan, we further evaluated the zebrafish *smad5* expression in the UIIβ MO embryos at 10 somite and 24hpf stage. Results showed that in contrast with the control, s*mad5* expression in UIIβ morphant embryos does not show any obvious deference (Fig. 3-18).

3.3.6 Overexpression of UIIβ also disturbs the normal L-R asymmetry

Using wild type fish line Tubingen at the 1-cell stage we injected the full-length mRNAs of UIIβ into zebrafish embryos. It is interesting that overexpression of UIIβ (150 pg mRNA) causes a similar L-R patterning defect as what caused by UIIβ

knockdown embryos (Fig. 3-22). Compared to MO effects on the L-R patterning of embryos, overexpression of UIIβ induced lower proportions (39.2%) of embryos with abnormal heart looping at 48 hpf (Fig. 3-22). This suggests that the level of UIIβ ligand is also critical for maintaining the natural balance of L-R patterning: either too much or too little of UIIβ will stir the signal balance and result in misorganization of L-R axis patterning in zebrafish embryos.

3.3.7 Overexpression of UIIβ perturbs the L-R patterning of embryos by altering Bmp signaling

Both overexpression and knockdown of UIIβ seem to adopt similar strategies to regulate asymmetrical development of embryos, for example, the way to change Bmp signaling is similar (Fig. 3-23. A). In contrast to the controls, at 22s the *bmp4* expression in heart field and LPM of UIIβ morphant embryos not only becomes symmetric but is also upregulated in the overexpression embryos. While at 10s the expression pattern of bmp4 has a distinct variation: up-regulated in polster regions, instead, in tail region surrounding KV, *bmp4* is down-regulated. As for *smad5*, the change of its expression pattern caused by overexpression of UIIβ is the same as that of UIIβ knockdown: *smad5* expression has no significantly change at 10 somite stage and 24 hpf. (Fig.3-23. B).

3.4. Discussion

Although UIIβ knockdown and overexpression of UIIβ have completely opposite effect on the UIIβ level, they all disrupt the L-R patterning of embryos, which perhaps suggests that the level of UIIβ peptides is also critical for maintaining

the natural balance of LR patterning either too much or too little of UIIβ will break the signal balance and result in misorganization of LR axis patterning in zebrafish embryos.

MOs and siRNAs have been extensive adopted by researchers to induce sequence-specific gene knockdown in multiple systems. However, the application of both technologies is sometimes limited by induction of off-target effects (Ekker et al., 2001; Scacheri et al. 2004; Lin et al. 2005; Jackson et al. 2003; Fedorov et al. 2006).

Approximately 15–20% of MOs used in zebrafish show off-targeting effects (Ekker et al., 2001), the off-target effects, which are represented by a neural death. The phenotype includes smaller heads and eyes, somite and notochord abnormalities, and eventually craniofacial defects. These MO-induced developmental defects are mediated by p53 upregulation at the transcriptional level in siRNA- and MO-treated vertebrate and target-independent because they fail to be reproduced by mutants in the respective genes.

Moreover, concurrent p53 knockdown provides a new approach to facilitate the identification of previously veiled gene functions by p53 activation.

.In this study, when initial performing the UIIβ knockdown experiment we use the wild type zebrafish line AB or Tubingen to inject UIIβ MO into their one-cell embryos. Embryos presented a consistent phenotype with doses 1.5 ng MO/embryo (Fig.3-24), however, the phenotypes of UIIβ morphants is similar with the general morphological features of MO-induced off-targeting neural death previously described. We characterized these defects using a series of neural marker such as *ngn-1, pax2a, crestin, rx3, egr2b, barhl2* and *mab21l2* (Fig.3-25). Morever we further found that these defects failed to be rescued.   Instead, it is not the case in the

UIIβ MO tp53M214K embryos. There are distinct different phenotypes between UIIβ MO-injected tp53M214K embryos (B in Fig.3-10). with UIIβ MO-injected wild-type embryo (A, B, and C in Fig.3-24) In the UIIβ MO tp53M214K embryos, no the neural death phenotypes, such as smaller heads and eyes, exhibit somite and notochord abnormalities, and eventually display craniofacial defects, were observed and we only found the pericardial edema and abnormal heart looping. Foremore, these defects may be successfully rescued.

Based on above information and reports (Robu et al., 2007) we think that when using the wild-type fish line to injecting the MO the phenotypes of UIIβ MO embryo are an off-targeting effect mediated through p53 activation by MO knockdown. In order to delete the off-targeting effect, we use the tp53M214K mutant line which is a p53(-/-) null zebrafish line. This zebrafish line harbors missense mutations in the tp53 DNA binding domain. Cells in the tp53M214K embryos failed to undergo apoptosis in response to radiation at both 28°C and 37°C. Unlike wild-type control embryos, irradiated tp53M214K embryos also failed to up-regulate p21 and did not arrest at the G1_S checkpoint. The mutant zebrafish lines provide a unique platform for deleting the off-target effect of some MO when injected into wild type embryos.
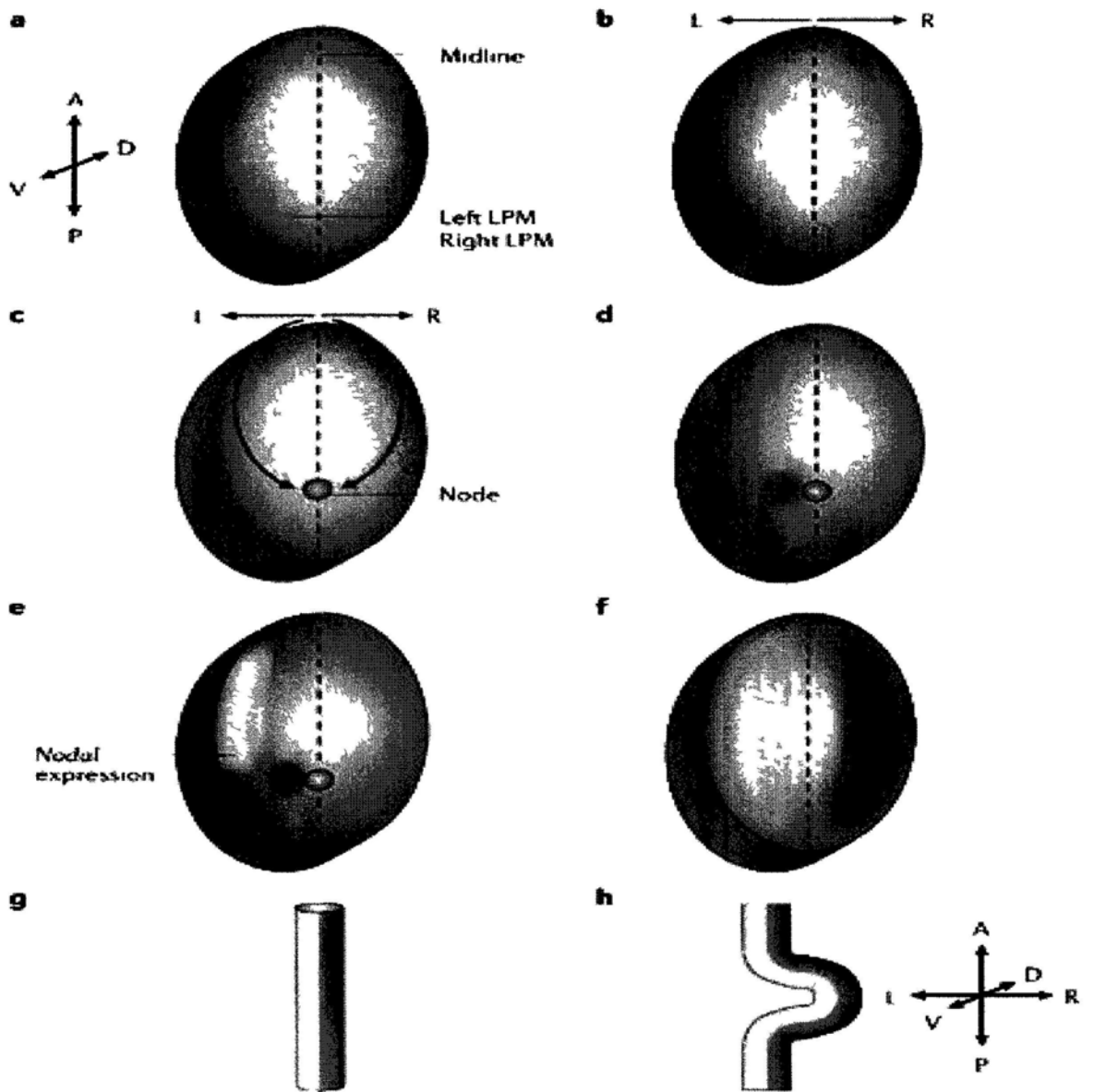
Fig.3-1. an overview of the determination of L-R axis of the vertebrate embryo

Fig.3-1. an overview of the determination of L-R axis of the vertebrate embryo.

(a) In early embryogenesis, an embryo that is aL-Ready patterned along the anterior–posterior and dorsal–ventral axes is bilaterally symmetrical. (b) A symmetry-breaking step generates initial L-R information, although the nature of this event is unknown. (c) The initial L-R information is then transferred to the embryo node (shown as a blue circle). (d) The node generates a directional output in the form of a discrete perinodal domain of *nodal* expression and/or lateralized hedgehog signaling, which results in local L-R asymmetries (shown as dark-blue shading). (e) These local asymmetries around the node are conveyed to the LPM in the form of side-specific *nodal* expression. (f) Broad domains of expression of left- and right-side specific genes (yellow and red, respectively) are then established, transferring laterality information to the organ primordia (a structure that represents a single primordium is shown in **g**), which, in turn, execute L-R asymmetrical morphogenetic programmers (illustrated as the directional looping of the organ primordium in **h**). A, anterior; P, posterior; D, dorsal; V, ventral; L, left; R, right. The figure is cited from Raya *et al.* (2006).
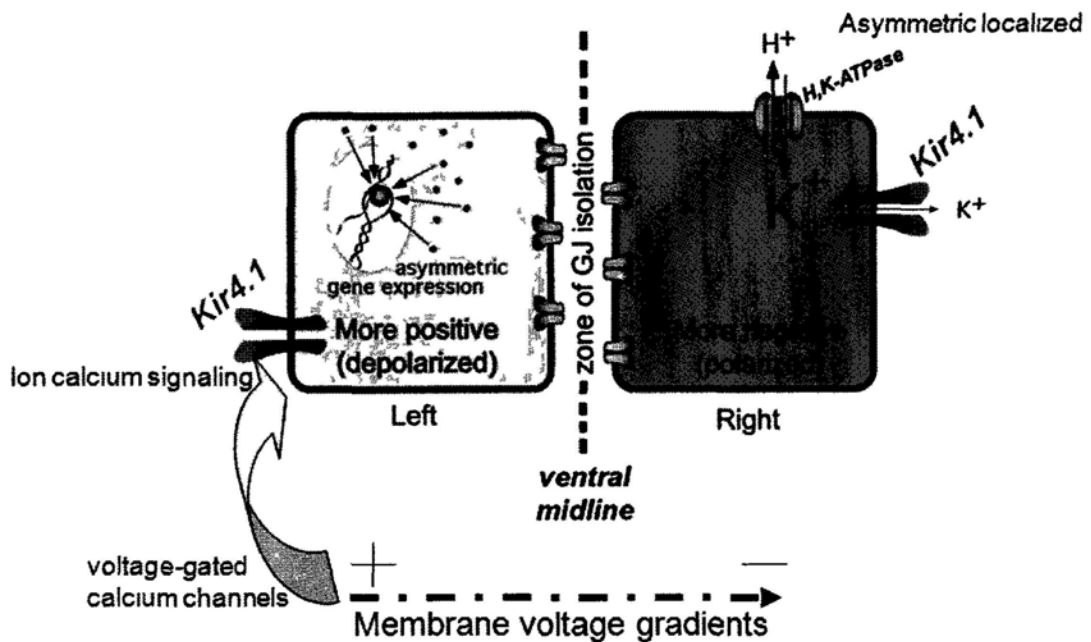
Fig.3-2. ion transporters / ion flux model.

This model is based on the observations about chicken, frog embryo. Depending on the cytoskeleton, the ion transporters, for example, the H+/K+-ATPase, are asymmetric localized on the right side of ventral midline. While symmetrical Kir4.1 presence in the ventral midline cells provides the controlled exit of excess K+ ions brought in by the H+/K+-ATPase on the right side. This allows the right cells to establish a pH and a membrane voltage that is different than that on the left side. Further the voltage gradient is transferred to some asymmetrical information, for instance, by the voltage-gated calcium channels, is translated into the calcium ion pulses or signaling to mediate the downstream asymmetric gene expression (Modified from Sherry et al., 2008 and Adams et al., 2006).
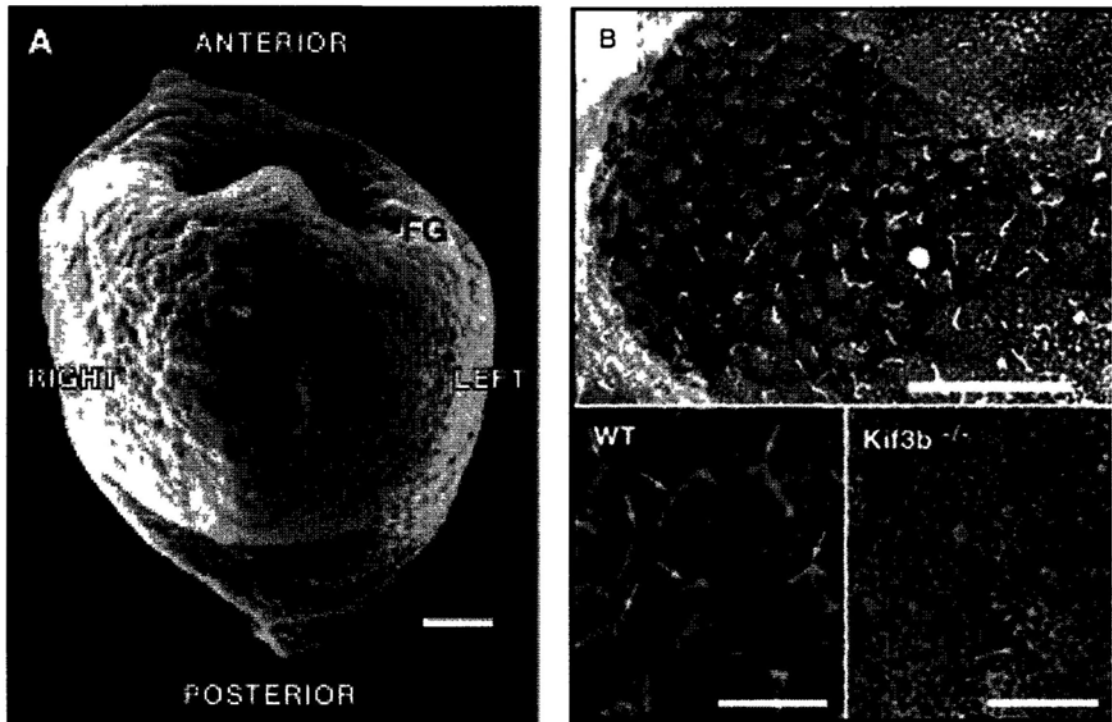
Fig. 3-3a. the ventral node of mouse embryo.

(A) A scanning electron micrograph shows the ventral view of a 7.5 dpc mouse embryo. VN, ventral node; NP, notochordal plate; FG, foregut; Bar, 100 μm. (B) Scanning electron micrographs of the mouse ventral node in lower (upper panel) and higher (lower panels) magnification are shown. The surface is normally ciliated in wild-type (arrows, lower left panel), whereas the nodal cilia were absent in *Kif3b*[/] embryos (lower right panel). Bars, 20 μm in upper panel, 5 μm in the lower panels. These figures are modified from
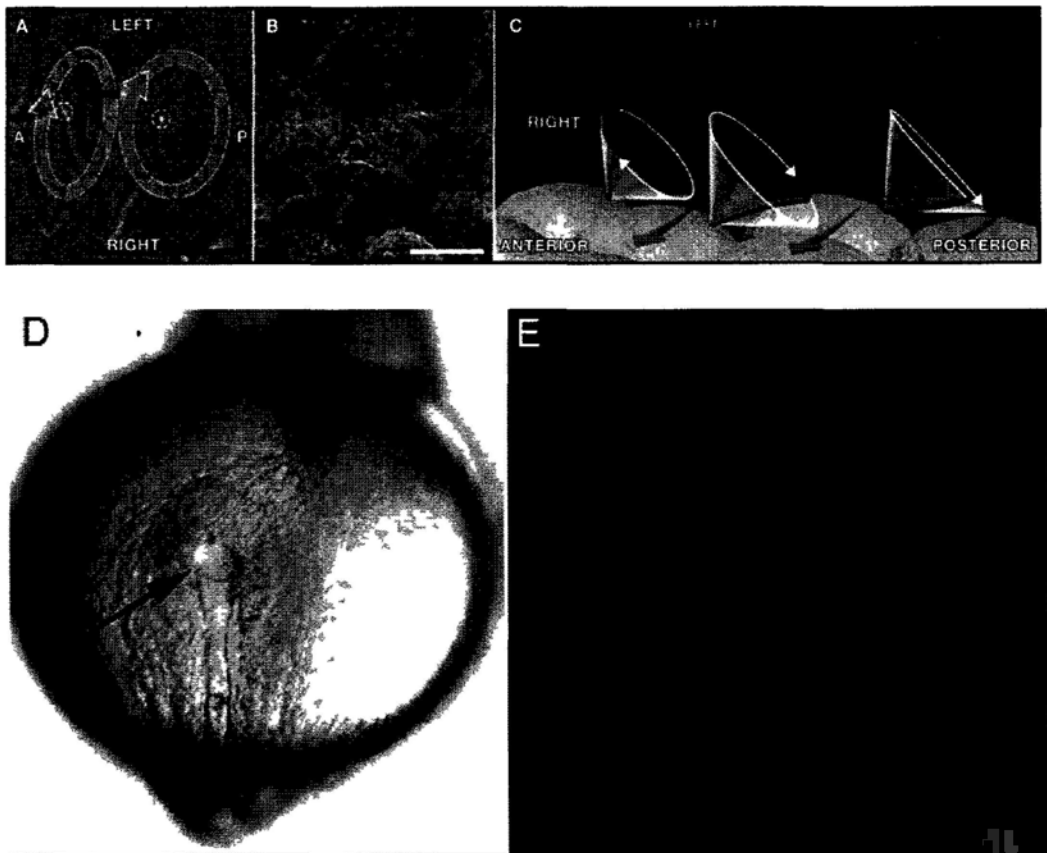
Fig, 3-3b. the mechanism of generation of leftward nodal flow.

Fig, 3-3b. the mechanism of generation of leftward nodal flow.

(A) The trajectory of the tips of nodal cilia (red circles on the white ellipse) is shifted toward the posterior when compared to the root of the cilia (yellow circles). (B) A scanning electron micrograph of ciliated cells of the ventral node of a rabbit embryo (at the presomite stage) is shown. The root of a cilium is most frequently found toward the posterior of a cell. The dome-like curvature of the apical plasma membrane helps explain the posterior tilt of the cilia. Bar, 5 μm. (C) A hydrodynamic mechanism generates leftward flow. Due to a gradient of shear resistance, a cilium cannot efficiently drive the extraembryonic fluid when it makes a rightward movement in the proximity of the surface. (D) The spherical KV (arrow) forms in the tailbud during early somite stages in wild-type embryos. Ventral view, anterior to the top. (E) Confocal images of cilia (red) labeled by fluorescent anti-acetylated tubulin immunohistochemistry. Cilia were organized within KV in wild-type embryos. Figures A-C from Hirokawa et al., (2006).Figure D and E modified from .Amack et al., (2004).
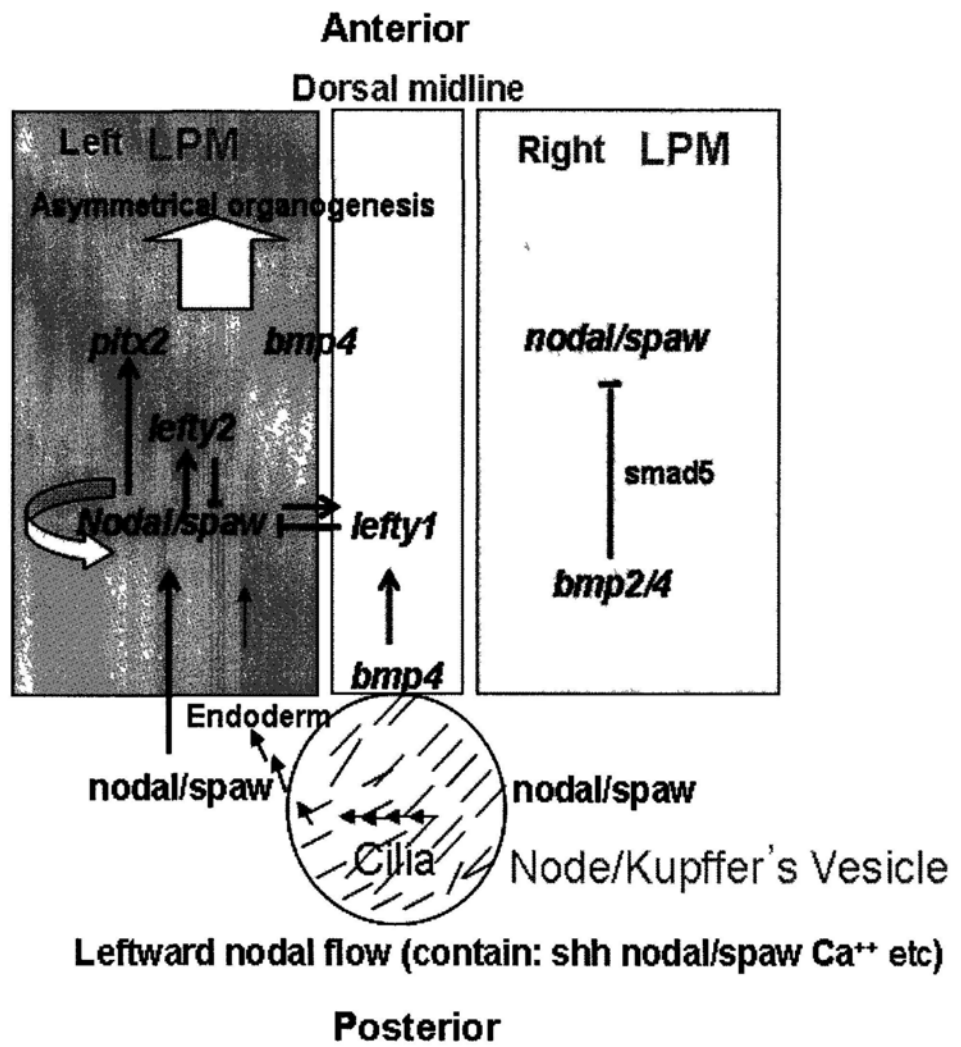
Fig. 3-3c. The nodal flow model.

Fig. 3-3c. The nodal flow model.

The nodal flow model shows that the rotation of the cilia lined on the ventral side cell of node produces a leftward flow of extracellular fluid that takes place in the nodal pit, which is called the nodal flow. The upstream asymmetrical information, such as nodal, shh and ion calcium, is transported to the left lateral mesoderm by nodal flow to induce the cascade of asymmetrical signaling (Note: as for the detail of this signal cascade, please refer to the section: 3.1.2 the asymmetryical genes), which assigns the left-right identity of embryo and further and initiates the asymmetrical morphorgenesis.

Table 3-1. Genes reported to be expressed L-R asymmetrically

Gene	Role	Species	Expression	Reference
Nodal	TGFβ signal (Nodal)	Chick	Left N, left LPM	(Levin et al ,[1995])
Nodal	TGFβ signal (Nodal)	Mouse	Left N, left LPM	(Collignon et al ,[1996], Lowe et al ,[1996])
Xnr1	TGFβ signal (Nodal)	*Xenopus*	Left LPM	(Lustig et al ,[1996])
cyclops	TGFβ signal (Nodal)	Zebrafish	Left LPM	(Sampath et al ,[1998])
southpaw	TGFβ signal (Nodal)	Zebrafish	Left LPM	(Long et al ,[2003])
Lefty1	TGFβ signal (divergent)	Mouse	Left PFP	(Meno et al ,[1996])
Lefty2	TGFβ signal (divergent)	Mouse	Left LPM	(Meno et al ,[1998])
Lefty1	TGFβ signal (divergent)	Chick	Left LPM, PFP	(Rodriguez-Esteban et al ,[1999])
Lefty	TGFβ signal (divergent)	*Xenopus*	Left LPM	(Cheng et al ,[2000])
Bmp-4	TGFβ signal (BMP)	Zebrafish	Left heart	(Chen et al ,[1997])
CFC	TGFβ co-receptor	Chick	Left N, left LPM	(Schlange et al ,[2001])
Caronte	TGFβ antagonist	Chick	Left LPM	(Rodriguez-Esteban et al ,[1999], Yokouchi et al ,[1999], Zhu et al ,[1999])
Shh	HH signal	Chick	Left N	(Levin et al ,[1995])
cPTC	HH receptor	Chick	Left N	(Pagan-Westphal and Tabin,[1998])
Dll1	Notch signal	Chick	Left N	(Raya et al ,[2004])
Lfng	Notch modulator	Chick	Left N	(Raya et al ,[2004])
eHAND	Transcription factor	Chick	Left heart	(Srivastava et al ,[1995])
eHAND	Transcription factor	Mouse	Left heart	(Srivastava et al ,[1995])
eHAND	Transcription factor	*Xenopus*	Left heart	(Sparrow et al ,[1998])
FoxA2	Transcription factor	Chick	Left LPM	(Levin et al ,[1995])
HoxC-8	Transcription factor	*Xenopus*	Left LPM	(Thickett and Morgan,[2002])
Islet-1	Transcription factor	Chick	Left gut	(Yuan and Schoenwolf,[2000])
NKX3 2	Transcription factor	Chick	Left LPM	(Schneider et al ,[1999])
Pitx2	Transcription factor	Chick	Left LPM	(Logan et al ,[1998], Piedra et al ,[1998], Ryan et al ,[1998], St Amand et al ,[1998], Yoshioka et al ,[1998])
Pitx2	Transcription factor	Mouse	Left LPM	(Piedra et al ,[1998], Ryan et al ,[1998], Yoshioka et al ,[1998])
Pitx2	Transcription factor	*Xenopus*	Left LPM	(Ryan et al ,[1998])
Pitx2	Transcription factor	Zebrafish	Left LPM	(Campione et al ,[1999])
LPlunc1	Lipid binding protein	Mouse	Left N	(Hou et al ,[2004])
Flectin	Extracellular matrix	Mouse	Left heart	(Tsuda et al ,[1998])
cAct-RIIa	TGFβ receptor	Chick	Right N	(Levin et al ,[1995])
BMP-4	TGFβ signal (BMP)	Chick	Right N	(Monsoro-Burq and Le Douarin,[2000])

Dante	TGFβ antagonist	Mouse	Right N	(Pearce et al ,[1999])
cWnt-8C	WNT signal	Chick	Right N	(Pagan-Westphal and Tabın,[1998])
FGF-8	FGF signal	Chick	Right N	(Boettger et al ,[1999])
FGF-18	FGF signal	Chick	Right N	(Ohuchı et al ,[2000])
cSnR	Transcription factor	Chick	Right LPM	(Isaac et al ,[1997])
dHAND	Transcription factor	Chick	Right heart	(Srıvastava et al ,[1995])
dHAND	Transcription factor	Mouse	Right heart	(Srıvastava et al ,[1995])
dHAND	Transcription factor	*Xenopus*	Right heart	(Angelo et al ,[2000])
dHAND	Transcription factor	Zebrafish	Right heart	(Angelo et al ,[2000])
NKX3 2	Transcription factor	Mouse	Right LPM	(Schneıder et al ,[1999])
Pcl2	Transcription factor	Chick	Right N	(Wang et al ,[2004])

N, node; LPM, lateral plate mesoderm; PFP, prospective floor plate
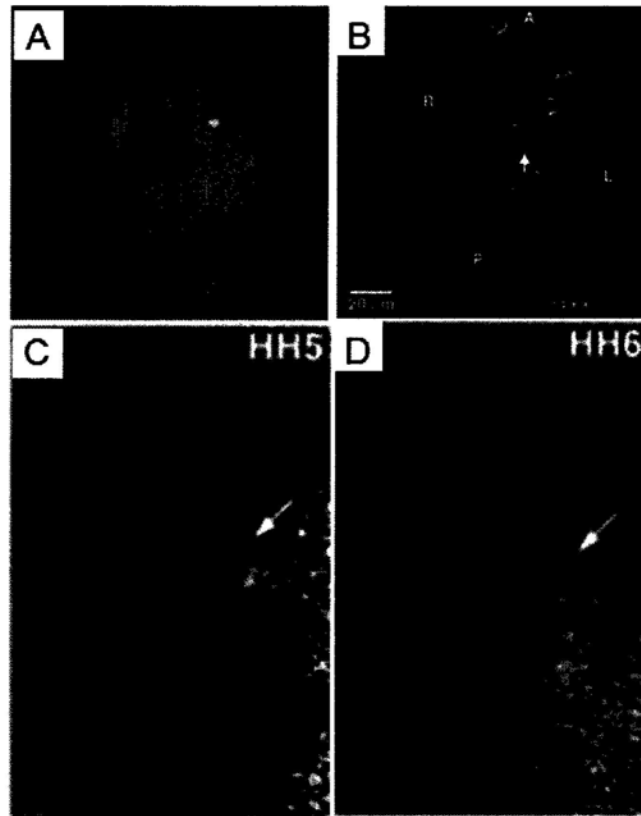
This table 3-1 is cited from Raya et al., (2008)

.

Fig. 3-4. L-R asymmetries in Ca2+ levels at the embryo node.

Fig. 3-4. L-R asymmetries in Ca2+ levels at the embryo node.

A: the left-sided accumulation of free cytoplasmic Ca2+ (intracellular Ca2+) at KV during zebrafisfe early somite stages (5s-8s). Embryos were injected at the 1 cell stage with mRNA encoding flash-pericam (fp), which is a Ca^{2+} indicator protein, a chimeric derivative of circularly permuted green fluorescent protein and calmodulin. It exhibits increased fluorescence emission with increasing cytosolic Ca^{2+} levels (Nagai et al., 2001). Ca^{2+} patterns at 5–8 SS were imaged by epi-fluorescence microscopy, and images were converted to an intensity scale (red indicating high intensity; yellow/green, moderate; blue/black, low). This figure modyfied from Sarmah et al., (2005).

B: calcium signaling at the node of e7.75 mouse embryos. This embryos show Fluo3 fluorescence at left margin of the node. The nodes ranged in width from 25 μm. Embryos are incubated with the cell-permeable calcium indicator Fluo3 and imaged by scanning confocal laser microscopy. Images are converted to an intensity scale. Red, high intensity; yellow/green, moderate intensity; blue/black, low intensity. This figure modyfied from McGrath et al (2003).

C and D: the asymmetric Ca^{2+} distribution during chick gastrulation was visualized with a cell-impermeant version of the Ca^{2+} indicator Calcium Green-5N. Asymmetric localized domains of Ca^{2+} (arrows) appeared on the left side of Hensen's node during HH4–HH6 and became symmetric at HH8. Two-photon excitation microscopy images of two representative experiments using chick embryos at HH5 and HH6 are shown. Embryo views are ventral, anterior is to the top. Ovals mark the position of Hensen's node. Grey levels representing fluorescence intensities have been pseudo-coloured with a purple (low intensity), yellow (moderate intensity) to white (high intensity) scale. This figure modyfied from Raya et al., (2004). L, left; R, right; nc, notochord; A, anterior; P, posterior
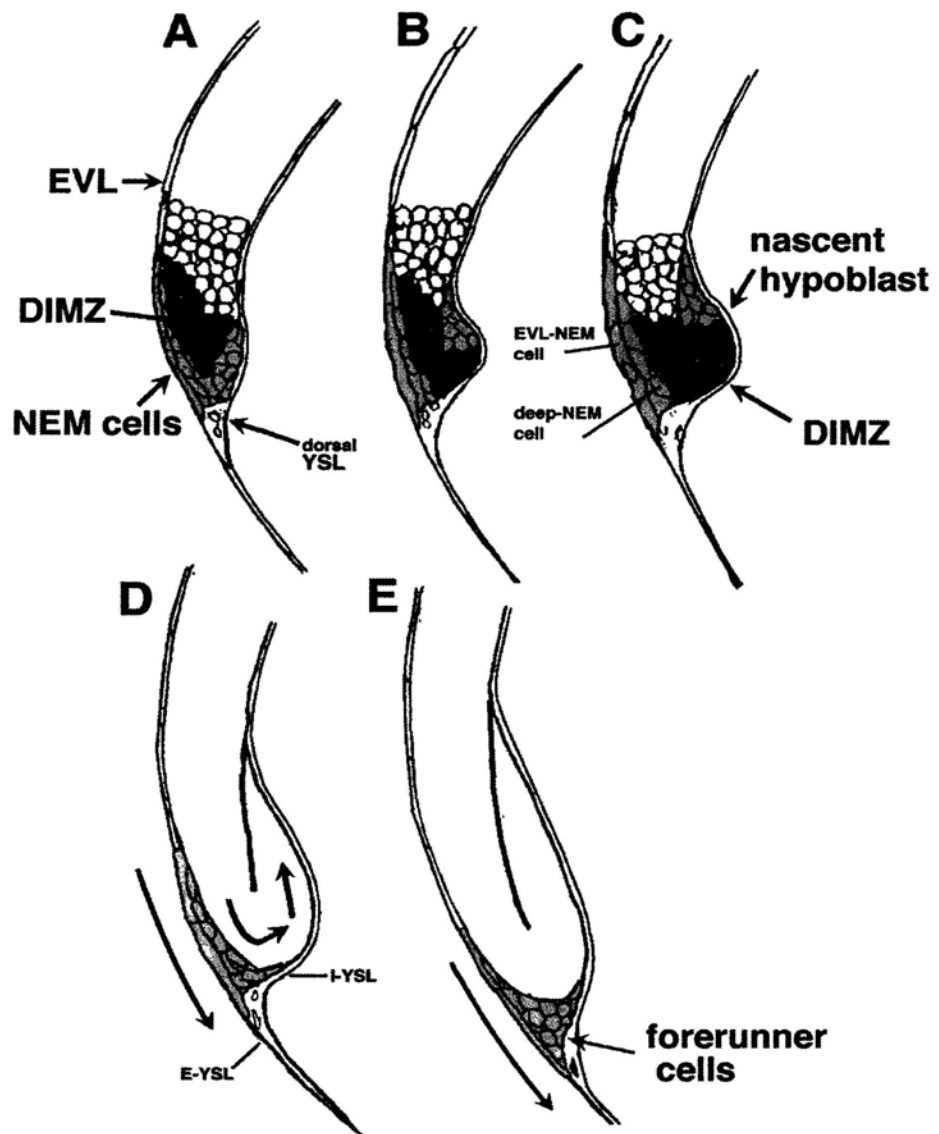
Fig. 3-5a The origin of KV during early zebrafish gastrulation.

Fig. 3-5a The origin of KV during early zebrafish gastrulation.

The cellular dynamics process taks place in the DMZ between 50 and 60% epiboly. (A) NEM cells are located superficially in the DMZ. The NEM cells (green) are composed of both EVL cells and 1–2 layers of underlying deep cells. The most marginal cells in the NEM cell cluster are in contact with the YSL. (B) Deep cells lying underneath the NEM cell cluster (red cells) in the DIMZ turn inward (i.e., involute) as gastrulation is initiated. Cells that are in close contact with the dorsal YSL (orange cells) are the first deep cells in the DIMZ to undergo a loss of coherence and begin moving toward the animal pole. (C) As involution continues in the DIMZ, cells in the nascent hypoblast (orange and red) move toward the animal pole. (D) A stylized view of the major cell movements occurring within the DMZ during early gastrulation. The NEM cell cluster remains in its superficial location and is displaced vegetally with the YSL as the syncytium undergoes epiboly. The site of EVL–YSL contact demarcates the YSL into two regions, known as the external YSL (E-YSL) and internal YSL (I-YSL), which are located external and internal to the EVL–YSL border, respectively (Trinkaus et al., 1993). (E) At 60% epiboly, deep cells of the NEM cell cluster become the forerunner cells, which lie at the leading edge of the blastoderm. At this developmental stage, the EVL cells of the original NEM cell cluster (EVL–NEM cells) lie directly above the forerunner cells. Once segregated, forerunner cells do not intercalate with other cell types in the DMZ. This picture comes from D'Amico LA et al., (1997).

Abbreviations: DIMZ, dorsal involuting marginal zone; DMZ, dorsal marginal zone; ERM, embryonic rearing medium; EVL, enveloping layer; NEM cells, noninvoluting endocytic marginal cells; YSL, yolk syncytial layer.
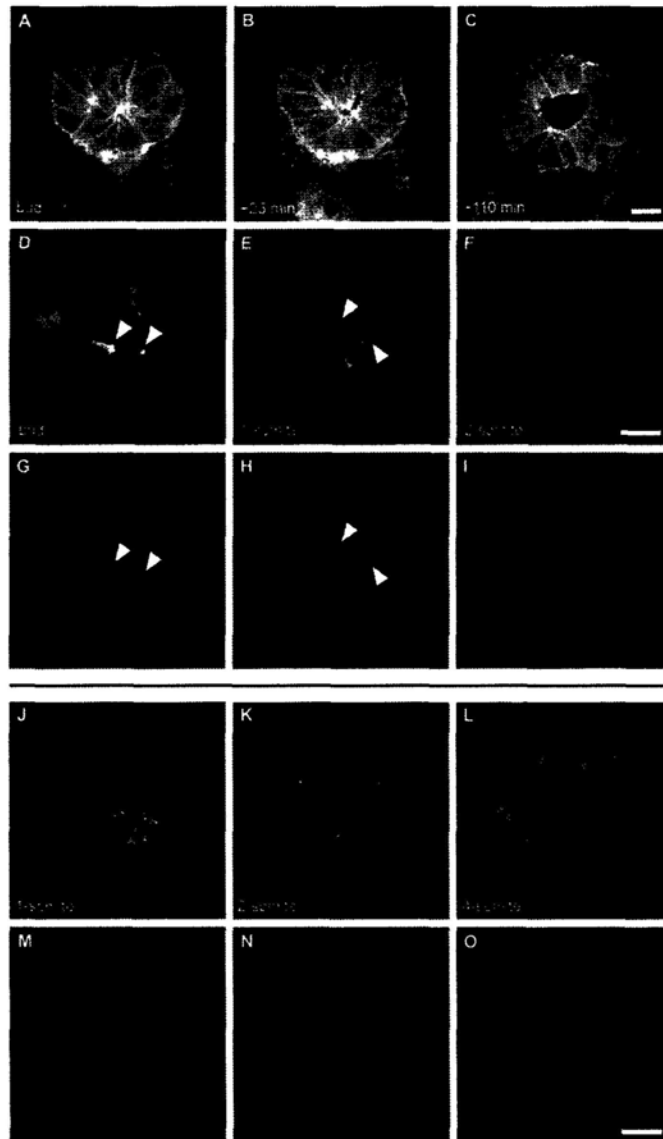
Fig. 3-5b. Lumen and cilia formation in Kupffer's vesicle.

96

Fig. 3-5b. Lumen and cilia formation in Kupffer's vesicle.

(A-C)Images of a time-lapse multi-photon confocal movie of a zebrafish embryo expressing *Tg(β-actin:HRAS-EGFP;sox17:GFP)*. Single focal planes at the interior of the DFC cluster are shown at the bud stage and subsequent time points, as indicated. Anterior is to the top. At the bud stage, bottle-shaped DFCs are arranged around two focal points (A, arrowheads). Shortly after, these focal points have coalesced into a single focal point (B, arrowhead) from which a single lumen forms (C). **(D-I)** Confocal images of *Tg(sox17:GFP)*-expressing embryos immunolabelled with an anti-ZO-1 antibody(ZO-1: tight-junction protein 1). GFP, green; anti-ZO-1, red. Single focal planes at the interior of the DFC cluster (D-F) and 3D renderings of the anti-ZO-1 labelling (G-I) are shown. Arrowheads mark equivalent structures in single focal planes and renderings. At the bud stage, multiple, widely spread ZO-1-rich accumulations are found in the interior of the DFC cluster (D,G). At the 1-somite stage, ZO-1 clusters are more connected and condensed, and small lumina are observed (E,H). At the 2-somite stage, a single, large lumen delineated by ZO-1 is observed inside the cluster (F,I). **(J-O)** Confocal images of *Tg(sox17:GFP)*-expressing embryos (green) double labelled with anti-ZO-1 (blue) and anti-acetylated α-tubulin (red) antibodies. Single focal planes are shown for merged (J-L) and single (M-O) channels. At the 1-somite stage, DFCs are positioned around multiple small lumina delineated by ZO-1, in which short, tubulin-rich cilia are observed (J,M). Between the 2- and 4-somite stages, a single, expanding lumen is observed (K,L), which contains cilia that are increasing in length (N,O). Scale bars: 30 μm. This picture comes from Oteíza et al., (2008).
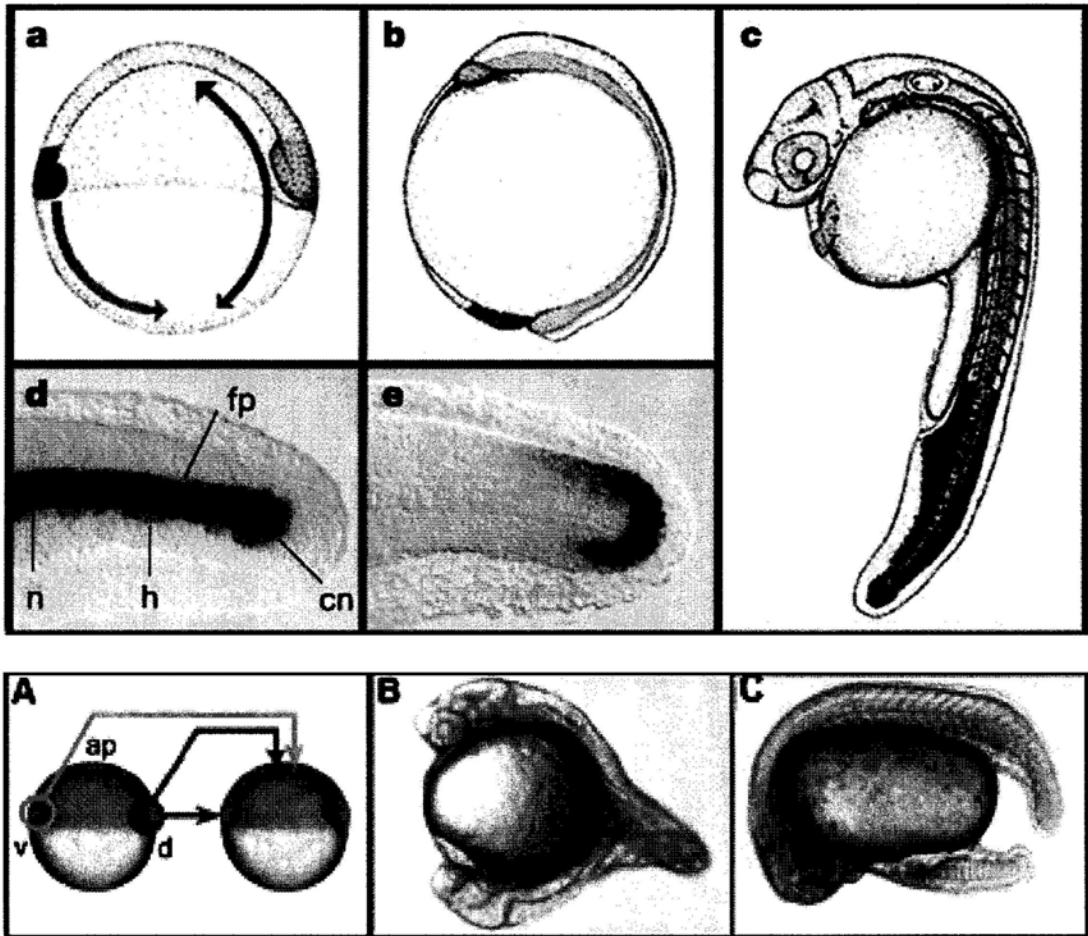
Fig. 3-6. The dorsal and ventral organizer dormains of zebrafish embryo.

Fig. 3-6. The dorsal and ventral organizer dormains of zebrafish embryo.

a, b, position and movement of ventral (red) and dorsal (blue) marginal cells at the shield stage (a), at the end of gastrulation (b) and at 24□h after fertilization (c). The dorsal margin (dorsal organizer) contributes to axial structures (blue); ventral margin (dorsal organizer) to non-axial tissues (red). d, e, labelling of parts of the tail at 24□h after fertilization. Axial parts are labelled by shh and CA2-IX (d); non-axial by eveI (e). cn, chordo-neural hinge; fp, floor plate; h, hypochord; n, notochord. (A) Dorsal (red) and ventral (green) marginal grafts of the early gastrula embryo. (B) Transplantation from the dorsal to ventral margin organizes secondary head and trunk. (C) A graft of the ventral margin at the animal pole results in the formation of a secondary tail, but no containing axis. ap, animal pole; v, ventral; d, dorsal. B, C, lateral view, anterior to the left, dorsal to the top; A, lateral view, anterior to the top and dorsal to the right (Modified from Agathon et al., 2003 and Fauny et al., 2009).

Table 3-2.   Prediction of possible functional *cis*-elements CRE and Smad BE.

Gene name	Type of cis element	Position	Sequence
URP	CRE	-459 to -470	TCTGACGTCATC
	Smad4 BS	no	
	Smad3-Smad4 BE	no	
UIIα	CRE	-3293 to -3286	TGACATCA
	Smad4 BS	no	
	Smad3-Smad4 BE	no	
UIIβ	CRE	no	
	Smad4 BS	-2361 to -2339	GACAGACAGACAGACTGACAAA
	Smad3-Smad4 BE	-1636 to -521	CAGACAGACAGACA [1]
bmp4	CRE	-2739 to - 2732	TGACGTCA
		-4032 to - 4025	TGACATCA
spaw	CRE	- 2568 to - 2561	TTACGTCA
cyclops	CRE	-1413 to -1404	GTGAGTTCAT
		- 207 to -200	TGACGTCA
smad5	CRE	-1052 to -1045	TGACGTCA
		-2821 to -2814	TGATGTCA
smad4	CRE	no	

Note: Search parameters: Expected mean number: 0.0100000; Statistical Siginicance Level: 0.9500000; Level of homology between known regulatory element/consensus and motif:80%; Variation of Distance between regulatory element/consensus Blocks: 20%; (1): from -1636 to -521, this sequence or extremely similar sequence is repeated 25 times.
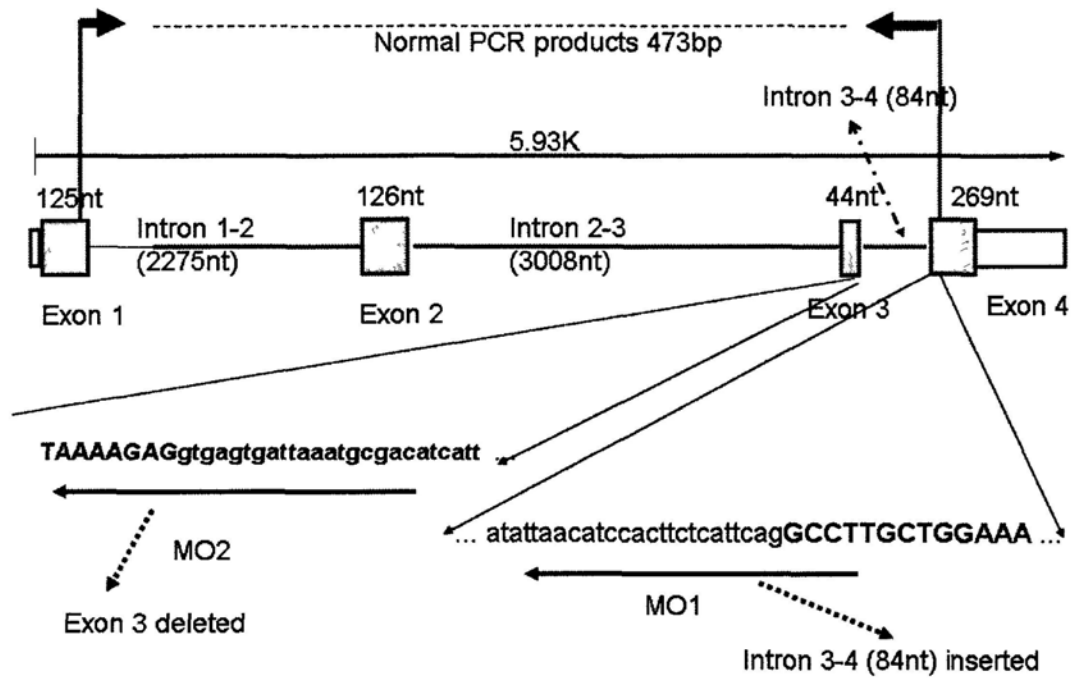
100

Fig. 3-7. Schematic of the strategy to block the pre-mRNA splicing by MO.

MO1 blocks the intron3-4-exon4 splice junction, which will result in the insertion of intron3-4 into the mRNA and generate a new stop codon in the interior of ORF. MO2 blocks the exon3-intron3-4 splice junction, which will cause the deletion of exon3. Red arrows represent primers used in the RT-PCR to tell the efficiency of splice-blocking MO.
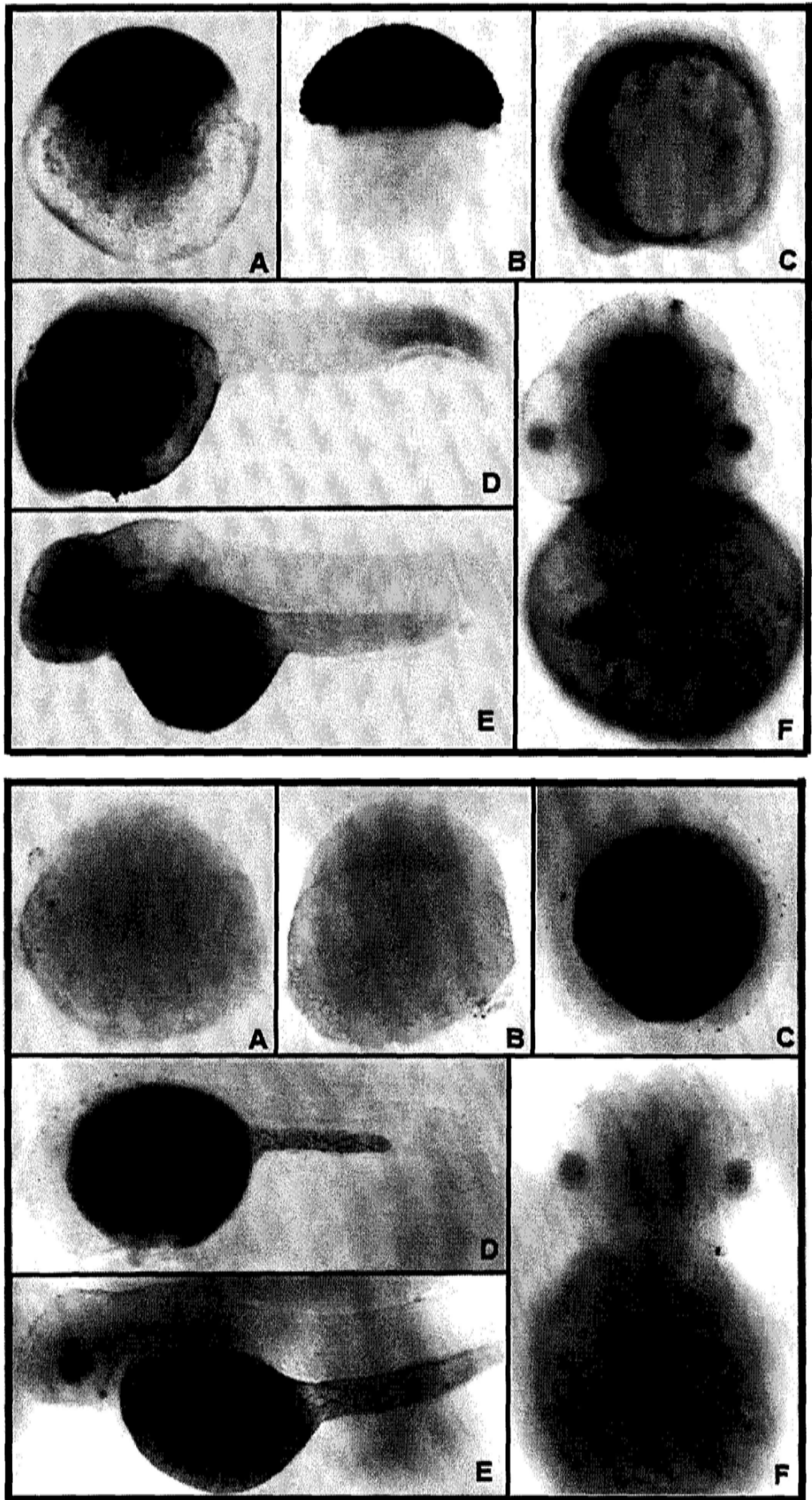
Fig. 3-8. Spatial and temporary expression of UIIβ during early embryonic development.

A: 1 cell (0 - 0.75 hpf), animoral pole to the top, lateral view; B: sphere (4hpf), animal pole to the top, lateral view; C: 10 somites (14hpf), anterial to the left, lateral view; D: Prim-5 (24 hpf), anterior to the left, lateral view; E: Long-pec (48 hpf), anterior to the left, lateral view; F: Long-pec (48 hpf); ventral view, anterior to the top. Panel I : RNA in situ hybridizations of whole embryo using the anti-sense RNA probe; Panel II : Control for the RNA in situ hybridizations of whole embryo using the sense RNA probe. This picture shows the expression of UIIβ during zebrafish embryogenesis. Note: hpf: hours post fertilization.
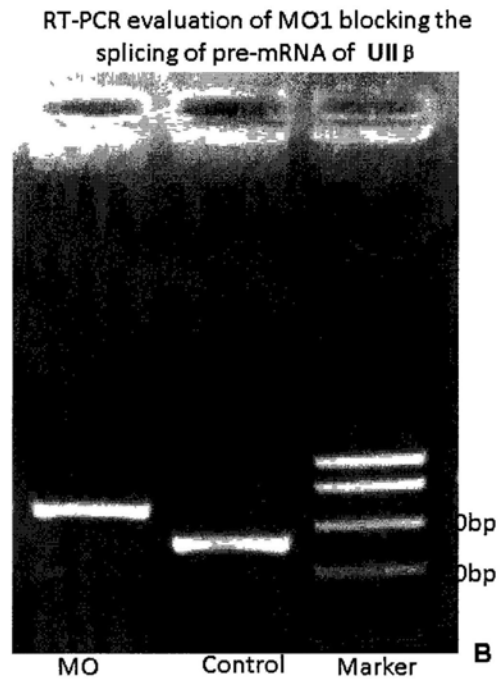
Fig. 3-9. Validation of MO1 (knockdown by splice-blocking).

RT-PCR was performed on wild-type embryos and embryos injected with 1.5 ng of the MO1.

The MO1 efficiently blocks **UIIβ** mRNA splicing by intron 3-4 insertion into the **UIIβ**

mRNA. Bands of 473 bp and 557bp (473 bp +84bp) represent wildtype and intron

3-4-inserted mRNA, respectively.
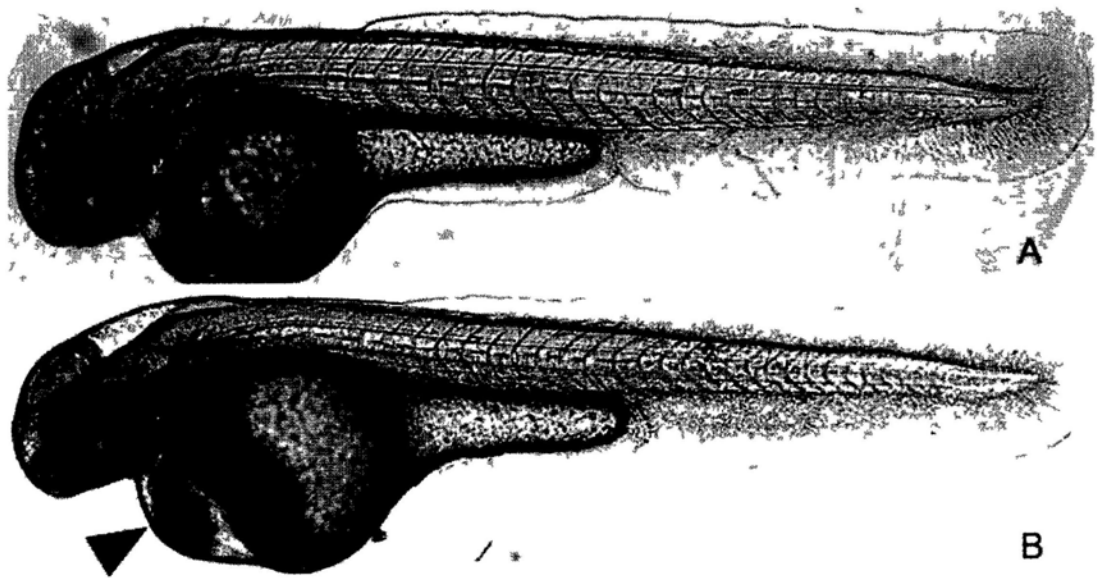
Fig. 3-10 UIIβ morphant phenotypes. Lateral views at 42 hpf.

A: Control-MO-injected embryos; B: UIIβ-MO-injected embryos. The UIIβ-MO1-injected embryos appeared morphologically normal except for distinctly pericardial edema (red rrowheads) and slightly somite-fused tail. A, B: lateral view, zebrafish line: tp53M214K, its p53 gene is mutated and loses the DNA-binding function.

Fig. 3-11a UIIβ knockdown randomizes the direction of cardiac jogging and heart looping.

Fig. 3-11a UIIβ knockdown randomizes the direction of cardiac jogging and heart looping.

A, Hearts were visualized via WISH for *nkx2.5* at 24 hpf, dorsal view and anterior to the top. Control embryos show the normal leftward-jogging heart. Arrow depicts the direction of atrium jogging with respect to the embryo m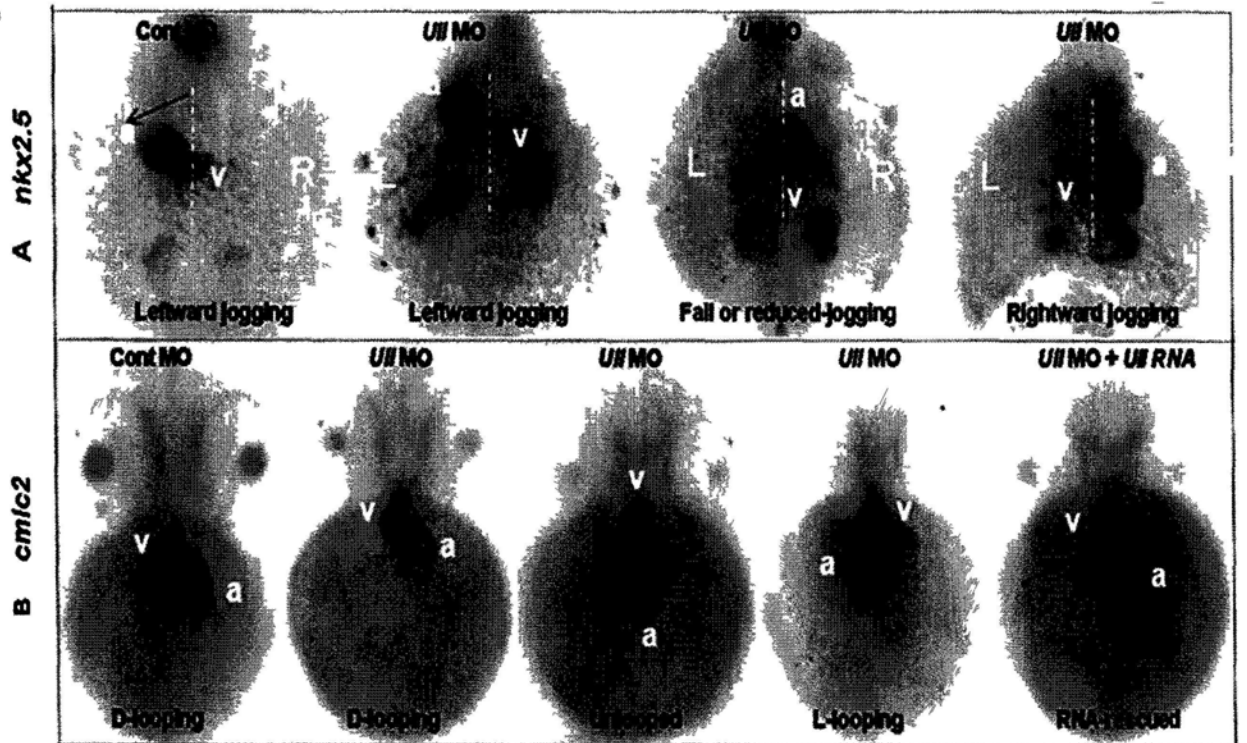idline. UIIβ-MO1-injected embryos display all kinds of cardiac jogging (rightward-jogging, fail or reduced-jogging or leftward-jogging heart). **B,** Hearts were visualized via WISH for *cmlc2* at 42 hpf, ventral views. Control embryos exhibit a normal heart looping (D-looping: the ventricle loops to the right and the atrium loops to the left). UIIβ-MO1-injected embryos manifest three types of heart looping (L-looping, no looping or D-looping). Co-injection of UIIβ mRNA with UIIβ-MO1 rescued the cardiac phenotype induced by UIIβ inhibition. a, atrium; v, ventricle; L, left; R, right; WISH, whole mount in situ hybridization.
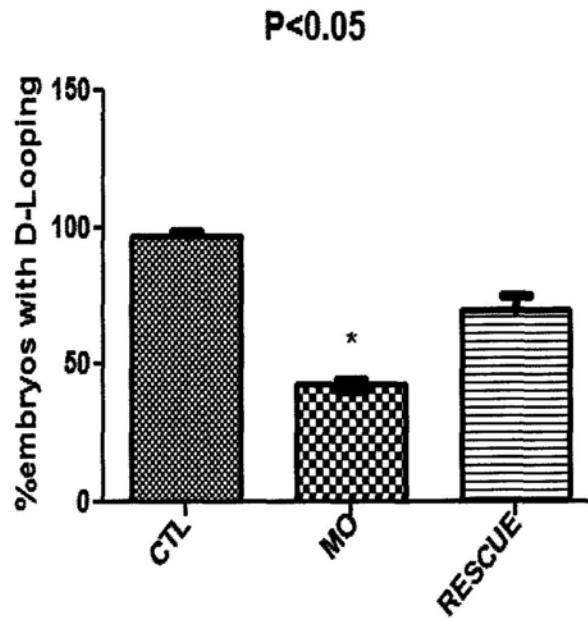
Fig.3-11b Graphical summary of the effect of UIIβ knockdown on the normal cardiac D-looping morphogenesis.

Calculation as % of embryos with D-looping in embryos injected with MO1(MO), Control MO (CTL) or MO1 and UIIβ mRNA (Rescue). The results were from 3 injection experiments. Error bars were ±SEM. *indicates statistical significance at $p<0.05$ by one-way ANOVA. The statistical analysis is performed using the software GraphPad PRISM Version 5.0. (GraphPad, San Diego, CA)(www.graphpad.com).
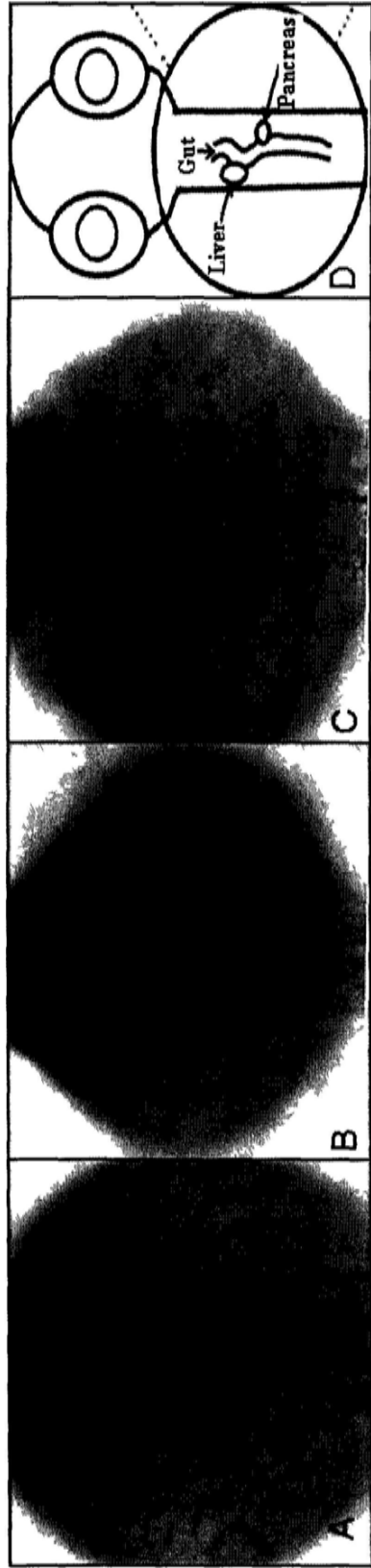
	% normal	% middle
Control MO	99	1
MO	19.4	80.6

Fig. 3-12 Laterality of visceral organs is perturbed by UIIβ knockdown. Visceral organs were were visualized via WISH for *foxa3* at 36hpf. A, Control embryos with normal distribution of visceral organs show that the liver is located at the left side of embryo and the pancreas posits at the right side of embryo with respect to midline; B, the minority (19.4%) of UIIβ-MO1-injected embryos with normal distribution of visceral organs; C, the majority (80.6%) of UIIβ-MO1-injected embryos with abnormal distribution of visceral organs. Their liver and pancreas are normally positioned on the midline and the looping of gut disappears. D, Cartoon indicates the wild-type distribution of visceral organs. All embryos, dorsal views and anterior to the top; L: liver; G: gut; P: pancreas.
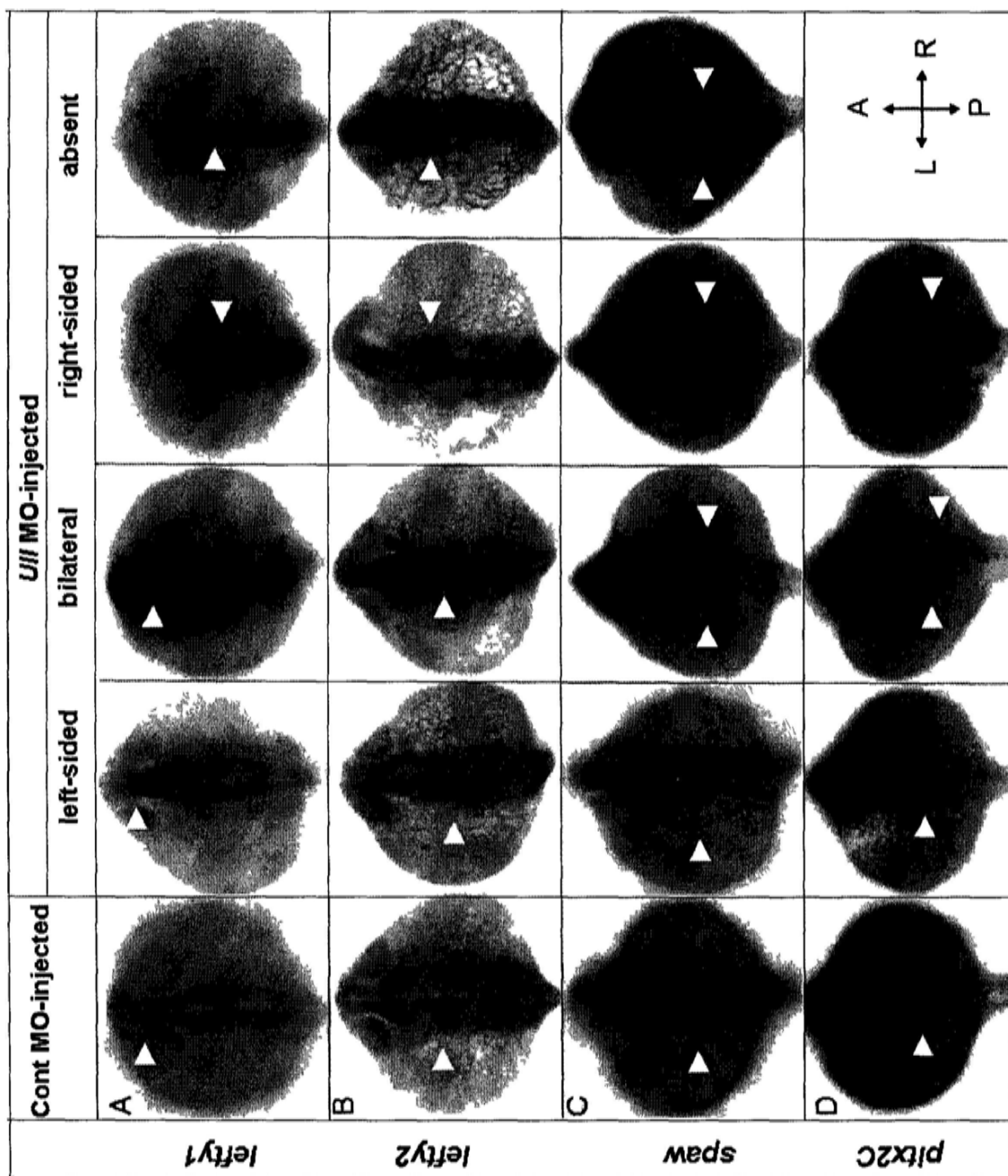
109

Fig. 3-13 the expression of asymmetric genes is randomized in UIIβ-knockdown embryos.

(A–D), analyses of the expression pattern of asymmetric gene *lefty1* (A), *lefty2* (B), *spaw* (C) and *pitx2c* (D) in control and UIIβ-knockdown embryos at 22-24s stages using the whole-mount mRNA *in situ* hybridization. L, *left* side; R, *right* side; A, anterior; P, posterior. All embryos are dorsal view and anterior to the top. The *lefty1* is normally expressed on the left side of diencephalon at 22–24s stages; however, among UIIβ-knockdown embryos it shows a randomized expression in the diencephalon and all kinds of expression patterns can be observed, including left-sided, right-sided, bilateral, or absent expression pattern.(A, arrowhead). The *lefty 2* is left-sided expressed on the heart primordial of wild-type embryos; but, like *lefty1*, UIIβ-knockdown also randomized the expression pattern of this gene (B, arrowhead). The *spaw*, a ligand for Nodal signaling pathway, is the earliest asymmetrically expressed molecular marker in zebrafish. This gene is expressed in the left LPM preceding asymmetric *lefty1* or *pitx2* expression. Our observation uncovered that the nodal related gene spaw was also randomized in UIIβ-MO-injected embryos (C, arrowhead). As for pitx2, the similar phenomenon can be observed (D). The frequency of randomized expression is shown in the Table 3-3.

Table 3-3 Frequency for the randomization expression of laterality genes

Effect of *UII* knockdown on *lefty1* expression in the diencephalon.

	% left	%bilateral	%right	%absent	Total embryos
Control	99	1	0	0	100
MO	16.9	45.0	16.7	21.3	160

Effect of *UII* knockdown on *lefty2* expression in the lateral plate mesoderm.

	% left	%bilateral	%right	%absent	Total embryos
Control	99.3	0.7	0	0	301
MO	33.3	47.1	14.1	5.4	276

Effect of *UII* knockdown on *spaw* expression in the lateral plate mesoderm.

	% left	%bilateral	%right	%absent	Total embryos
Control	98.7	0.6	0.6	0.0	311
MO	20.5	62.1	12.1	5.4	298

Effect of *UII* knockdown on *pitx2* expression in the lateral plate mesoderm.

	% left	%bilateral	%right	%absent	Total embryos
Control	100	0	0	0	80
MO	27.7	56.9	15.4	0	65
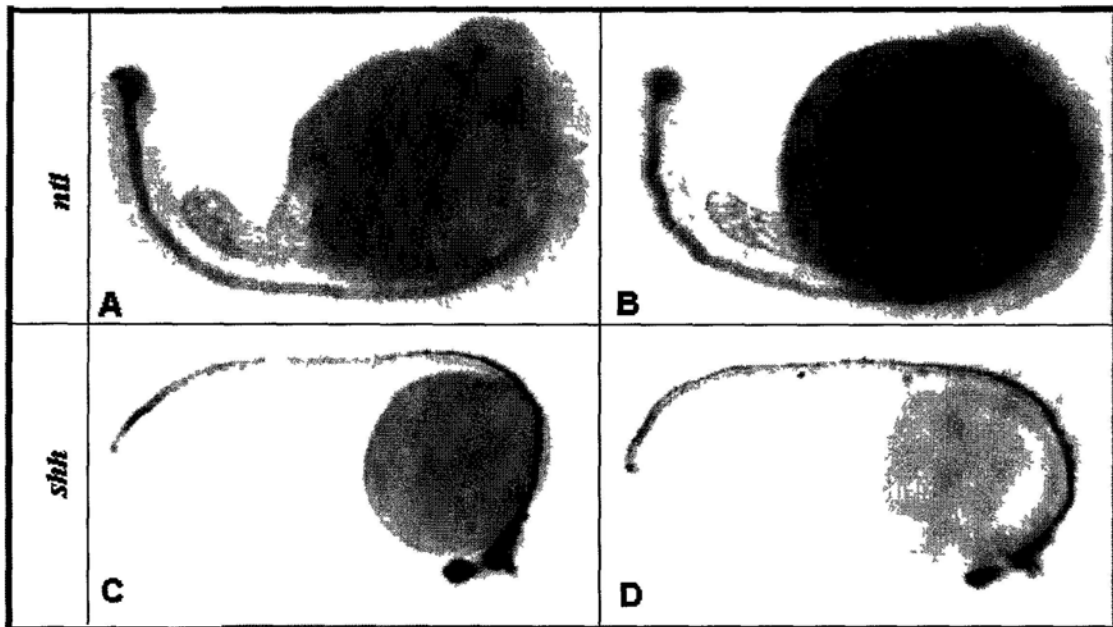
Fig.3-14 Midline development is normal in UIIβ knockdown embryos

(A, B) RNA in situ hybridization (ISH) analysis of *ntl* expression, which marks the notochord in the midline, In contrast with the control (A) no sharp difference is observed in UIIβ morphants except for little zigzag notochord in tail (B). (C, D) RNA ISH analysis of *shh* expression, which marks the floor plate and hypochord in the midline, there is no clear differentia between the controls (C) with UIIβ morphants (D). All embryos is lateral view at 22-24 somite stage.

Fig. 3-15a Reducing of UIIβ levels perturbs KV morphogenesis

114

Fluorescent

Injected Calcium
Green indicator
+ MO

Injected Calcium
Green indicator
+ U2b mRNA

DIC

MO or Overexpression

Fluorescent

DIC

Control

Un-injected Calcium
Green indicator

Injected Calcium
Green indicator

Injected Calcium
Green indicator +
control MO

Injected Calcium
Green indicator
+ control RNA
(antisense RNA of
EGFP)

Fig.3-15b

115
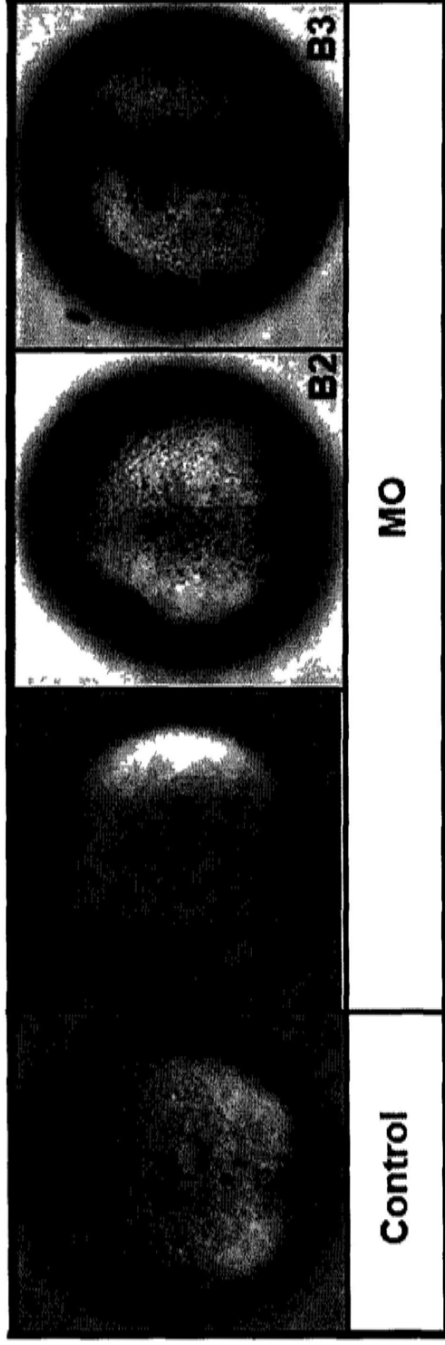
Fig. 3-15 Reducing of UIIβ levels perturbs KV morphogenesis and stirs the asymmetrical distribution of intracellular Ca²⁺ flux around the KV region.

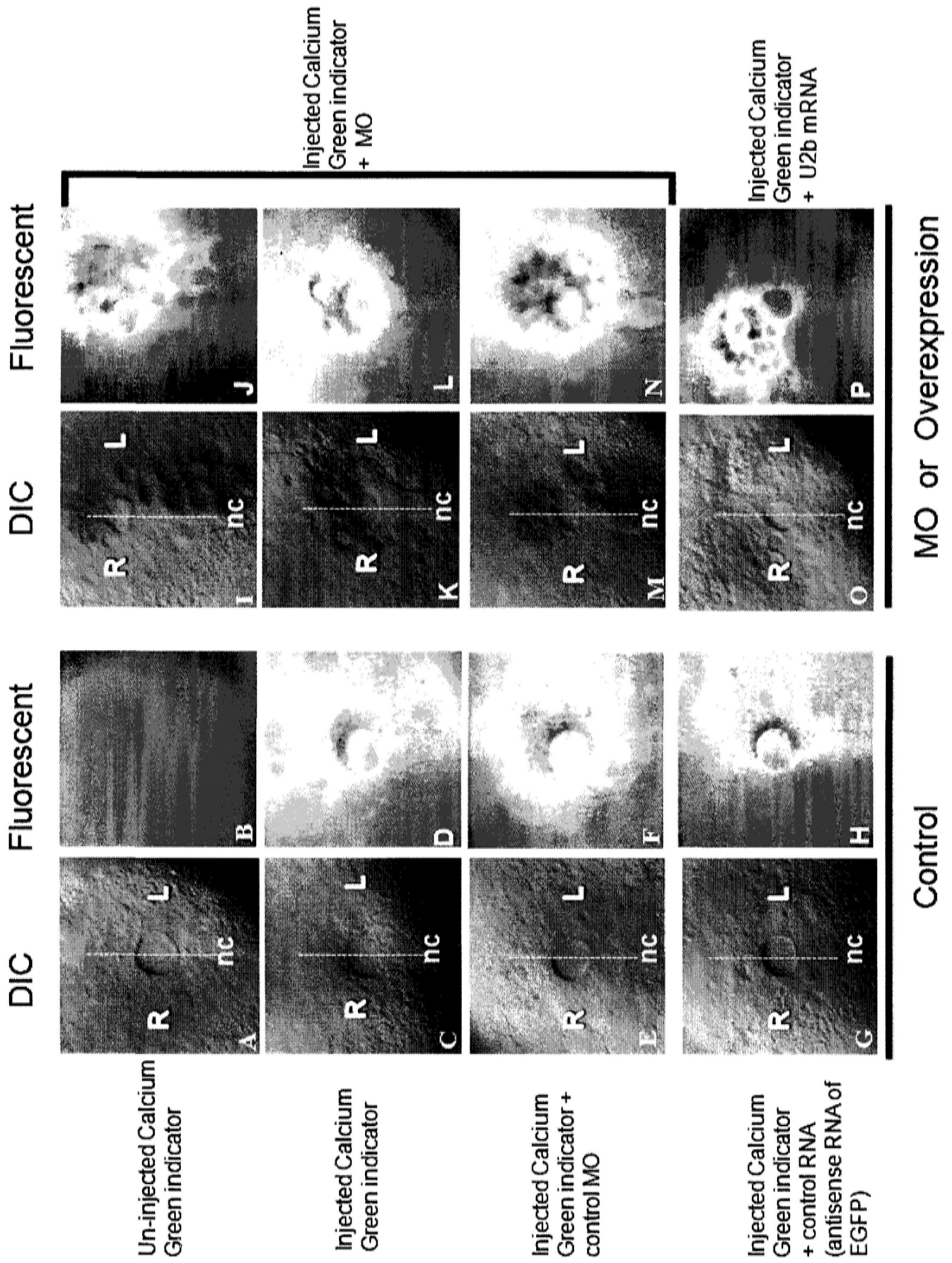(Fig.3-15a) repression of UIIβ levels results in reduced KV size and multi-KV structure. Embryos coinjected with Ca²⁺ indicator and UIIβ-MO exhibit different extents of morphology defect of KV (B1, B2, B3), when compared with embryos coinjected with Ca²⁺ indicator and control MO (A). These pictures from the differential interference contrast (DIC) microscopy show the defect of developing KV.

(Fig.3-15b) the distribution of free cytoplasmic Ca²⁺ (intracellular Ca²⁺) at KV during zebrafisfe early somite stages (5s-8s) was visualized with a Ca²⁺ indicator. Ca²⁺ patterns at 5–8 SS were imaged by fluorescence microscopy, and images were converted to an intensity scale (red indicating high intensity; yellow/green, moderate; blue/black, low). (A and B): Autofluorescence of an uninjected 5–8 SS embryo (B) with corresponding DIC (A). (C and D): A representative embryo injected with only Ca²⁺ indicator and showing fluorescence at KV (D). (E and F): Embryos injected with Ca²⁺ indicator and the control MO. (G–H): Embryos coinjected with Ca²⁺ indicator and the control RNA (antisense RNA of EGFP). (I–N): Embryos coinjected with Ca²⁺ indicator and UIIβ-MO exhibit different extents of defect of KV(I, K, M) and different kinds of abnormal distribution of intracellular Ca²⁺ flux around the KV region (J, K, N). (O and P): Embryos coinjected with Ca²⁺ indicator and UIIβ mRNA L, left; R, right; nc, notochord. All embryos is showed at 5s-6s stage, focued on the KV region, ventral view and anterior to the top. KV is in the ventral tailbud region.

116
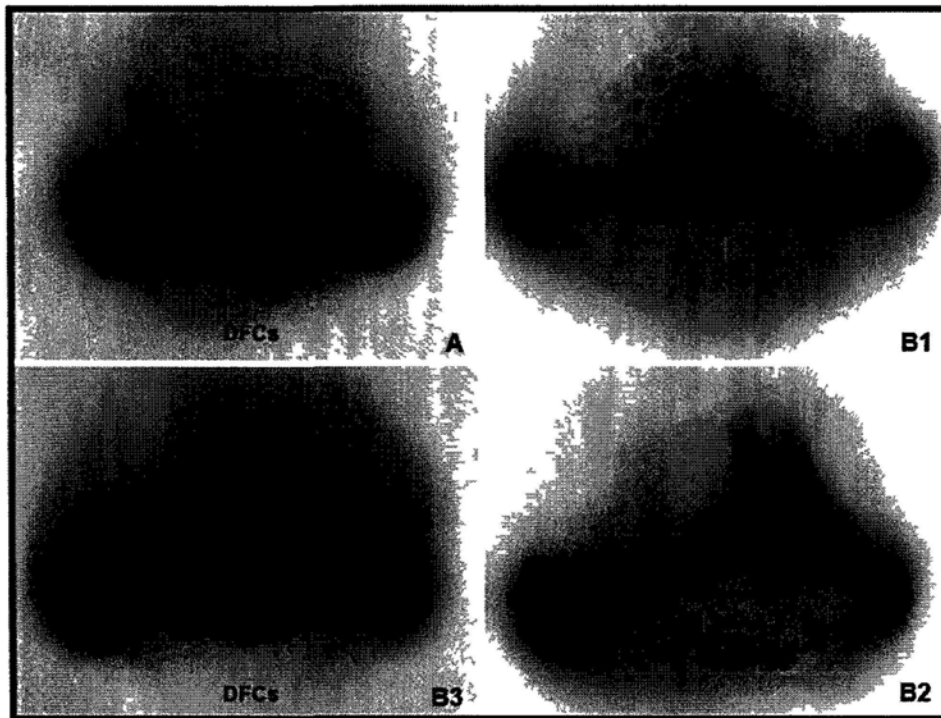
Fig.3-16 UIIβ knockdown alters DFCs development

During gastrulation, in addition to being expressed in margin cells, including the dorsal organizer margin region and ventral margin, paraxial mesoderm and prechordal plate *ntl* is also expressed in DFCs. RNA in situ analysis of *ntl* at 80% epiboly stage embryos to appear the morphology of DFCs. In a control embryo, DFCs form a single, compact DFC cluster (A); but in UIIβ knockdown embryos the morphological defect of DFCs can be observed (B1, B2 and B3), which mainly displays absent (minority or significantly smaller but multiple DFC clusters (majority) and disperse at the ahead of dorsal organizer magian (B1-B3, arrow).
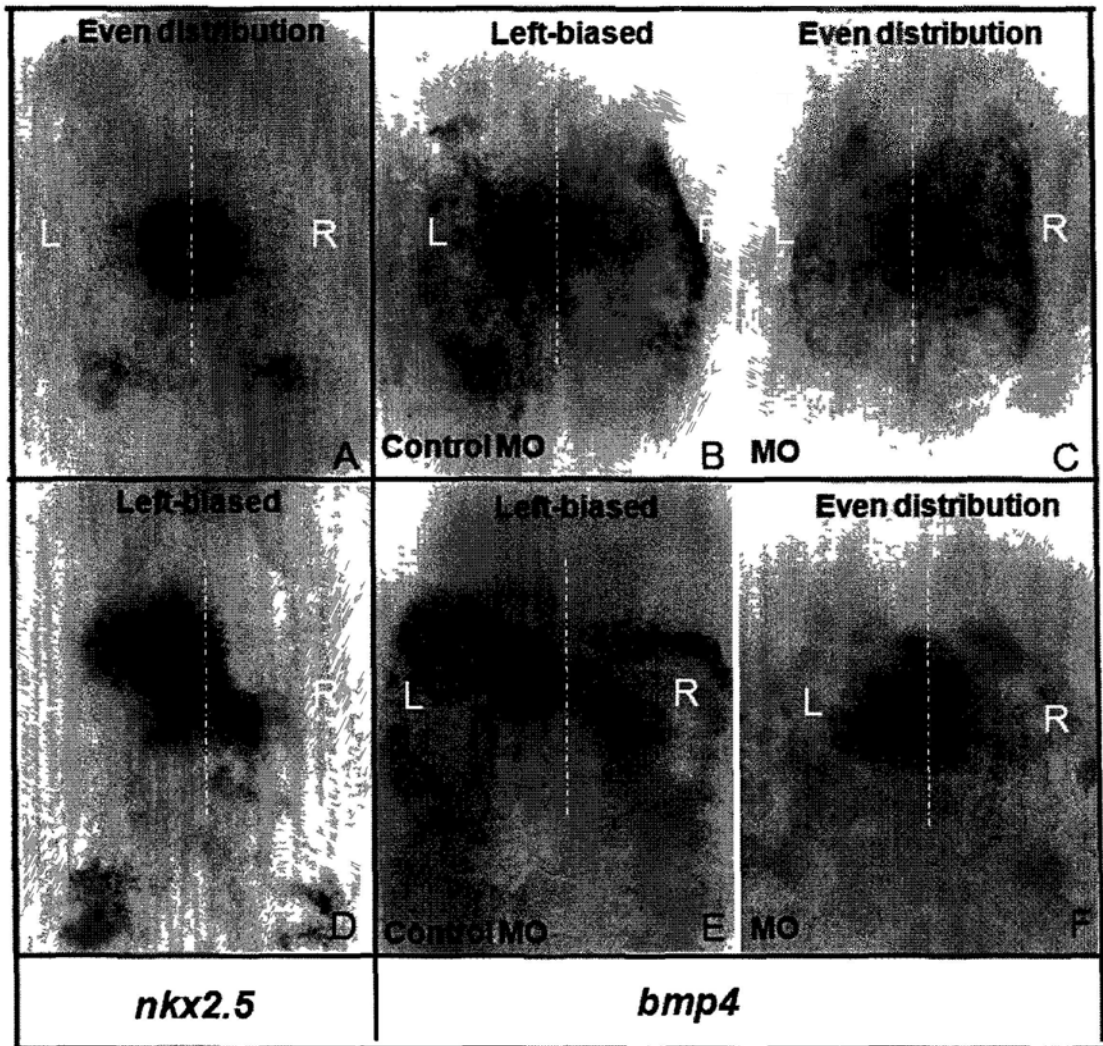
Fig.3-17 UIIβ-knockdown altered the asymmetrical expression pattern of *bmp4* in cardiac field and LPM at the 20–22 somite stage.

Fig.3-17 UIIβ-knockdown altered the asymmetrical expression pattern of *bmp4* in cardiac field and LPM at the 20–22 somite stage.

A, the shape of cardiac cone of wild-type embryo were visualized via WISH for *nkx2.5* at the 20–22 somite stage; D, the shape of heart tube of wild-type embryo were visualized via WISH for *nkx2.5* at the 24hpf stage. At late segmentation stages, *bmp4* expression is confined to the cardiac field and LPM. from 20s stage, *bmp4* expression in the left LPM is transiently up-regulated and is stronger on the left compared with the right side LPM. *bmp4* shows an asymmetric expression pattern (B, from 22s to 24s stage; E, 24hpf). However the asymmetrical distribution of bmp4 transcript can be disrupted by UIIβ knockdown. The injection of UIIβ-MO results in a down-regulation of *bmp4* expression in the left LPM (C, from 22s to 24s stage; E, 24hpf). At 24hpf the difference of bmp4 expression pattern between the controls (E) and UIIβ morphant embryos became much more distinct (F). All embryos are lateral views with anterior to the top.
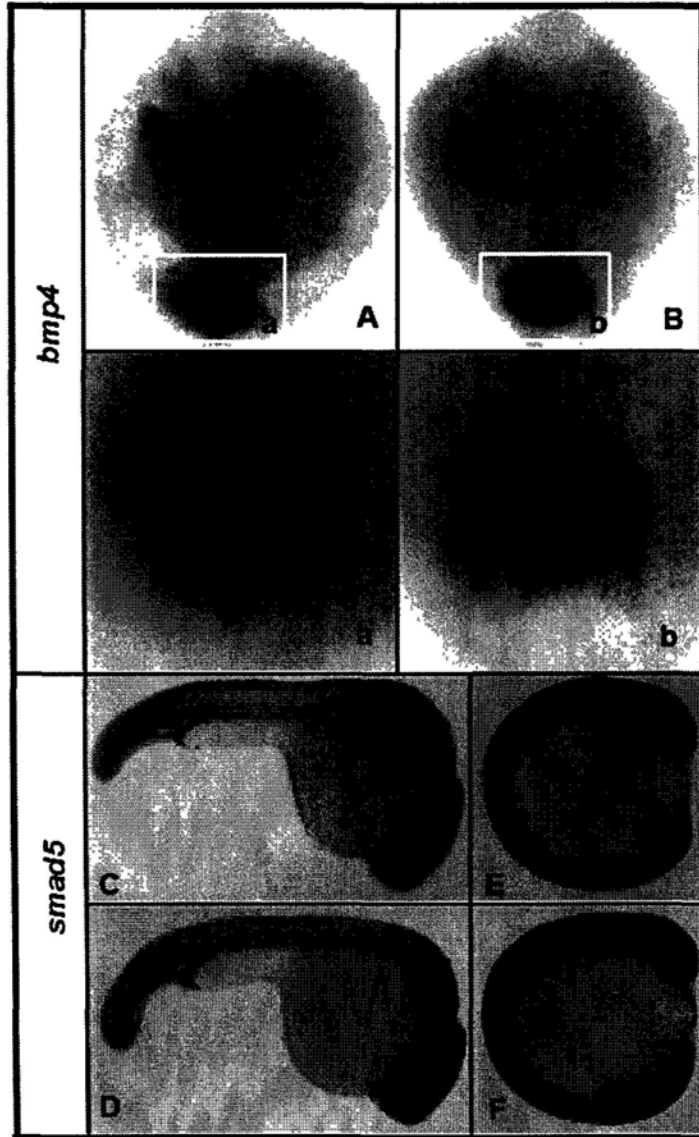
Fig.3-18 At the early segmentation stage the *bmp4* expression is significantly down-regulated by UIIβ knockdown.

Fig.3-18 At the early segmentation stage the *bmp4* expression is significantly down-regulated by UIIβ knockdown.

Boxed area in A (MO) and B (Control) show the *bmp4* expression in the tailbud and at the periphery of Kupffer's vesicle at 10s stage embryo and are enlarged in a (MO) and b (Control). The *bmp4* expression in the tailbud and at the periphery of Kupffer's vesicle is down-regulated by UIIβ Knockdown (a, b); on contrary, in polster the transcripts of *bmp4* are up-regulated by UIIβ Knockdown (A, B). Tthe transcripts of *smad5* were visualized via WISH at 10s stage and the 24hpf stage and no distinct difference is observed between UIIβ-MO-injected embryos (D and F) and the control (C and E). A and B, ventral view with anterior to the top at 10s stage; C and D, lateral view at 24hpf stage; E and F, lateral view at 10s stage. MO-injected embryos, A, a, D and F; Control-MO-injected embryos, B, b, C and E.
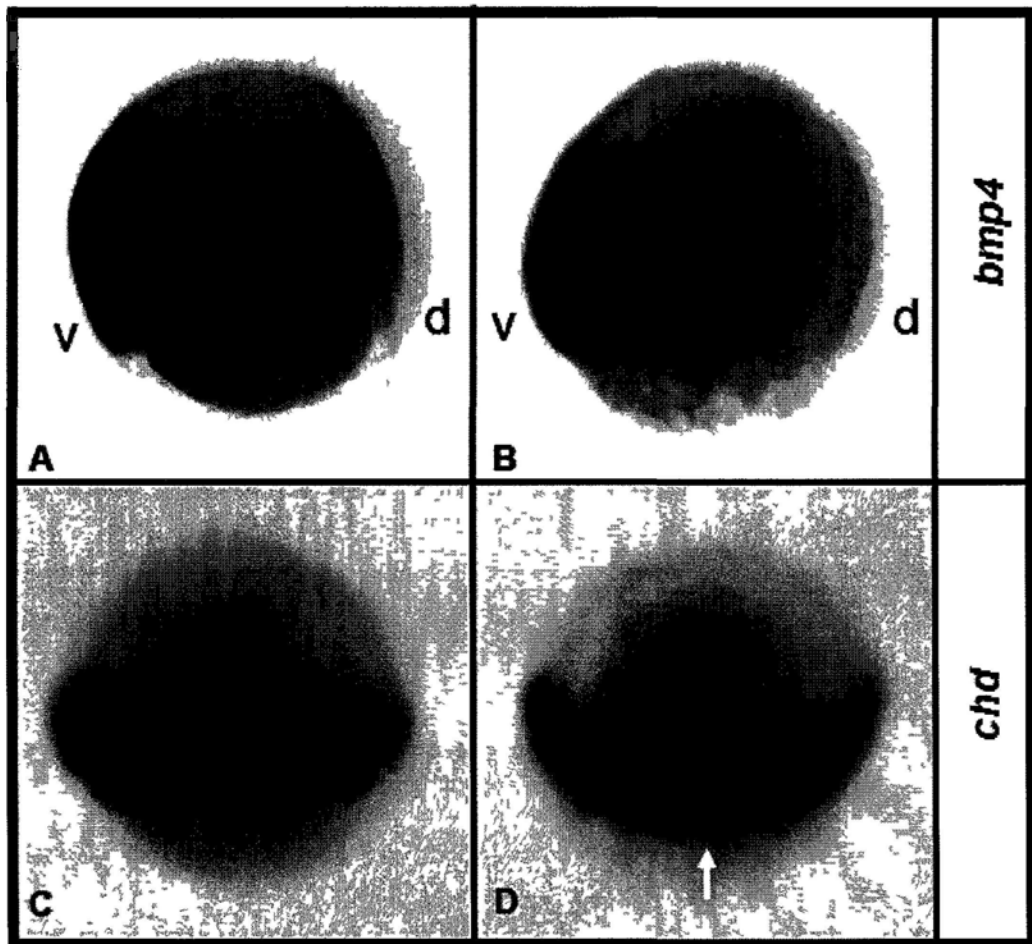
Fig.3-19 During zebrafish gastrulation gradient distribution of *bmp4* along ventral-to-dorsal axis *in* UIIβ morphant embryos is reduced.

Fig.3-19 During zebrafish gastrulation gradient distribution of *bmp4* along ventral-to-dorsal axis *in* UIIβ morphant embryos is reduced.

A (The control embryos) and B (UIIβ morphant embryo) show the bmp4 expression along ventral-to-dorsal axis at 85% epiboly stage. The gradient distribution of *bmp4 along* ventral-to-dorsal axis *in* UIIβ morphant embryos is reduced by UIIβ knockdown. A and B, lateral view, the dorsal to right and animal pole to the top at 85% epiboly stage. C (The control embryos) and D (UIIβ morphant embryo) show the *chd* expression in the dorsal side at 85% epiboly stage. It is worthy of noting that the BMP antagonist gene, *chordin*, not only appears significantly up-regulated expression in dorsal Spemnna organizer region and margin along dorsal-ventral axis in UIIβ morphant embryos but also shows ectopic expression in the DFCs domain (D arrow). C and D, lateral view, the dorsal to right and animal pole to the top at 85% epiboly stage. V, ventral side; D, dorsal side.
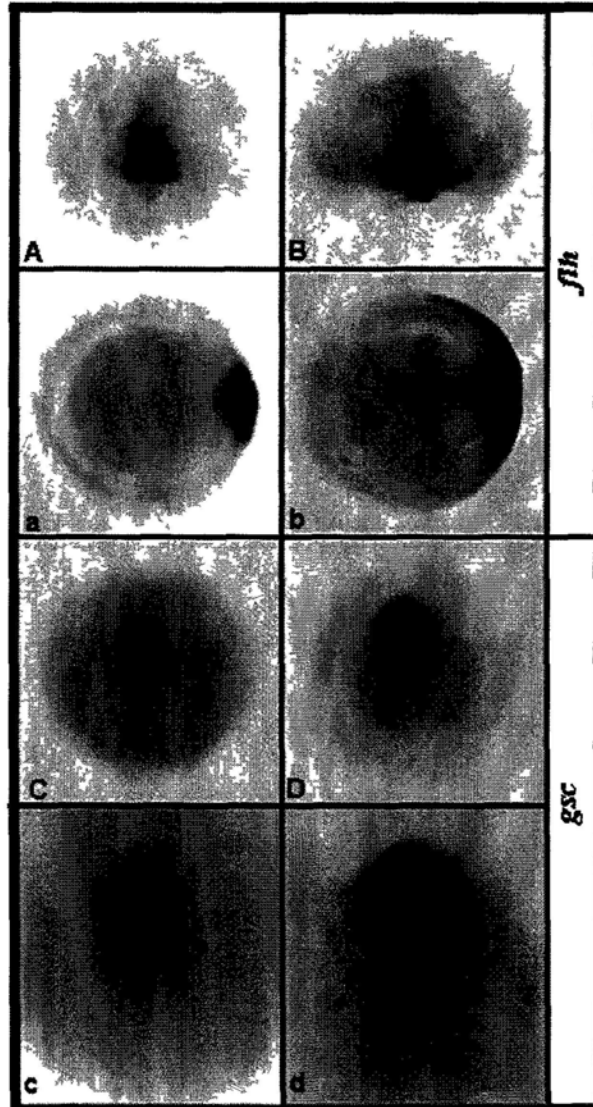
Fig.3-20a Enlargement of dorsal organizer
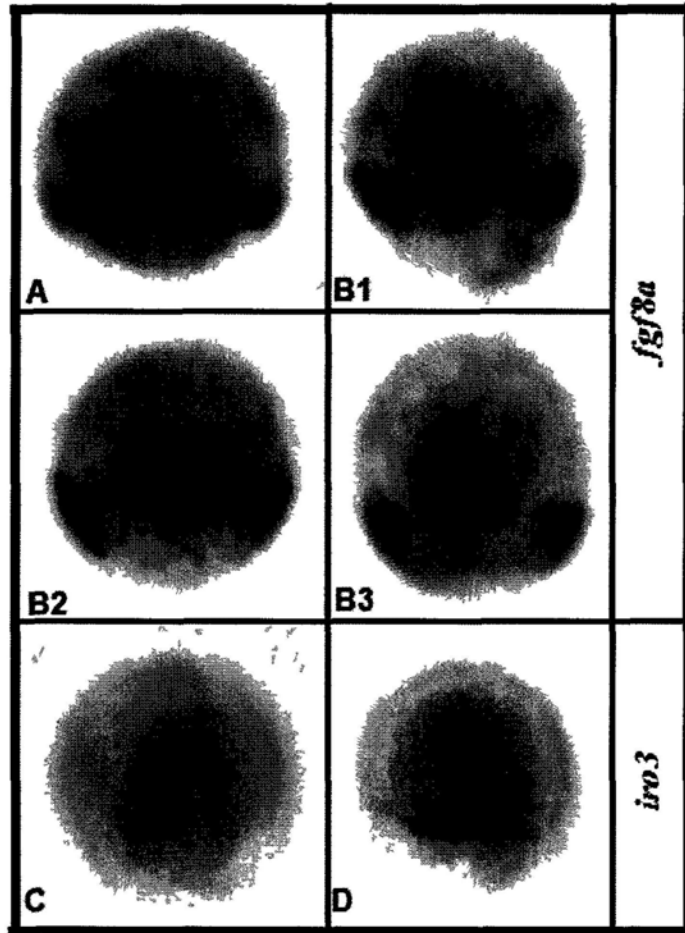
Fig.3-20b WISH analyses of organizer-regulating genes

Fig.3-20 Enlargement of dorsal organizer in UIIβ -Knockdown embryos

Fig.3-20a: UIIβ restricts dorsal organizer formation through suppressing fgf8 and iro3 activity. WISH analyses of organizer markers *flh* (A, B, a, b), *gsc* (C, D, c and d) in the control (A, a, C and c) and UIIβ MO1-injected embryos (B, b, D and d) at 80% epiboly stage. organizer markers *flh* shows territories of dorsal organizer. Embryos are dorsal views with the animal pole to the top in the A, B, C, D, c, and d. The a and b are animal views with the dorsal side to the right.

Fig.3-20b: WISH analyses of organizer-regulating genes *fgf8a* (A, B1, B2 and B3) *iroquois3* (C and D). the expression domains of organizer-regulating genes *fgf8a* and *iroquois3* are enlarged in reduced UIIβ embryos (B1,2,3; C, D), in contrast with the control embryos (A, and C), which indicates that **UIIβ** acts as a negative regulator to restrict the size of the dorsal organizer.
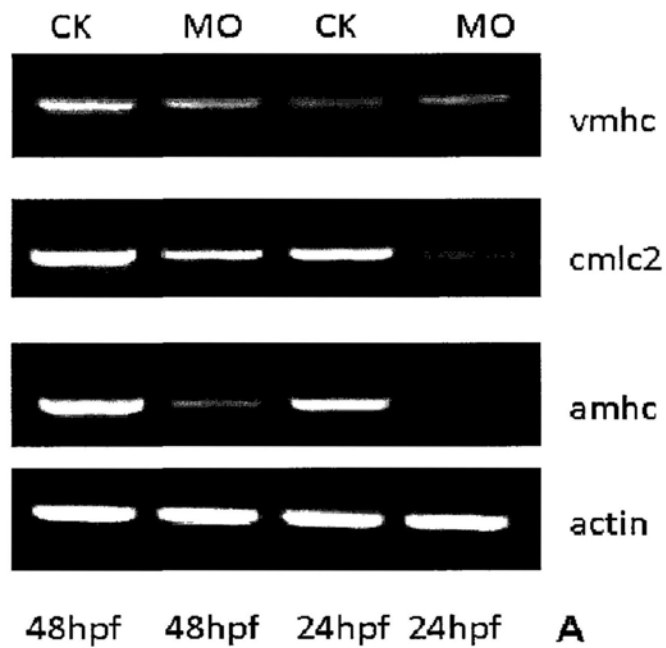
Fig.3-21 UIIβ knockdown interferes in the myocardium development

Using RT-PCR, we have evaluated the heart tube. At 24hpf and 48hpf, the myocardial marker *cmlc2* and atrial marker *amhc* were down-regulated by the UIIβ knockdown, but ventricular marker *vmhc* had no distinct change (Fig. 3-2 left panel). It appears that myocardium development suffered from some impact from the UIIβ knockdown

127
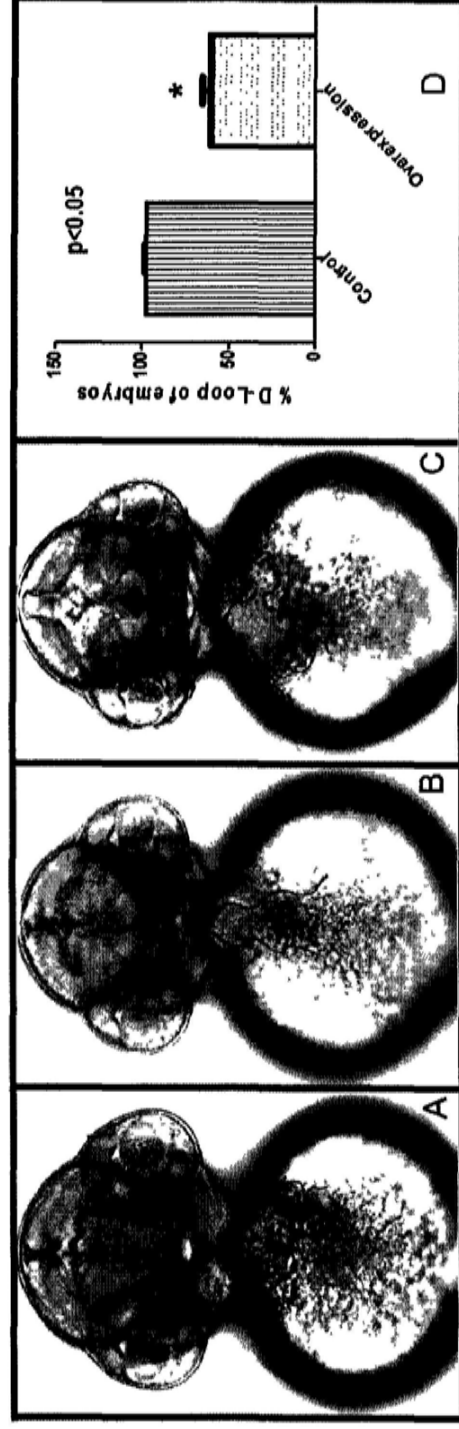
Fig. 3-22. Overexpression of UIIβ disrupts cardiac looping morphogenesis.

A: Control, D-looping; B: UIIβ-overexpression embryos, un-looping; C: UIIβ-overexpression embryos, L-looping; D: Graphical summary of

UIIβ overexpression disrupted normal cardiac D-looping morphogenesis at 48 hpf. Calculation as % of embryos with D-looping in control, Error bars were

±SEM.   * indicated statistical significance at $p<0.05$ with t-test (DIC picture, ventral view).
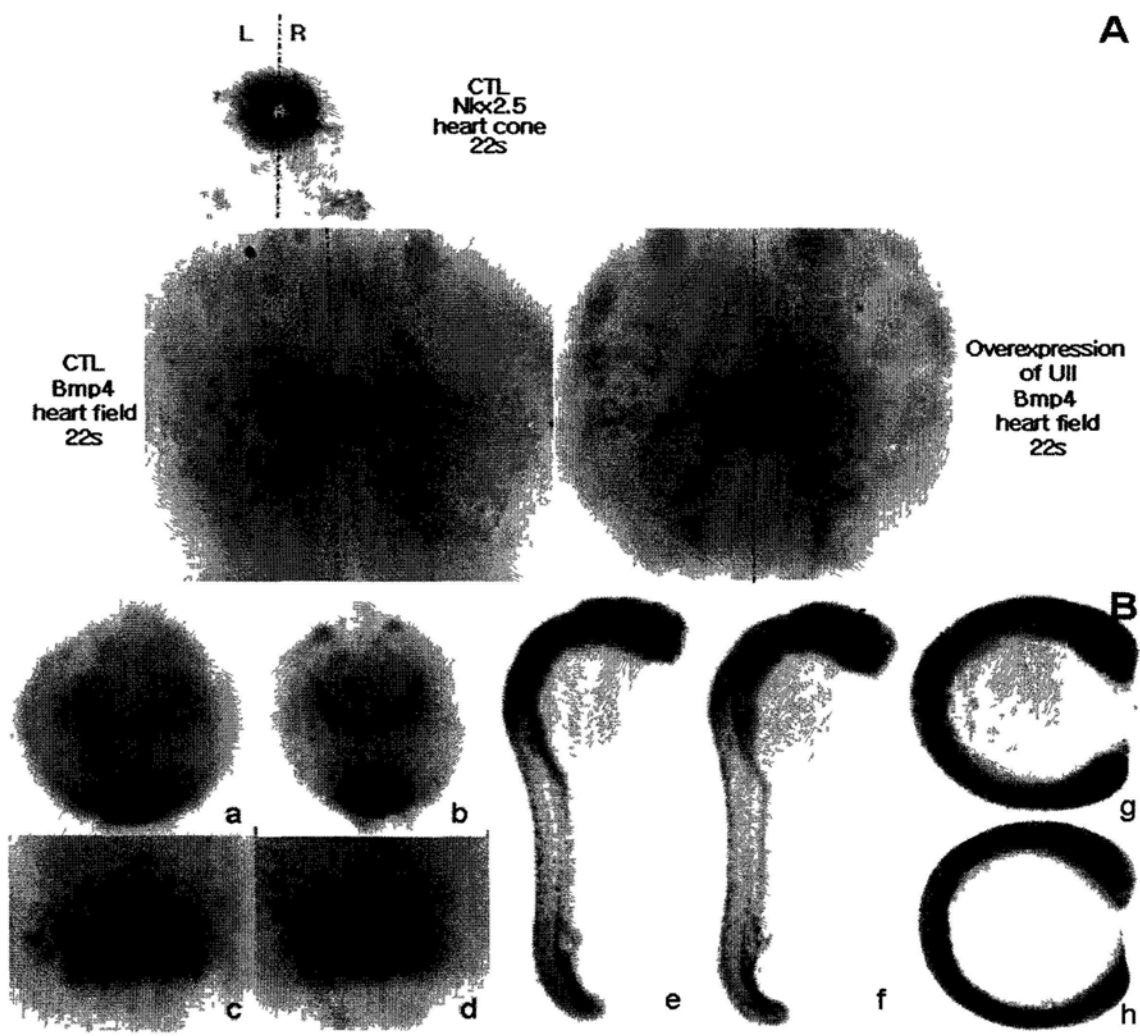
128

Fig. 3-23. Overexpression of UIIβ perturbs the L-R patterning of embryos by

altering Bmp signaling.

Fig. 3-23. Overexpression of UIIβ perturbs the L-R patterning of embryos by altering Bmp signaling.

A: *bmp4* at 22s dorsal view; B (a-d): *bmp4* at 10s ventral view; B (e f): *smad5* at 24. hpf lateral view; B(g, h): *smad5* at 10 s lateral view. Control: a, c e and g; UIIβ overexpression embryos: b, d f and h.

Both overexpression and knockdown of UIIβ seem to adopt similar strategies to regulate asymmetrical development of embryos, for example, the way to change Bmp signaling is similar (Fig. 3-23. A). In contrast to the controls, at 22s the *bmp4* expression in heart field and LPM of UIIβ morphant embryos not only becomes symmetric but is also upregulated in the overexpression embryos. While at 10s the expression pattern of bmp4 has a distinct variation: up-regulated in polster regions, instead, in tail region surrounding KV, *bmp4* is down-regulated. As for *smad5*, the change of its expression pattern caused by overexpression of UIIβ is the same as that of UIIβ knockdown: *smad5* expression has no significantly change at 10 somite stage and 24 hpf. (Fig.3-23. B).

Morphological phenotypes of WT zebrafish embryos
(AB or Tubingen) derived from fertilized eggs injected with MO

D, control MO at 85hpf

A, 3.2%   B, 37.8%   C, 46.0%
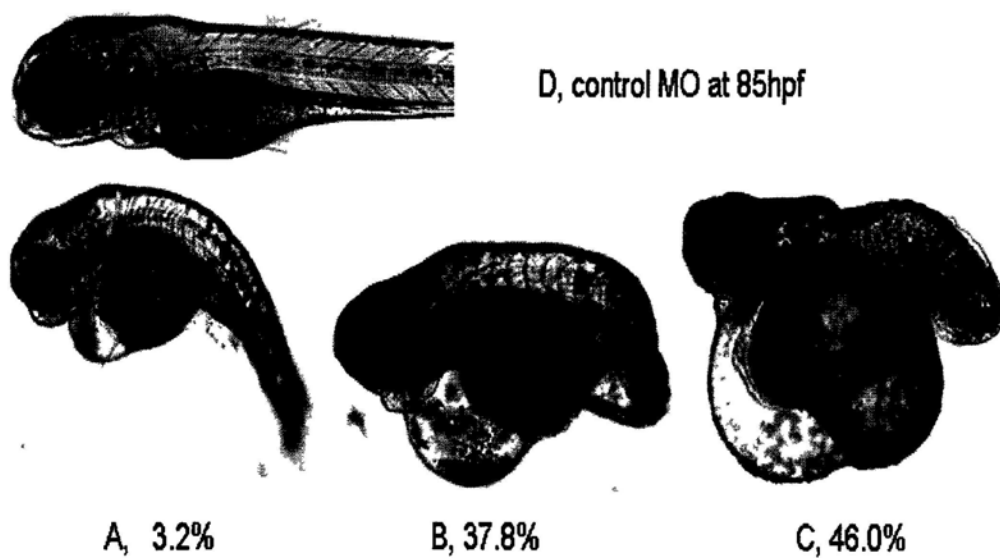
Fig. 3-24 Off-target effect of MO knockdown mediated through p53 activation.

A-C: UIIβ morphant embryos (AB or tubingen lines); D: Control. In this study, when initial

performing the UIIβ knockdown experiment we use the wild type zebrafish line AB or

Tubingen to inject UIIβ MO into their one-cell embryos. Embryos presented a consistent

phenotype with doses 1.5 ng MO/embryo (A, B and C), however, the phenotypes of UIIβ

morphants is similar with the general morphological features of MO-induced off-targeting neural

death as previously described by Robu et al., (2007).
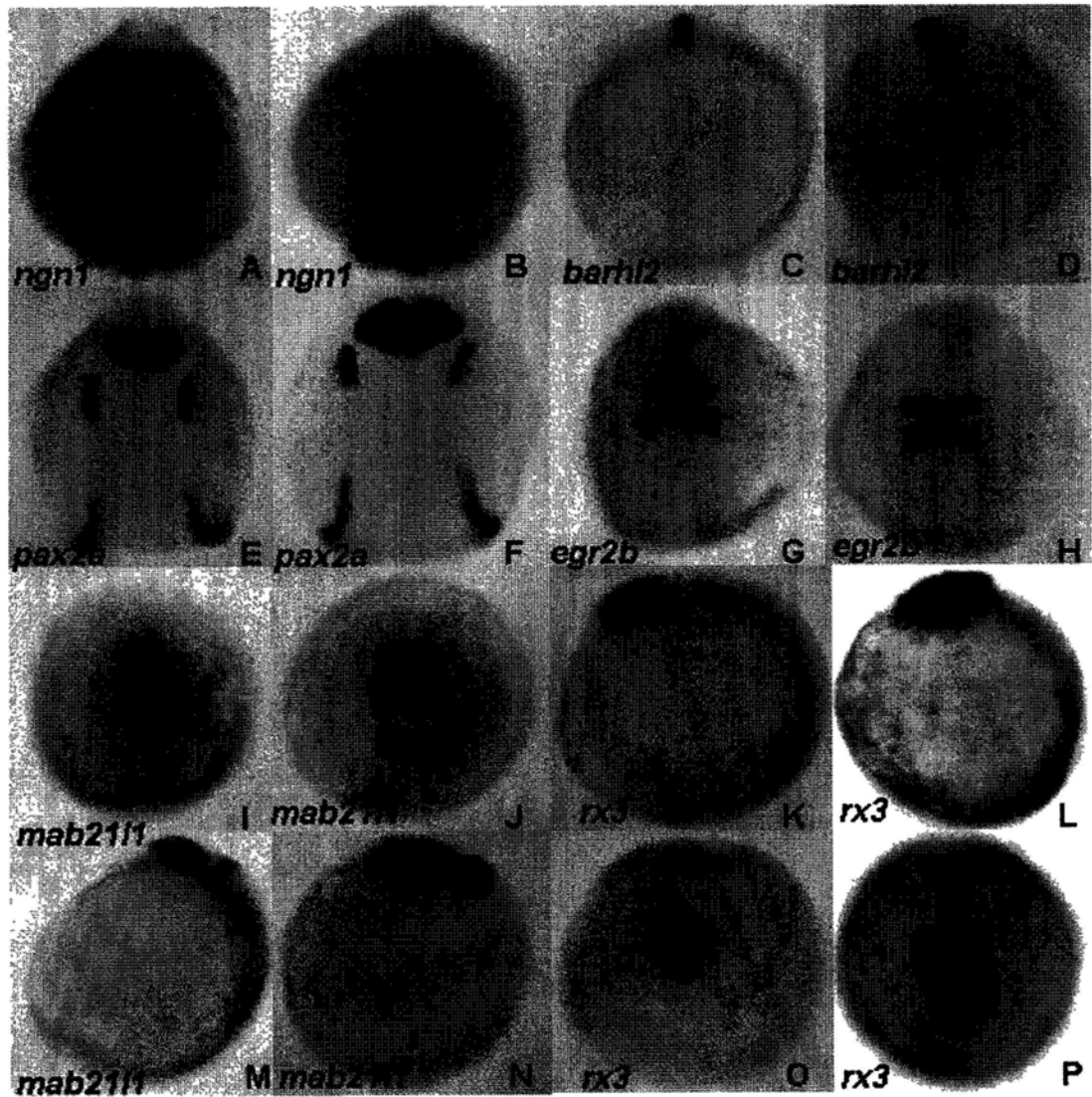
Fig. 3-25. Off-target effect of MO knockdown mediated through p53 activation.

Fig. 3-25. Off-target effect of MO knockdown mediated through p53 activation.

A-P: all embryos at 3 s belonging to the wild-type zebrafish AB or Tubingen line. A: UIIβ MO embryos show the neural progenitor cell marker *ngn1*; B: Control MO embryos show the *ngn1*; C: UIIβ MO embryos show the diencephalon marker *barhl2;* D: Control MO embryos show the *barhl2;* E: UIIβ MO embryos show the midbrain marker *pax2a;* F: Control MO embryos show the *pax2a;* G: UIIβ MO embryos show the rhombomere marker *egr2b;* H: Control MO embryos show the *egr2b;* I and M: UIIβ MO embryos show the eye anlage and midbrain marker *mab21l1;* J and N: Control MO embryos show the *mab21l1;* K and O: UIIβ MO embryos show the eye field marker *rx3;* Lnd P: Control MO embryos show the *rx3;* C, D, K, L , M and N: anterior up and lateral view. A, B, E and F: anterior up and dorsal view; I, J, O and P: focused on the top of eye field. As showed in the Fig.3-24 (A, B, and C), the phenotypes of UIIβ morphants is similar with the general morphological features of MO-induced off-targeting neural death previously described by RObu et al., (2007). We characterized these defects using a series of neural marker such as *ngn-1, pax2a, crestin, rx3, egr2b, barhl2* and *mab21l2* (Fig.3-25). Moreover we further found that these defects failed to be rescued. Instead, it is not the case in the UIIβ MO tp53M214K embryos; the phenotypes of UIIβ morphant in tp53M214K embryos can be rescued by injecting the UIIβ mRNA with UIIβ MO1. There are distinct different phenotypes between UIIβ MO tp53M214K embryos (B in Fig.3-10). with UIIβ MO wild-type embryo (A, B, and C in Fig.3-24) In the UIIβ MO tp53M214K embryos, no the neural death phenotypes, such as smaller heads and eyes, exhibit somite and notochord abnormalities, and eventually display craniofacial defects, were observed and we only found the pericardial edema and abnormal heart looping. Foremore, these defects may be successfully rescued.

Chapter 4 General Discussion

4.1 Overview

Although observations from different model organisms suggested several signals might be implicated into the process of vertebrate embryonic L-R patterning, the majority reports indicated that Nodal signaling and Bmp signaling are the two major pathways involved. In mouse, *nodal* is expressed in the node, and its asymmetric expression in the left LPM is directly regulated by itself (Shen et al., 2007). The *nodal* expression throughout the left LPM further results in induction of *pitx2* and *lefty2* expression in the left LPM, and of *lefty1* in the axial midline; In turn *lefty1* and *lefty2* antagonize nodal activity. Through the negative feedback loop the duration and extent of nodal signalling in the left LPM is elegantly regulated (Raya et al., 2006). In zebrafish two Nodal genes, *cyclops* (*cyc*) and *southpaw* (*spaw*), are also expressed symmetrically. Around the 20-somite stage, expression of *cyc* is confined to the left lateral plate and the presumptive epiphysis, which lies on the left side of the dorsal diencephalons (Rebagliati et al., 1998). The initial expression of *spaw* is limited in bilateral domains flanking KV at the 4–6 s (Long et al., 2008). At the 10–12 s, its expression becomes asymmetrical in the left lateral plate mesoderm. The *spaw*-deficient embryos display the orientation defects of visceral and diencephalon left-right asymmetry. Consistent with the morphological changes, the left-biased expression of downstream genes (*cyclops, pitx2, lefty1 and lefty2*) is severely downregulated or abolished within the lateral plate mesoderm of

spaw-deficient embryos (Long et al., 2003).

In zebrafish, the first evidence for bilateral symmetry breaking is from the observation of Chen et al., (1997), the left-sided expression of *bmp4* in the heart field directs the normal leftward jogging and subsequent D-looping of heart tube. Further report from Chocron et al (2007) indicated *bmp4* is involved in the establishment of L-R asymmetry of zebrafish embryo by repressing *spaw* expression in the right lateral plate mesoderm and regulating left-sided gene expression in the left lateral plate mesoderm. Smad5 is a downstream component in Bmp signaling cascade. In mice homozygous for a mutation in *smad5* the lack of or bilateral expression of *nodal, lefty2* and *pitx2* suggests that as repressor, Bmp signaling acts on upstream of Nodal signaling to repress Nodal signaling in the right LPM (Chang et al., 2000). Using *bmp4* null ES cells and *bmp4* mutant mouse embryos Fujiwara et al (2002) found that *bmp4* expression is required for node morphogenesis, *nodal* expression in the node is severely reduced and no expression was observed in the left LPM. Furthermore, the *bmp4* mutants show an abnormal flat shape of the node in contrast to the concave structure of the node in the wild-type embryos. In frog similar observations were also obtained (Branford et al., 2000; Schilling et al.,1999) and overexpression of *bmp4* on the right, but not on the left, induces reversal of heart looping, supporting the idea that enhanced one-sided *bmp4* expression in the heart field determines the laterality of embryos. These results suggest that *bmp4* signaling is critical for establishment of asymmetrical axis.

4.2. Contribution of the present study

Herein we presented five lines of evidence supporting the hypothesis that UII/

UIIR signaling pathway is required for normal determination of asymmetric axis during early embryogenesis. First, function-loss of UII results in a concordant randomization of viscus asymmetries in embryos, including abnormalities in cardiac looping and positioning of visceral organs. Second, knockdown of UII randomizes the left-sided expression of asymmetrical genes including *lefty2, spaw* and *pitx2c* in the lateral plate mesoderm (LPM) and *bmp4* in the developing heart domain and the LPM. Third, reducing the UII level interferes with the normal organogenesis of Kupffer's vesicle (KV), an organ implicated in the early steps of left-right (L-R) patterning of embryos. Fourth, repression of UII function perturbed the asymmetrical distribution of free Ca^{2+} (intracellular Ca^{2+}) at the region surrounding embryo KV during early somitogenesis, which is one of the signaling mechanisms that propagandize and amplify the early clue of L-R asymmetry. Fifth, loss of UII function alters the normal Bmp and Nodal signaling pathway, which modulate the establishment of L-R asymmetry of developmental embryo. Collectively, these observations support a model in which UII/UIIR signal system takes part in the early molecular events of L-R asymmetry patterning of embryo by modulating Bmp and Nodal signaling, regulating KV normal morphogenesis, so then, maintaining the asymmetrical distribution of free intracellular Ca^{2+} at the region surrounding embryo KV. This study documents a role of UII/UIIR signaling pathway in the establishment of L-R axis of embryos which promises to reveal the molecular mechanisms responsible for human congenital diseases with heterotaxy.

4.2.1 UII acts as an important factor for defining the left-sidedness of embryo in establishment of asymmetrical axis of embryos

Our results from the loss-of-function or overexpression experiment of UII uncovered that by modulating *nodal* and *bmp4* signaling UII is implicated in the early determination of L-R patterning of embryos. Evidence derives from these observations that in UII knockdown embryos the Bmp signaling is severally altered, the left-biased expression of *lefty*, which act as inhibitors of Nodal signaling, is affected and *nodal* itself (*spaw*) asymmetrical expression in left LPM is randomized or deleted. Moreover, the expression profile of *pitx2c*, a downstream target of nodal signaling, also shows similar change. Collectively, our data shed light on a previously unexpected role of UII in L-R patterning of zebrafish embryos.

4.2.2 UII acts in the earlier stages of L-R patterning of embryo and is required for the KV morphogenesis

The vertebrate body plan develops along three geometric axes: anterior-posterior, dorsal-ventral, and left-right. The establishment of all three body axes is induced by the Spemann organizer (Jansen et al 2007; Saúdel et al 2000; Agathon et al 2003; Fauny et al 2009; Vandenberg et al 2010). Observations demonstrate that the LR axis is set with respect to the anterior–posterior and dorsa-ventral (dorsal-anterior) axes and the alteration in dorsal-anterior development will perturb the orientation of left-right axis (Danos MC et al 1995); the detailed mechanism on how the LR axis is coordinated (linked) with dorsal-anterior axis and is correctly oriented by the Spemann organizer still is elusive.

Observations from zebrafish suggest that the BMPs show a degressive gradient

distribution from ventral to dorsal and are required for dorsoventral patterning during gastrulation. Our work suggests that through maintaining proper BMP gradient along ventral to dorsal axis UIIβ controls limits the territory of dorsal Spemann organizer and then affects the specification, migration and convergence of DFCs. These phenomena seem imply it is through normal DFCs development that .LR axis is coordinated with dorsal-anterior axis and is correctly oriented. Our experimental observations suggests UII is involved in the process of L-R patterning of embryos before the onset of KV morphogenesis

In short, this is the first report on the UII acting in the establishment of L-R axis during vertebrate embryogenesis.

4.2.3 Model on UII modulating the correct orientation of L-R axis of embryos

Fig.4-1 suggests the basic timeline of UII modulating the correct orientation of L-R axis of embryos. During gastrulation UIIβ regulates *bmp* ligand expression to maintain the gradient balance of BMP/WNT along the ventral-dorsal axis. UIIβ negatively regulates the organizer regulation gene directly, or indirectly through the rate of BMP/WNT along ventral-to-dorsal axis, regulates, for example fga8a and iro3 etc., to limit the territory of dorsal organizer which is essential for dorsal-ventral patterning of embryos. The appropriately boundary of dorsal organizer is required for the normal development of DFCs.

During early segmentation through directly, or indirectly regulating *bmp4* expression in tailbud and periphery of KV, UII induces the inhibiting effect of *lefty1* on the *spaw* expression in the right LPM . During later segmentation by directly, or

indirectly inducing *bmp4* asymmetrical expression in heart field and LPM, UII affects the cardiac jogging towards the left side and heart looping..

4. 3 Future prospects

To fully understand the UII role in the L-R patterning during embryogenesis, the following issues should be addressed in the future.

● **Whether UII is regulated by Smad4 and Smad3?**

Our results from bioinformatics analysis revealed that the promoter of zebrafish UIIβ not only embodies more different kinds of *cis*-elements, but also possesses a *cis* Smad4 binding element (GACAGACAGACAGACTGACAAA) between-2361 and -2339 and a 25-times-repeated *cis* Smad3-Smad4 binding elements region (CAGACAGACAGACA) between -1636 and -521 (Table. 3-1). The 25-times repetition of the *cis* element might reflect its potential to sense the concentration gradient of Smad factors and to give the differential transcriptional activity. Previously studies have been shown that Bmp and Nodal common belong to the TGF-β superfamily. Smad4 is a common transduction factor for both Bmp and Nodal/activin/TGF-β pathways. It acts as comediator to merge this two signaling pathway together and mediates the crosstalk between this two signaling pathway at the downstream of their signaling transduction by modulating the translocation of transcriptional complexes into nuclei and activation of target genes. Instead, Smad3 only acts at the downstream of Nodal Nodal/activin/TGF-β pathway and is specific for Nodal signaling (Wu et al., 2002; Davis et al., 2008; Kim et al., 2006; Inman et al., 2002; Chen et al., 2002; Zhou et al., 1998; Shioda et al., 1998; Kishigami et al., 2005). Therefore, it will be of interest to investigate whether the crosstalk among the

UII signaling pathway, Nodal signaling pathway and Bmp signaling pathway is modulated by Smad4 or Smad4-Smad3. If it is true, then what is the role of other factor cAMP among three signaling system? Interesting we found that the promoters of zebrafish *bmp4*, *smad5*, *cyclops* and *spaw* possess one or two cAMP responsive element respectively. These works should be undertaken at the next step to obtain a full insight into the above issues: in the context of loss-of-function and overexpression of *smad4*, *smad3+smad4* to monitor expression of *UIIβ*, *bmp4 and nodal*, and to evaluate the corresponding phenotypes.

- **Whether UIIβ mediates the initial breaking of embryo symmetry?**

Our observations suggested that UII functions on the upstream of KV organogenesis, being essential for the normal KV development. In zebrafish, KV organogenesis originates from the dorsal forerunner cells (DFCs) and DFCs are specified during the blastula period by a number of yet unidentified factors. DFCs express two genes, *foxj1a* and *L-Rdr1*. Previous results demonstrated that the two genes are required for KV organogenesis from DFCs (Essner et al., 2005; Tian et al., 2009); while other earlier genes required for proper DFC formation are still unclear. Therefore, in order to determine whether UII functions at the initial breaking of embryo symmetry stage the relationship of UII with these genes should be investigated. .
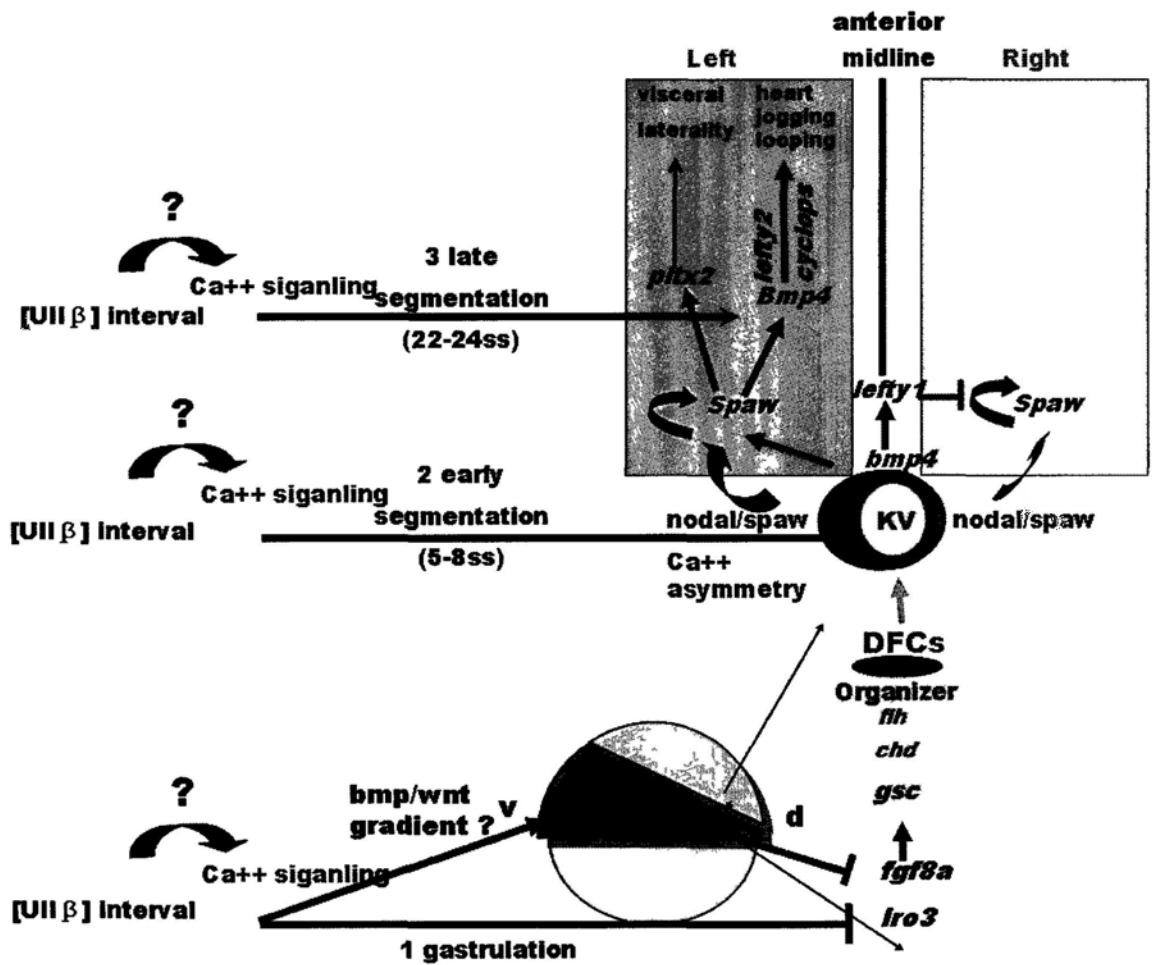
Fig.4-1 Model on UIIβ modulating the correct orientation of L-R axis of embryos.

Fig.4-1 Model on UIIβ modulating the correct orientation of L-R axis of embryos.

During gastrulation UIIβ regulates *bmp* ligand expression to maintain the gradient balance of BMP or BMP/WNT along the ventral-dorsal axis. UIIβ directly negatively regulates, or indirectly through the rate of BMP/WNT along ventral-to-dorsal axis, regulates the organizer regulation gene (fga8a and iro3) to limit the territory of dorsal organizer which is essential for dorsal-ventral patterning of embryos. The appropriately boundary of dorsal organizer is required for the normal development of DFCs. During early segmentation stages, Bmp4 in Kupffer's vesicle represses *spw* expression in the right LPM possibly by regulating *lefty1* expression in the notochord. Lefty1 is a negative regulator of Nodal signaling. Due to the absence of this negative regulation cascade in the left LPM, *spaw* is expressed on the left LPM where it regulates visceral organ and heart morphogenesis. UIIβ might directly regulate the *bmp4* expression in Kupffer's vesicle and acts at the uptream of *spaw*. During late segmentation stages, *spaw* in the left LPM induces *bmp4* expression in the left LPM and heard field, and *pitx2* expression in the gut primordium. This late *bmp4* expression is required for left-sided gene expression in the cardiac field and regulates cardiac jogging towards the left side without affecting morphogenesis of the visceral organs at later stages. UIIβ might indirectly regulate the *bmp4* expression in heart field and LPM and acts at the downstream of *spaw*.

Reference

Aiyar N, Johns DG, Ao Z, Disa J, Behm DJ and Foley JJ. (2005). Cloning and pharmacological characterization of the cat urotensin-II receptor (UT). *Biochem Pharmacol*, 69, 1069–79.

Alewijnse AE, Timmerman H, Jacobs EH, Smit MJ, Roovers E and Cotecchia S. (2000). The effect of mutations in the DRY motif on the constitutive activity and structural instability of the histamine H (2) receptor. *Mol Pharmacol*, 57, 890–98.

Allende ML, Amsterdam A, Becker T, Kawakami K, Gaiano N and Hopkins N. (1996). Insertional mutagenesis in zebrafish identifies two novel genes, pescadillo and dead eye, essential for embryonic development. *Genes Dev,*10:3141–3155.

Amack JD and Yost HJ. (2004). The T box transcription factor no tail in ciliated cells controls zebrafish left-right asymmetry. *Curr Biol* 14: 685-690.

Ames RS, Sarau HM, Chambers JK, Willette RN, Aiyar NV, Romanic AM, et al. (1999). Human urotensin-II is a potent vasoconstrictor and agonist for the orphan receptor GRP14. *Nature*, 401, 282–86.

Angelo S, Lohr J, Lee KH, et al. 2000. Conservation of sequence and expression of Xenopus and zebrafish dHAND during cardiac, branchial arch and lateral mesoderm development. *Mech Dev* 95: 231-237.

Aw S, Levin M. (2008). What's left in asymmetry? *Dev Dyn*, 237, 3453-63.

Balat O, Aksoy F, Kutlar I, Ugur MG, Iyikosker H, Balat A and Anarat R. (2005). Increased plasma levels of Urotensin-II in preeclampsia-eclampsia: a new mediator in pathogenesis? *Eur J Obstet Gynecol Reprod Biol*, 120, 33-38.

Ballesteros JA, Jensen AD, Liapakis G, Rasmussen SG, Shi L, Gether U, et al. (2001). Activation of the beta 2-adrenergic receptor involves disruption of an ionic lock between the cytoplasmic ends of transmembrane segments 3 and 6. *J Biol Chem*, 276, 29171–77.

Barak LS, Oakley RH, Laporte SA and Caron MG. (2001). Constitutive arrestin-mediated desensitization of a human vasopressin receptor mutant associated with nephrogenic diabetes insipidus. *Proc Natl Acad Sci USA*, 98,

93–98.

Bern HA, Pearson D, Larson BA and Nishioka RS. (1985). Neurohormones from fish tails: the caudal neurosecretory system. I. "Urophysiology" and the caudal neurosecretory system of fishes. *Recent Prog Horm Res*, 41, 533–52.

Bichet DG. (1998). Nephrogenic diabetes insipidus. *Am J Med*, 105, 431–42.

Bihoreau C, Monnot C, Davies E, Teutsch B, Bernstein KE and Corvol P, et al. (1993). Mutation of Asp74 of the rat angiotensin II receptor confers changes in antagonist affinities and abolishes G-protein coupling. *Proc Natl Acad Sci USA*, 90, 133–37.

Bisgrove BW, Essner JJ and Yost HJ. (1999). Regulation of midline development by antagonism of lefty and nodal signaling. *Dev*, 126, 3253-62.

Bisgrove BW, Essner JJ and Yost HJ. (2000). Multiple pathways in the midline regulate concordant brain, heart and gut left-right asymmetry. *Dev*, 127, 3567-79.

Bisgrove BW, Morelli SH and Yost HJ. (2003). Genetics of human laterality disorders: insights from vertebrate model systems. *Annu Rev Genomics Hum Genet*, 4, 1-32.

Boettger T,Wittler L,Kessel M.(1999). FGF8 functions in the specification of the right body side of the chick. *Curr Biol*, 9: 277-280.

Bonnafe E, Touka M, AitLounis A, et al. (2004). The transcription factor RFX3 directs nodal cilium development and left-right asymmetry specification. *Mol Cell Biol*, **24**: 4417-4427.

Bottrill FE, Douglas SA, Hiley CR and White R. (2000). Human urotensin-II is an endothelium dependent vasodilator in rat small arteries. *Br J Pharmacol*, 130, 1865–70.

Boucard AA, Sauve SS, Guillemette G, Escher E and Leduc R. (2003). Photolabelling the rat urotensin II/GPR14 receptor identifies a ligand-binding site in the fourth transmembrane domain. *Biochem J*, 370, 829–38.

Bousette N, Patel L, Douglas SA, Ohlstein EH and Giaid A. (2004). Increased expression of urotensin II and its cognate receptor GPR14 in atherosclerotic lesions of the human aorta. *Atherosclerosis*, 176, 117–23.

Bousette N, Pottinger J, Ramli W, Ohlstein EH, Dhanak D and Douglas SA. (2006). Urotensin-II receptor

blockade with SB-611812 attenuates cardiac remodeling in experimental ischemic heart disease. *Peptides*, 27,

2919–26.

Branford WW, Essner JJ and Yost HJ. (2000). Regulation of gut and heart left–right asymmetry by

context-dependent interactions between Xenopus lefty and BMP4 signaling. *Dev Biol*, 223, 291–306.

Brend T and Holley SA. (2009). Balancing segmentation and laterality during vertebrate development. *Semin*

Cell Dev Bio,l 20, 472-78.

Brennan J, Norris DP and Robertson EJ. (2002). Nodal activity in the node governs left–right asymmetry.

Genes Dev, 16, 2339–44.

Brown NA,Wolpert L. (1990). The development of handedness in left/right asymmetry. *Dev,* 109: 1-9.

Buceta J,Ibanes M,Rasskin-Gutman D, et al. (2005). Nodal cilia dynamics and the specification of the

left/right axis in early vertebrate embryo development. *Biophys J,* 89: 2199-2209.

Bunney TD, De Boer AH,Levin M. (2003). Fusicoccin signaling reveals 14-3-3 protein function as a novel step

in left-right patterning during amphibian embryogenesis. *Dev,* 130: 4847-4858.

Burdine RD and Schier AF. (2000). Conserved and divergent mechanisms in leftright axis formation. *Genes Dev,*

14, 763-76

Camarda V, Rizzi A, Calo G, Gendron G, Perron SI and Kostenis E. (2002). Effects of human urotensin II in

isolated vessels of various species; comparison with other vasoactive agents. *Naunyn Schmiedebergs Arch*

Pharmacol, 365, 141–49.

Campione M, Steinbeisser H, Schweickert A, Deissler K, van Bebber F, Lowe LA, Nowotschin S, Viebahn

C, Haffter P, Kuehn MR and Blum M. (1999). The homeobox gene Pitx2: mediator of asymmetric left-right

signaling in vertebrate heart and gut looping. *Dev,* 126, 1225-34.

Capdevila J, Vogan KJ, Tabin CJ, Izpisua-Belmonte JC. (2000). Mechanisms of left–right determination in

vertebrates. *Cell,* 101, 9–21.

Cartwright JH, Piro O, Tuval I. (2004). Fluid-dynamical basis of the embryonic development of left-right asymmetry in vertebrates. *Proc Natl Acad Sci USA* **101**: 7234-7239.

Castel H, Diallo M, Chatenet D, Leprince J, Desrues L and Schouft MT, et al. (2006). Biochemical and functional characterization of high-affinity urotensin II receptors in rat cortical astrocytes. *J Neurochem*, 99, 582–95.

Chang H, Zwijsen A, Vogel H, Huylebroeck D and Matzuk MM. (2000). Smad5 is essential for left–right asymmetry in mice. *Dev Biol*, 219, 71–8.

Chatenet D, Dubessy C, Leprince J, Boularan C, Carlier L, Segalas-Millazo I, et al. (2004). Structure–activity relationships and structural conformation of a novel urotensin II-related peptide. *Peptides*, 25, 1819–30.

Chen CR, Kang Y, Siegel PM and Massague J. (2002). E2F4/5 and p107 as Smad cofactors linking the TGF-beta receptor to c-myc repression. *Cell*, 110, 19-32.

Chen JN, van Eeden FJ, Warren KS, Chin A, Nusslein-Volhard C, Haffter P and Fishman MC. (1997). Left–right pattern of cardiac BMP4 may drive asymmetry of the heart in zebrafish. *Dev*, **124**: 4373-4382.

Cheng AM, Thisse B, Thisse C, Wright CV. (2000). The lefty-related factor Xatv acts as a feedback inhibitor of nodal signaling in mesoderm induction and L-R axis development in xenopus. *Development* **127**: 1049-1061.

Cheung BM, Leung R, Man YB and Wong LY. (2004). Plasma concentration of urotensin II is raised in hypertension. *J Hypertens*, 22, 1341–44.

Chocron S, Verhoeven MC, Rentzsch F, Hammerschmidt M, Bakkers J. (2007). Zebrafish Bmp4 regulates left-right asymmetry at two distinct developmental time points. *Dev Biol*, 305, 577-88.

Chung DA, Wade SM, Fowler CB, Woods DD, Abada PB and Mosberg HI, et al. (2002). Mutagenesis and peptide analysis of the DRY motif in the alpha2A adrenergic receptor: evidence for alternate mechanisms in G protein-coupled receptors. *Biochem Biophys Res Commun*, 293, 1233–41.

Chung FZ, Wang CD, Potter PC, Venter JC and Fraser CM. (1988). Site-directed mutagenesis and

continuous expression of human beta-adrenergic receptors. Identification of a conserved aspartate residue involved in agonist binding and receptor activation. *J Biol Chem,* 263, 4052–55.

Clark SD, Northacker HP, Wang Z, Saito Y, Leslie FM and Civelli O. (2001). The urotensin II receptor is expressed in the cholinergic mesopontine tegmentum of the rat. *Brain Res,* 923, 120–27.

Collignon J, Varlet I, Robertson EJ. (1996). Relationship between asymmetric nodal expression and the direction of embryonic turning. *Nature,* 381:155–58.

Collignon J, Varlet I, Robertson EJ. (1996) Relationship between asymmetric nodal expression and the direction of embryonic turning. *Nature* 381: 155-158

Conlon J M, O'Harte F, Smith DD, Tonon MC and Vaudry H. (1992). *Biochem Biophys Res Commun,* 188, 578-83.

Conlon JM, Arnold-Reed D and Balment RJ. (1990). Post-translational processing of prepro-urotensin II. *FEBS lett,* 66, 7-40.

Conlon JM, O'Harte F, Smith DD, Tonon MC and Vaudry H. (1992). Isolation and primary structure of urotensin II from the brain of a tetrapod, the frog Rana ridibunda. *Biochem Biophys Res Commun,* 97, 103–10.

Conlon JM, Tostivint H and Vaudry H. (1997). Somatostatin- and urotensin II-related peptides: molecular diversity and evolutionary perspectives. *Regul Pept,* 69, 95–103.

Coulouarn Y, Je´gou S, Tostivint H, Vaudry H and Lihrmann I. (1999). Cloning, sequence analysis and tissue distribution of the mouse and rat urotensin-II precursors. *FEBS Lett,* 457, 28–32.

Coulouarn Y, Lihrmann I, Je´gou S, Anouar Y, Tostivint H, Beauvillain JC, et al. (1998). Cloning of the cDNA encoding the urotensin-II precursor in frog and human reveals intense expression of the urotensin-II gene in motoneurons of the spinal cord. *Proc Natl Acad Sci USA,* 95, 15803–8.

D'Amico LA and Cooper MS. (1997). spatially distinct domains of cell behavior in the zebrafish organizer region. *Biochem. Cell Biol,* 75: 563–577.

DahmR and Geisler R. (2006). Learning from small fry: the zebrafish as a genetic model organism for

aquaculture fish species. *Marine Biotech,* 8, 324-45.

Dathe V,Prols F,Brand-Saberi B. (2004). Expression of kinesin kif5c during chick development. *Anat Embryol (Berl)* **207**: 475-480.

Davis BN, Hilyard AC, Lagna G and Hata A. (2008). SMAD proteins control DROSHA- mediated microRNA maturation. *Nature,* 454, 56-61.

Davis EE, Brueckner M and Katsanis N. (2006). The emerging complexity of the cilium: vertebrate new functional roles for an ancient organelle. *Dev Cell,* 11, 9–19.

Davis NM, Kurpios NA, Sun X, Gros J, Martin JF and Tabin CJ. (2008). The chirality of gut rotation derives from left-right asymmetric changes in the architecture of the dorsal mesentery. *Dev Cell,* 15, 134–45.

Delmas, P. (2004). Polycystins: from mechanosensation to gene regulation. *Cell,* 118.

do Rego JC, Chatenet D, Orta MH, Naudin B, Le Cudennec C, Leprince J, et al. (2005). Behavioral effects of urotensin-II centrally administered in mice. *Psychopharmacol,* 183, 103–17.

Douglas SA, Naselsky D, Ao Z, Disa J, Herold CL and Lynch F, et al. (2004). Identification and pharmacological characterization of native, functional human urotensin-II receptors in rhabdomyosarcoma cell lines. *Br J Pharmacol,* 142, 921–32.

Douglas SA, Sulpizio AC, Piercy V, Sarau HM, Ames RS and Aiyar NV, et al. (2000). Differential vasoconstrictor activity of human urotensin-II in vascular tissue isolated from the rat, mouse, dog, pig, marmoset and cynomolgus monkey. *Br J Pharmacol,* 131, 1262–74.

Douglas SA. (2003). Human urotensin-II as a novel cardiovascular target: "heart" of the matter or simply a fi shy "tail"? *Curr Opin Pharmacol,* 3, 159–67.

Driever W, Solnica-Krezel L, Schier AF, Neuhauss SC et al. (1996). A genetic

Dschietzig T, Richter C, Bartsch C, Böhme C, Heinze D, Ott F, Zartnack F, Baumann G and Stangl K. (2001). Flow-induced pressure differentially regulates endothelin-1, urotensin II, adrenomedullin, and relaxin in pulmonary vascular endothelium. *Biochem Biophys Res Commun,* 289, 245-51.

Dubruille R,Laurencon A,Vandaele C, et al. (2002). Drosophila regulatory factor X is necessary for ciliated sensory neuron differentiation. *Dev*, **129**: 5487-5498.

Dutt P, Kjoller L, Giel M, Hall A and Toksoz D. (2002). Activated Galphaq family members induce Rho GTPase activation and Rho-dependent actin filament assembly. *FEBS Lett*, 531, 565–69.

Eimon PM and Ashkenazi A. (2009). The zebrafish as a model organism for the study of apoptosis. *Apoptosis*, Dec 24 (On line).

Ekker SC, Larson JD (2001) Morphant technology in model developmental systems. *Genesis* 30: 89–93

Elshourbagy NA, Douglas SA, Shabou U, Harrison S, Duddy G and Sechler JL, et al. (2002). Molecular and pharmacological characterization of genes encoding urotensin-II peptides and their cognate G-protein-coupled receptors from the mouse and monkey. *Br J Pharmacol*, 136, 9–22.

Essner JJ, Amack JD, Nyholm MK, Harris EB and Yost HJ. (2005). Kupffer's vesicle is a ciliated organ of asymmetry in the zebrafish embryo that initiates left–right development of the brain, heart and gut. *Dev*, 132, 1247–60.

Essner JJ, Amack JD, Nyholm MK, Harris EB and Yost HJ. (2005). Kupffer's vesicle is a ciliated organ of asymmetry in the zebrafish embryo that initiates left-right development of the brain, heart and gut, *Dev*, 132, 1247–1260.

Essner JJ, Branford WW, Zhang J and Yost HJ. (2000). Mesendoderm and left-right brain, heart and gut development are differentially regulated by pitx2 isoforms. *Dev*, 127, 1081-93.

Essner J, Vogan J, Wagner K, et al. (2002). Conserved function for embryonic nodal cilia. *Nature* 418: 37-38.

Faucourt M, Houliston E, Besnardeau L, Kimelman D and Lepage T.(2001). The pitx2 homeobox protein is required early for endoderm formation and nodal signaling. *Dev Biol*, 229, 287-06.

Fauny JD, Thisse B, Thisse C. Development. (2009). The entire zebrafish blastula-gastrula margin acts as an organizer dependent on the ratio of Nodal to BMP activity. *Dev*, 136(22):3811-9.

Favre N, Fanelli F, Missotten M, Nichols A, Wilson J and di Tiani M. (2005). The DRY motif as a molecular

switch of the human oxytocin receptor. *Biochem,* 44, 9990–08.

Fedorov Y, Anderson EM, Birmingham A, Reynolds A, Karpilow J, et al. (2006) Off-target effects by siRNA can induce toxic phenotype. *RNA* 12: 1188–1196.

Feng W and Song ZH. (2003). Effects of D3.49A, R3.50A, and A6.34E mutations on ligand binding and activation of the cannabinoid-2 (CB2) receptor. *Biochem Pharmacol,* 65, 1077–85.

Flohr S, Kurz M, Kostenis E, Brkovich A, Fournier A and Klabunde T. (2002). Identification of nonpeptidic urotensin II receptor antagonists by virtual screening based on a pharmacophore model derived from structure–activity relationships and nuclear magnetic resonance on urotensin II. *J Med Chem,* 45, 1799–05.Foley JE, Maeder ML, Pearlberg J, Joung JK, Peterson RT and Yeh JR. (2009). Targeted mutagenesis in zebrafish using customized zinc-finger nucleases. ***Nat Protoc,*** **4:1855-67.**

Francescatto L, Rothschild SC, Myers AL and Tombes RM. (2010). The activation of membrane targeted CaMK-II in the zebrafish Kupffer's vesicle is required for left-right asymmetry. *Dev.* 137, 2753-2762.

Fromm C, Coso OA, Montaner S, Xu N and Gutkind JS. (1997). The small GTP-binding protein Rho links G protein-coupled receptors and Galpha12 to the serum response element and to cellular transformation. Proc Natl Acad Sci USA, 94, 10098–03.

Fujiwara T, Dehart DB, Sulik KK and Hogan BL. (2002). Distinct requirements for extra-embryonic and embryonic bone morphogenetic protein 4 in the formation of the node and primitive streak and coordination of left–right asymmetry in the mouse. *Dev,* 29, 4685–96.

Gaio U,Schweickert A,Fischer A, et al. (1999). A role of the cryptic gene in the correct establishment of the left-right axis. *Curr Biol* 9: 1339-1342.

Garcia-Castro MI,Vielmetter E,Bronner-Fraser M. (2000) N-Cadherin, a cell adhesion molecule involved in establishment of embryonic left-right asymmetry. *Science* **288**: 1047-1051.

Gohla A, Harhammer R and Schultz G. (1998). The G-protein G13 but not G12 mediates signaling from lysophosphatidic acid receptor via epidermal growth factor receptor to Rho. *J Biol Chem,* 273, 4653–59.

Gonzalez GC, Martinez-Padron M, Lederis K and Lukowiak K. (1992). *Pepti*(Tarrytown, NY), 13, 695–03.

Granata A,Quaderi NA. (2003). The Opitz syndrome gene MID1 is essential for establishing asymmetric gene expression in Hensen's node. *Dev Biol* **258**: 397-405. Links

Grunwald DJ and Streisinger G. (1992). Induction of recessive lethal and specific locus mutations in the zebrafish with ethyl nitrosourea. *Genet Res*, 59:103–116.

Hackett BP. (2002). Formation and malformation of the vertebrate left-right axis. *Curr Mol Med*, 2: 39-66.

Haffter P, Granato M, Brand M, Mullins MC, Hammerschmidt M, et al. (1996). The identification of genes with unique and essential functions in the development of the zebrafish, *Danio rerio*. *Dev*, 123:1–36.

Hamada H, Meno C,Watanabe D, Saijoh Y. (2002). Establishment of vertebrate left-right asymmetry. *Nat Rev Genet* **3**: 103-113. Links

Hamburger V,Hamilton HL. (1951). A series of normal stages in the development of the chick embryo. *J Morphol* **88**: 49-92. Links

heart in zebrafish. *Dev*, 124, 4373–82.

Hirokawa N, Tanaka Y, Okada Y and Takeda S. (2006). Nodal flow and the generation of left-right asymmetry. *Cell*, 125, 33-45.

Hirokawa N. (2000). Stirring up development with the heterotrimeric kinesin KIF3. *Traffic* **1**: 29-34.

Hirshman CA and Emala CW. (1999). Actin reorganization in airway smooth muscle cells involves Gq and Gi-2 activation of Rho. *Am J Physiol*, 277, 653–61.

Horne-Badovinac S, Rebagliati M and Stainier DY. (2003). A cellular framework for gut-looping morphogenesis in zebrafish. *Science*, 302, 662-65.

Hou J, Yashiro K, Okazaki Y, et al. 2004. Identification of a novel left-right asymmetrically expressed gene in the mouse belonging to the BPI/PLUNC superfamily. *Dev Dyn* **229**: 373-379.

Huitron-Resendiz S, Kristensen MP, Sanchez-Alavez M, Clark SD, Grupke SL and Tyler C, et al. (2005). Urotensin II modulates rapid eye movement sleep through activation of brainstem cholinergic neurons. *J*

Neurosci, 25, 5465–74.

Isman GJ, Nicolas FJ and Hill CS. (2002). Nucleocytoplasmic shuttling of Smads 2, 3, and 4 permits sensing of TGF-beta receptor activity. *Molec Cell,* 10, 283-94.

Isaac A, Sargent MG, Cooke J. (1997). Control of vertebrate left-right asymmetry by a snail-related zinc finger gene. *Science* **275**: 1301-1304.

Ishihata A, Sakai M and Katano Y. (2006). Vascular contractile effect of urotensin II in young and aged rats: infl uence of aging and contribution of endothelial nitric oxide. *Peptides,* 27, 80–86.

Itoh H, McMaster D and Lederis K. (1988). Functional receptors for fi sh neuropeptide urotensin II in major rat arteries. *Eur J Pharmacol,* 149, 61–66.

Jackson AL, Bartz SR, Schelter J, Kobayashi SV, Burchard J, et al. (2003) Expression profiling reveals off-target gene regulation by RNAi. *Nat Biotechnol* 21: 635–637.

Je´gou S, Cartier D, Dubessy C, Gonzalez BJ, Chatenet D, Tostivint H, et al. (2006). Localization of the urotensin II receptor in the rat central nervous system. *J Comp Neurol,* 495, 21–36.

Joyal D, Huynh T, Aiyar N, Guida B, Douglas S and Giaid A. (2006). Urotensin-II levels in acute coronary syndromes. *Int J Cardiol,* 108, 31-5.

Katoh H, Aoki J, Yamaguchi Y, Kitano Y, Ichikawa A and Negishi M. (1998). Constitutively active Galpha12, Galpha13, and Galphaq induce Rho-dependent neurite retraction through different signaling pathways. *J Biol Chem,* 273, 28700–07.

Kawakami M, Nakanishi N. (2001). The role of an endogenous PKA inhibitor, PKIalpha, in organizing left-right axis formation. *Dev,* 128: 2509-2515.

Kawakami Y,Raya A,Raya RM, et al. 2005. Retinoic acid signalling links left-right asymmetric patterning and bilaterally symmetric somitogenesis in the zebrafish embryo. *Nature* 435: 165-171.

Kemp W, Roberts S and Krum H. (2005). Urotensin II: a vascular mediator in health and disease. *Curr Vasc Pharmacol,* 3, 159-68.

Khan SQ, Bhandari SS, Quinn P, et al. (2007). Urotensin II is raised in acute myocardial infarction and low levels predict risk of adverse clinical outcome in humans. *Int J Cardio,* 117, 323–28.

Kim BG, Li C, Qiao W, Mamura M, Kasprzak B, Anver M, Wolfraim L, Hong S, Mushinski E, Potter M, Kim SJ, Fu XY, Deng C and Letterio JJ. (2006). Smad4 signalling in T cells is required for suppression of gastrointestinal cancer. *Nature,* 441, 1015-19.

Klein, P.S., and Melton, D.A. (1996). A molecular mechanism for the effect of lithium on development. *Proc. Natl. Acad. Sci. U.S.A.* **93**: 8455–8459.

Klingensmith J, Kemp C, et al. (2000). The organizer factors Chordin and Noggin are required for mouse forebrain development. *Nature,* 403, 658–61.

Kramer-Zucker AG, Olale F, Haycraft CJ, Yoder BK, Schier AF, Drummond IA. (2005). Cilia-driven fluid flow in the zebrafish pronephros, brain and Kupffer's vesicle is required for normal organogenesis. *Dev,* 132, 1907–21.

Krebs LT,Iwai N,Nonaka S, et al. (2003). Notch signaling regulates left-right asymmetry determination by inducing Nodal expression. *Genes Dev* 17: 1207-1212.

Lancien F, Leprince J, Mimassi N, Mabin D, Vaudry H and Le Me´ vel JC. (2004). Central effects of native urotensin II on motor activity, entilatory movements and heart rate in the trout Oncorhynchus mykiss. *Brain Res,* 1023, 167–74.

Lee JD and Anderson KV. (2008) Morphogenesis of the node and notochord: The cellular basis for the establishment and maintenance of left-right asymmetry in the mouse. *Dev Dyn,* 237, 3464–76.

Leprince J, Tonon MC and Vaudry H. (2008). Structure-activity relationships of urotensin II and URP. *Peptides,* 29, 658-73.

Levin M and Mercola M. (1998). The compulsion of chirality: towards an understanding of left-right asymmetry. *Genes Dev,* 12, 763–69.

Levin M and Mercola M. (1998b). Evolutionary conservation of mechanisms upstream of asymmetric Nodal

expression: reconciling chick and Xenopus. *Dev Genet,* 23:185–93.

Levin M and Mercola M. (1998c). Gap junctions are involved in the early generation of left-right asymmetry. *Dev Biol,* 202, 90–05.

Levin M and Mercola M. (1999). Gap junction-mediated transfer of left-right patterning signals in the early chick blastoderm is upstream of Shh asymmetry in the node. *Dev,* 126, 4703–14.

Levin M, Johnson RL, Stern CD, Kuehn M and Tabin C. (1995). A molecular pathway determining left-right asymmetry in chick embryogenesis. *Cell,* 82, 803–14.

Levin M, Pagan S, Roberts DJ, Cooke J, Kuehn M and Tabin CJ. (1997). Left/right patterning signals and the independent regulation of different aspects of situs in the chick embryo. *Dev Biol,* 189, 57–67.

Levin M, Thorlin T, Robinson K, Nogi T and Mercola M. (2002). Asymmetries in H+/K+-ATPase and cell membrane potentials comprise a very early step in left-right patterning. *Cell,* 111, 77–89.

Levin M, Johnson RL, Stern CD, et al. (1995). A molecular pathway determining left-right asymmetry in chick embryogenesis. *Cell* 82: 803-814.

Levin M, Mercola M. (1999). Gap junction-mediated transfer of left-right patterning signals in the early chick blastoderm is upstream of Shh asymmetry in the node. *Dev,* 126: 4703-4714.

Levin M,Thorlin T,Robinson K, et al. (2002). Asymmetries in H(+)/K(+)-ATPase and cell membrane potentials comprise a very early step in left-right patterning. *Cell* 111: 77-89.

Levin M. (1998). The roles of activin and follistatin signaling in chick gastrulation. *Int J Dev Biol,* 42:553–59.

Levin M. (2003). Motor protein control of ion flux is an early step in embryonic left-right asymmetry. *Bioessays* 25: 1002-1010.

Levin M. (2006). Is the early left–right axis like a plant, a kidney, or a neuron? The integration of physiological signals in embryonic asymmetry. *Birth Defects Res C Embryo Today,* 78, 191–23.

Lin X, Ruan X, Anderson MG, McDowell JA, Kroeger PE, et al. (2005) siRNA-mediated off-target gene silencing triggered by a 7 nt complementation. *Nucleic Acids Res* 33: 4527–4535

Linask KK,Han MD,Artman M,Ludwig CA. (2001). Sodium-calcium exchanger (NCX-1) and calcium modulation: NCX protein expression patterns and regulation of early heart development. *Dev Dyn* **221**: 249-264.

Liu QY, Pong SS, Zeng ZZ, Zhang Q, Howard AD and Williams DL, et al. (1999). Identification of urotensin II as the endogenous ligand for the orphan G-protein-coupled receptor GPR14. *Biochem Biophys Res Commun*, 266, 174–78.

Logan M, Pagan-Westphal SM, Smith DM, et al. (1998). The transcription factor Pitx2 mediates situs-specific morphogenesis in response to left-right asymmetric signals. *Cell* **94**: 307-317. Links

Lohr JL, Danos MC, Yost HJ. (1997). Left-right asymmetry of a nodal-related gene is regulated by dorsal midline structures during Xenopus development. *Dev*, 124, 1465–72.

Long S., Ahmad N and Rebagliati M. (2003) The zebrafish nodal-related gene southpaw is required for visceral and diencephalic left-right asymmetry. *Dev*, 130, 2303–16

Lowe LA, Supp DM, Sampath K, Yokoyama T and Wright CVE, et al. (1996). Conserved left-right asymmetry of nodal expression and alterations in murine situs inversus. *Nature*, 381, 158–61.

Lowe LA, Yamada S and Kuehn MR. (2001). Genetic dissection of nodal function in patterning the mouse embryo. *Dev*, 128, 1831–43.

Lu Z, Jiang YP, Ballou LM, Cohen IS and Lin RZ. (2005). Galpha q inhibits cardiac L-type Ca2+ channels through phosphatidylinositol 3-kinase. *J Biol Chem*, 280, 40347–54.

Lustig KD, Kroll K, Sun E, et al. (1996). A Xenopus nodal-related gene that acts in synergy with noggin to induce complete secondary axis and notochord formation. *Development* **122**: 3275-3282.

MacLean MR, Alexander D, Stirrat A, Gallagher M, Douglas SA, Ohlstein EH, Morecroft I and Polland K. (2000). Contractile responses to human urotensin-II in rat and human pulmonary arteries: effect of endothelial factors and chronic hypoxia in the rat. *Br J Pharmacol*, 130, 201–04.

Mallamaci F, Cutrupi S, Pizzini P, et al. (2005) Urotensin II in end-stage renal disease: an inverse correlate of sympathetic function and cardiac natriuretic peptides. *J Nephrol*, 18, 727–32.

155

Mallamaci F, Cutrupi S, Pizzini P, et al. (2006) Urotensin II and biomarkers of endothelial activation and atherosclerosis in end-stage renal disease. *Am J Hypertens,* 19, 505-10.

Männer J. (2001). Does an equivalent of the "ventral node" exist in chick embryos? A scanning electron microscopic study. *Anat Embryol (Berl),* 203, 481-90.

Marchese A, Heiber M, Nguyen T, Heng HH, Saldivia VR and Cheng R, et al. (1995). Cloning and chromosomal mapping of three novel genes, GPR9, GPR10 and GPR14, encoding receptors related to interleukin 8, neuropeptide Y, and somatostatin receptors. *Genomics,* 29, 335–44.

Marques S, Borges AC, Silva AC, Freitas S, Cordenonsi and Belo JA. (2004). The activity of the Nodal antagonist Cerl-2 in the mouse node is required for correct L/R body axis. *Genes Dev,* 18, 2342.

Massagué J. (1998). TGF-beta signal transduction. *Annu Rev Biochem,* 67, 753-91.

Matsumoto Y, Abe M, Watanabe T, Adachi Y, Yano T, Takahashi H, et al. (2004). Intracerebroventricular administration of urotensin II promotes anxiogenic-like behaviors in rodents. *Neurosci Lett,* 358, 99–02.

Matsushita M, Shichiri M, Imai T, Iwashina M, Tanaka H and Takasu N, et al. (2001). Co-expression of urotensin-II and its receptor (GPR14) in human cardiovascular and renal tissue. *J Hypertens,* 19, 2185–90.

McDonald J, Batuwangala M and Lambert DG. (2007). Role of urotensin II and its receptor in health and disease. *J Anesth,* 21, 378-89.

McGrath J and Brueckner M. (2003). Cilia are at the heart of vertebrate left–right asymmetry. *Curr Opin Genet Dev,* 13, 385–92.

McGrath J, Somlo S, Makova S, Tian X and Brueckner M. (2003).Two populations of node monocilia initiate left–right asymmetry in the mouse. *Cell,* 114, 61–73.

Meno C, Ito Y, Saijoh Y, et al. (1997). Two closely-related left–right asymmetrically expressed genes, lefty-1 and lefty-2: their distinct expression domains, chromosomal linkage and direct neuralizing activity in Xenopus embryos. *Genes Cells,* 2, 513–24.

Meno C, Saijoh Y, Fujii H, et al. (1996.) Left-right asymmetric expression of the TGF beta-family member lefty in mouse embryos. *Nature* 381: 151-155

Meno C, Shimono A, Saijoh Y, et al. (1998.) lefty-1 is required for left-right determination as a regulator of lefty-2 and nodal. *Cell* 94: 287-297.

Mercola M and Levin M. (2001). Left-right asymmetry determination in verterbrates. *An Rev of Cell and Dev Bio,* 17, 779-05

Mercola M, Levin M. (2001.) Left-right asymmetry determination in vertebrates. *Annu Rev Cell Dev Biol* 17: 779-805.

Meyers EN and Martin GR. (1999). Differences in left-right axis pathways in mouse and chick: functions of FGF8 and SHH. *Science,* 285, 403–06.

Meyers EN, Martin GR. (1999) Differences in left-right axis pathways in mouse and chick: functions of FGF8 and SHH. *Science* 285: 403-406.

Mhaouty-Kodja S, Barak LS, Scheer A, Abuin L, Diviani D and Caron MG, et al. (1999). Constitutively active alpha-1b adrenergic receptor mutants display different phosphorylation and internalization features. *Mol Pharmacol,* 55, 339–47.

Monsoro-Burq A, Le Douarin N. (2000) Left-right asymmetry in BMP4 signalling pathway during chick gastrulation. *Mech Dev* 97: 105-108.

Mori M, Sugo T, Abe M, Shimomura Y, Kurihara M and Kitada C. (1999). Urotensin II is the endogenous ligand of G-proteincoupled orphan receptor SENR (GPR14). *Biochem Biophys Res Commun,* 265, 123–29.

Nagai T, Sawano A, Park ES and Miyawaki A. (2001). Circularly permuted green fluorescent proteins engineered to sense Ca^{2+}, *Proc. Natl. Acad. Sci. USA* **98** pp. 3197–3202

Nagayoshi S, Hayashi E, Abe G, Osato N, Asakawa K, Urasaki A, Horikawa K, Ikeo K, Takeda H, Kawakami K. (2008). Insertional mutagenesis by the Tol2 transposonmediated enhancer trap approach generated mutations in two developmental genes: tcf7 and synembryn-like. *Dev,* 135:159–169.

Nauli SM and Zhou J. (2004). Polycystins and mechanosensation in renal and nodal cilia. *Bioessays,* 26, 844–856.

Neve KA, Cox BA, Henningsen RA, Spanoyannis A and Neve RL. (1991). Pivotal role for aspartate-80 in the regulation of dopamine D2 receptor affinity for drugs and inhibition of adenylyl cyclase. *Mol Pharmacol,* 39, 733–39.

Nonaka S, Shiratori H, Saijoh Y and Hamada H. (2002). Determination of left-right patterning of the mouse embryo by artificial nodal flow. *Nature,* 418, 96-9.

Nonaka S, Tanaka Y, Okada Y, Takeda S, Harada A, et al. (1998). Randomization of left-right asymmetry due to loss of nodal cilia generating leftward flow of extraembryonic fluid in mice lacking KIF3B motor protein. *Cell,* 95, 829–37.

Nonaka S,Shiratori H,Saijoh Y,Hamada H. (2002). Determination of left-right patterning of the mouse embryo by artificial nodal flow. *Nature* **418**: 96-99.

Nonaka S,Tanaka Y,Okada Y, et al. (1998). Randomization of left-right asymmetry due to loss of nodal cilia generating leftward flow of extraembryonic fluid in mice lacking KIF3B motor protein. *Cell* **95**: 829-837.

Norris DP, Robertson EJ. (1999). Asymmetric and node-specific nodal expression patterns are controlled by two distinct cis-acting regulatory elements. *Genes Dev* 13: 1575-1588.

Obara T, Mangos S, Liu Y, Zhao J, Wiessner S, Kramer-Zucker AG, Olale F, Schier AF and Drummond IA. (2006). Polycystin-2 immunolocalization and function in zebrafish. *J Am Soc Nephrol,* 17, 2706–18.

Oh SP. & Li E. (1997) The signaling pathway mediated by the type IIB activin receptor controls axial and lateral asymmetery in the mouse. *Genes Dev.* 11, 1812–1826.

Ohuchi H,Kimura S,Watamoto M,Itoh N. (2000). Involvement of fibroblast growth factor (FGF)18-FGF8 signaling in specification of left-right asymmetry and brain and limb development of the chick embryo. *Mech Dev* 95: 55-66.

Okada Y,Nonaka S,Tanaka Y, et al. (1999.) Abnormal nodal flow precedes situs inversus in iv and inv mice. *Mol Cell* 4: 459-468.

Onan D, Hannan RD and Thomas WG. (2004).Urotensin II: the old kid in town. *Trends Endocrinol Metab,* 15, 175–82.

Onan D, Pipolo L, Yang E, Hannan RD and Thomas WG. (2004). Urotensin II promotes hypertrophy of cardiac myocytes via mitogen-activated protein kinases. *Mol Endocrino,* 118, 2344–54.

Ong KL, Lam KS and Cheung BM. (2005). Urotensin II: its function in health and its role in disease. *Cardiovasc Drugs Ther,* 19(1), 65-75.

Oteíza P, Köppen M, Concha ML, Heisenberg CP. (2008). Origin and shaping of the laterality organ in zebrafish. *Dev,* 135: 2807-13.

Otto EA, Schermer B, Obara T, O'Toole, Hildebrandt F. (2003). Mutations in INVS encoding inversin cause nephronophthisis type 2, linking renal cystic disease to the function of primary cilia and left–right axis determination. *Nat Genet,* 34, 413–20.

Pagan-Westphal SM, Tabin CJ. (1998). The transfer of left-right positional information during chick embryogenesis. *Cell* 93: 25-35

Pearce JJ, Penny G, Rossant J. (1999) A mouse cerberus/Dan-related gene family. *Dev Biol* 209: 98-110.

Pearson D, Shively JE, Clark BR, Geschwind II, Barkley M, Nishioka RS, et al. (1980). Urotensin II: a somatostatin-like peptide in the caudal neurosecretory system of fishes. *Proc Natl Acad Sci USA,* 77, 5021–24.

Peeters H and Devriendt K. (2006). Human laterality disorders. *Eur J Med Genet,* 49, 349-62.

Peeters H, Voz ML, Verschueren K, De and Devriendt K. (2006). Sesn1 is a novel gene for left-right asymmetry and mediating nodal signaling. *Hum Mol Genet,* 15, 3369-77.

Pelletier G, Lihrmann I and Vaudry H. (2002). Role of androgens in the regulation of urotensin II precursor mRNA expression in the rat brainstem and spinal cord. *Neurosci,* 115, 525–32.

Pelletier G, Lihrmann I, Dubessy C, Luu-The V, Vaudry H and Labrie F. (2005). Androgenic

down-regulation of urotensin II precursor, urotensin II-related peptide precursor and androgen receptor mRNA in the mouse spinal cord. *Neuroscie,* 132, 689–96.

Piedra ME and Ros MA. (2002). Bmp signaling positively regulates Nodal expression during left right specification in the chick embryo. *Dev,* 129, 3431–40.

Piedra ME, Icardo JM, Albajar M, et al. (1998) Pitx2 participates in the late phase of the pathway controlling left- right asymmetry. *Cell* 94: 319-324.

Proulx CD, Holleran BJ, Lavigne P, Escher E, Guillemette G and Leduc R. (2008). Biological properties and functional determinants of the urotensin II receptor. *Peptides,* 29, 691-99.

Psychoyos D, Stern CD. (1996) Restoration of the organizer after radical ablation of Hensen's node and the anterior primitive streak in the chick embryo. *Dev,* **122**: 3263-3273.

Qiu D, Cheng SM, Wozniak L, McSweeney M, Perrone E, Levin M. (2005). Localization and loss-of-function implicates ciliary proteins in early, cytoplasmic roles in left-right asymmetry. *Dev Dyn,* 234:176-89.

Ramsdell AF and Yost HJ. (1999). Cardiac looping and the vertebrate left–right axis: antagonism of left-sided Vg1 activity by a right-sided ALK2-dependent Bmp pathway. *Dev,* 126, 5195–205..

Rankin CT, Bunton T, Lawler AM, Lee SJ. (2000) Regulation of left-right patterning in mice by growth/differentiation factor-1. *Nat Genet* 24: 262-265.

Raya A and Izpisúa Belmonte JC, (2006). Left-right asymmetry in the vertebrate embryo: from early information to higher-level integration. *Nat Rev Genet,* 7, 283-93.

Raya A, Izpisúa Belmonte JC. (2008). Insights into the establishment of left-right asymmetries in vertebrates. *Birth Defects Res C Embryo Today.* 84: 81-94.

Raya A, Kawakami Y, Rodriguez-Esteban C, Buscher D, Koth CM, Itoh T, et al. (2003a). Notch activity induces Nodal expression and mediates the establishment of left–right asymmetry in vertebrate embryos. *Genes Dev,* 17, 1213–18.

Raya A, Kawakami Y, Rodriguez-Esteban C, Ibanes M, Rasskin-Gutman D, Rodriguez-Leon J, et al.

(2004). Notch activity acts as a sensor for extracellular calcium during vertebrate left–right determination. *Nature*, 427, 121–28.

Raya A,Izpisúa Belmonte JC. (2004b) Unveiling the establishment of left-right asymmetry in the chick embryo. *Mech Dev* **121**: 1043-1054.

Raya A,Izpisúa Belmonte JC.(2004a) Sequential transfer of left-right information during vertebrate embryo development. *Curr Opin Genet Dev* **14**: 575-581.

Raya A,Kawakami Y,Rodriguez-Esteban C, et al. (2003). Notch activity induces Nodal expression and mediates the establishment of left-right asymmetry in vertebrate embryos. *Genes Dev* **17**: 1213-1218.

Raya A,Kawakami Y,Rodriguez-Esteban C, et al. (2004). Notch activity acts as a sensor for extracellular calcium during vertebrate left-right determination. *Nature* **427**: 121-128.

Rebagliati MR, Toyama R, Fricke C, Haffter P and Dawid IB. (1998). Zebrafish nodal-related genes are implicated in axial patterning and establishing left-right asymmetry. *Dev Biol*, 199, 261–72.

Rebagliati MR, Toyama R, Fricke C, Haffter P and Dawid IB. (1998). Zebrafish nodal-related genes are implicated in axial patterning and establishing left-right asymmetry. *Dev Biol*, 199, 261-72.

Robu ME, Larson JD, Nasevicius A, Beiraghi S, Brenner C, Farber SA and Ekker SC.(2007). p53 activation by knockdown technologies. *PLoS Genet*, 25;3:e78.

Rodriguez Esteban C, Capdevila J, Economides AN, Pascual J, Ortiz A and Izpisua Belmonte JC. (1999). The novel Cer-like protein Caronte mediates the establishment of embryonic left–right asymmetry. *Nature*, 401, 243–51.

Rodriguez-Esteban C, Capdevila J, Kawakami Y, Izpisua Belmonte JC. (2001). Wnt signaling and PKA control nodal expression and left-right determination in the chick embryo. *Dev,* 128: 3189-3195

Rodriguez-Esteban C,Capdevila J,Economides AN, et al. (1999). The novel Cer-like protein Caronte mediates the establishment of embryonic left-right asymmetry. *Nature* 401: 243-251.

Rossowski WJ, Cheng BL, Taylor JE, Datta R and Coy DH. (2002). Human urotensin II-induced aorta ring

contractions are mediated by protein kinase C, tyrosine kinases and Rho-kinase: inhibition by somatostatin receptor antagonists. *Eur J Pharmacol,* 438, 159–70.

Russell FD and Molenaar P. (2004). Investigation of signaling pathways that mediate the inotropic effect of urotensin-II in human heart. *Cardiovasc Res,* 63, 673–81.

Ryan AK, Blumberg B, Rodriguez-Esteban C, et al. (1998). Pitx2 determines left-right asymmetry of internal organs in vertebrates. *Nature* Raya A,Izpisúa Belmonte JC. 545-551.

Saetrum Opgaard O, Nothacker H, Ehlert FJ and Krause DN. (2000). Human urotensin II mediates vasoconstriction via an increase in inositol phosphates. *Eur J Pharmacol,* 406, 265–71.

Sagi SA, Seasholtz TM, Kobiashvili M, Wilson BA, Toksoz D and Brown JH. (2001). Physical and functional interactions of Galphaq with Rho and its exchange factors. *J Biol Chem,* 276, 15445–52.

Saijoh Y,Oki S,Ohishi S,Hamada H. (2003). Left-right patterning of the mouse lateral plate requires nodal produced in the node. *Dev Biol,* 256: 160-172.

Sampath K, Cheng AM, Frisch A and Wright CV. (1997). Functional differences among Xenopus nodal-related genes in left-right axis determination. *Dev,* 124, 3293–02.

Sampath K, Rubinstein AL, Cheng AM, Liang JO and Fekany K. (1998). Induction of the zebrafish ventral brain and floorplate requires cyclops/nodal signalling. *Nature,* 395, 185–89.

Sarmah B, Latimer AJ, Appel B, Wente SR. (2005). Inositol polyphosphates regulate zebrafish left–right asymmetry. *Dev Cell,* 9, 133–45.

Sauzeau V, Le Mellionnec E, Bertoglio J, Scalbert E, Pacaud P and Loirand G. (2001). Human urotensin II-induced contraction and arterial smooth muscle cell proliferation are mediated by RhoA and Rho-kinase. *Circ Res,* 88, 1102–04.

Scacheri PC, Rozenblatt-Rosen O, Caplen NJ, Wolfsberg TG, Umayam L, et al. (2004) Short interfering RNAs can induce unexpected and divergent changes in the levels of untargeted proteins in mammalian cells. *Proc Natl Acad Sci U S A* 101: 1892–1897.

Schilling TF,Concordet JP,Ingham PW. (1999). Regulation of left-right asymmetries in the zebrafish by Shh and BMP4. *Dev Biol* 210: 277-287.

Schlange T, Arnold HH and Brand T. (2002). BMP2 is a positive regulator of Nodal signaling during left–right axis formation in the chicken embryo. *Dev,* 129, 3421–29.

Schlange T, Schnipkoweit I, Andree B, et al. (2001). Chick CFC controls Lefty1 expression in the embryonic midline and nodal expression in the lateral plate. *Dev Biol,* 234: 376-389.

Schneider A,Mijalski T,Schlange T, et al. (1999). The homeobox gene NKX3.2 is a target of left-right signalling and is expressed on opposite sides in chick and mouse embryos. *Curr Biol* 9: 911-914

Schottenfeld J, Sullivan-Brown J and Burdine RD. (2007). Zebrafish curly up encodes a Pkd2 ortholog that restricts left-side-specific expression of southpaw. *Dev,* 134, 1605-15.

screen for mutations affecting embryogenesis in zebrafish. *Dev,* 123:37–46.

Shenouda A, Douglas SA, Ohlstein EH and Giaid A. (2002). Localization of urotensin-II immunoreactivity in normal human kidneys and renal carcinoma. *J Histochem Cytochem,* 50, 885-89.

Shimeld SM. (2004). Calcium turns sinister in left-right asymmetry. *Trends Genet,* 20, 277-80.

Shioda, T, Lechleider RJ, Dunwoodie SL, Li H, Yahata T, de Caestecker MP, Fenner MH, Roberts AB and Isselbacher KJ. (1998). Transcriptional activating activity of Smad4: roles of SMAD hetero-oligomerization and enhancement by an associating transactivator. *Proc Nat Acad Sci USA,* 95, 9785-90.

Shiratori, H., Sakuma, R., Watanabe, M., et al. (2001) Two step regulation of asymmetric *Pitx2* expression: initiation by Nodal signaling and maintenance by Nkx2. *Mol. Cell* 7, 137–149

Solnica-Krezel L, Schier AF, et al. (1994). Efficient recovery of ENU-induced mutations from the zebrafish germline. *Genetics,* 136:1401–1420

Somlyo AP and Somlyo AV. (2003). Ca2+ sensitivity of smooth muscle and nonmuscle myosin II: modulated by G proteins, kinases, and myosin phosphatase. *Physiol Rev,* 83, 1325–58.

Song W, Abdel AEL, Lu W, Ao Z, Johns DG, Douglas SA, et al (2006) Urotensin II and renal function in the rat *Kidney Int,* 69 1360–1368

Sparrow DB, Kotecha S, Towers N, Mohun TJ (1998) Xenopus eHAND a marker for the developing cardiovascular system of the embryo that is regulated by bone morphogenetic proteins *Mech Dev* **71** 151-163

Srivastava D, Cserjesi P, Olson EN (1995) A subclass of bHLH proteins required for cardiac morphogenesis *Science* 270 1995-1999

St Amand R, Ra J, Zhang Y, et al. (1998) Cloning and expression pattern of chicken Pitx2 a new component in the SHH signaling pathway controlling embryonic heart looping *Biochem Biophys Res Commun* **247** 100-105

Stachel E, Grunwald J, and Myers Z. (1993) Lithium perturbation and *goosecoid* expression identify a dorsal specification in the pregastrula zebrafish Development (Cambridge), **117** 1261–1274

Sternfeld L, Duddenhoffer M, Ludes A, Heinze D, Anderie I and Krause E. (2007) Activation of muscarinic receptors reduces store-operated Ca2+ entry in HEK293 cells *Cell Signal,* 19, 1457–64

Streisinger G, Walker C, Dower N, Knauber D and Singer F. (1981) Production of clones of homozygous diploid zebra fish (*Brachydanio rerio*) *Nature,* 291 293–296

Sugo T, Murakani Y, Shimomura Y, Harade M, Abe M and Ishibashi Y. (2003) Identification of urotensin II-related peptide as the rat brain *Biochem Biophys Res Commun,* 310, 860-68

Suguro T, Watanabe T, Ban Y, Kodate S, Misaki A, Hirano T, Miyazaki A and Adachi M. (2007) Increased human urotensin II levels are correlated with carotid atherosclerosis in essential hypertension *Am J Hypertens,* 20, 211-17

Sulik K, Dehart DB, Iangaki T, Carson JL, Vrablic T, Gesteland K and Schoenwolf GC. (1994) Morphogenesis of the murine node and notochordal plate *Dev Dyn,* 201, 260-78

Sun Z, Amsterdam A, Pazour GJ, Cole DG, Miller MS and Hopkins N (2004) A genetic screen in zebrafish identifies cilia genes as a principal cause of cystic kidney *Dev,* 131, 4085–93

Sutherland MJ and Ware SM (2009) Disorders of left–right asymmetry heterotaxy and situs inversus *Am J*

Med Genet C Semin Med Genet, 151C, 307-17.

Swoboda P, Adler HT, Thomas JH. (2000). The RFX-type transcription factor DAF-19 regulates sensory neuron cilium formation in C. elegans. *Mol Cell* **5**: 411-421.

Tabin CJ and Vogan KJ. (2003). A two-cilia model for vertebrate left-right axis specification. *Genes Dev,* 17, 1–6.

Takahashi M, Narushima M and Oda Y. (2002). In vivo imaging of functional inhibitory networks on the mauthner cell of larval zebrafish. *J Neurosci,* 22, 3929–38.

Takeda S,Yonekawa Y,Tanaka Y, et al. (1999). Left-right asymmetry and kinesin superfamily protein KIF3A: new insights in determination of laterality and mesoderm induction by kif3A-/- mice analysis. *J Cell Biol* **145**: 825-836.

Tal M, Ammar DA, Karpuj M, Krizhanovsky V, Naim M and Thompson DA. (1995).A novel putative neuropeptide receptor expressed in neural tissue, including sensory epithelia. *Biochem Biophys Res Commun,* 209, 752–9.

Tanaka Y, Okada Y and Hirokawa N. (2005). FGF-induced vesicular release of Sonic hedgehog and retinoic acid in leftward nodal flow is critical for left-right determination. *Nature,* 435, 172–77.

Tasaki K, Hori M, Ozaki H, Karaki H and Wakabayashi I. (2004). Mechanism of human urotensin II-induced contraction in rat aorta. *J Pharmacol Sci,* 94, 376–83.

Thickett C, Morgan R. (2002) Hoxc-8 expression shows left-right asymmetry in the posterior lateral plate mesoderm. *Gene Expr Pattern* **2**: 5-6

Tian T, Zhao L, Zhang M, Zhao X and Meng A. (2009). Both foxj1a and foxj1b are implicated in left-right asymmetric development in zebrafish embryos. *Biochem Biophys Res Commun,* 380, 537-42.

Tostivint H, Joly L, Lihrmann I, Parmentier C, Lebon A and Morisson M. (2006). Comparative genomics provides evidence for close evolutionary relationships between the urotensin II and somatostatin gene families. *Proc Natl Acad Sci USA,* 103, 2237–42.

Totsune K, Takahashi K, Arihara Z, Sone M, Ito S and Murakami O. (2003). Increased plasma urotensin II levels in patients with diabetes mellitus. *Clin Sci (Lond),* 104, 1-5.

Totsune K, Takahashi K, Arihara Z, Sone M, Satoh F, Ito S, et al.(2001). Role of urotensin II in patients on dialysis. *Lancet,* 358, 810–11.

Trinkaus JP. (1993). The yolk syncytial layer of *Fundulus*: its origin and history and its significance for early embryogenesis. *J. Exp. Zool.* **265**: 258–284.

Tsuda T, Majumder K, Linask KK. (1998). Differential expression of flectin in the extracellular matrix and left-right asymmetry in mouse embryonic heart during looping stages. *Dev Genet* **23**: 203-214.

Tsukui T, Capdevila J, Tamura K, et al. (1999). Multiple left-right asymmetry defects in Shh(-/-) mutant mice unveil a convergence of the shh and retinoic acid pathways in the control of Lefty-1. *Proc Natl Acad Sci USA* **96**: 11376-11381.

Tzanidis A, Hannan RD, Thomas WG, et al. (2003). Direct actions of urotensin II on the heart: Implications for cardiac fibrosis and hypertrophy. *Circ Res,* 93, 246–53.

Ulloa L and Tabibzadeh S. (2001). Lefty inhibits receptor-regulated Smad phosphorylation induced by the activated transforming growth factor-beta receptor. *J Biol Chem,* 276, 21397–04.

Veldman MB and Lin S. (2008). Zebrafish as a developmental model organism for pediatric research. *Pediatr Res,* 64, 470-76.

Wang D, Jao LE, Zheng N, Dolan K, Ivey J, Zonies S, Wu X, Wu K, Yang H, Meng Q, Zhu Z, Zhang B, Lin S and Burgess SM. (2007). Efficient genome-wide mutagenesis of zebrafish genes by retroviral insertions. *Proc Natl Acad Sci USA,* 104:12428–12433.

Wang S,Yu X,Zhang T, et al. (2004). Chick Pcl2 regulates the left-right asymmetry by repressing Shh expression in Hensen's node. *Development* **131**: 4381-4391.

Waugh D, Youson JH, Mims SD, Sower SA and Colon JM. (1995). Urotensin II from the river lamprey (Lampetra fluviatilis), the sea lamprey (Petromyzon marinus) and the paddlefish (Polyodon spathula). *Gen Comp*

Endocrino, 199, 323-32.

Waugh D. and Conlon JM. (1993). Purification and characterization of urotensin II from the brain of a teleost (trout, Oncorhynchus mykiss) and an elasmobranch (skate, Raja rhina). *Gen Comp Endocrinol*, 92, 419–427.

Wu JW, Krawitz AR, Chai J, Li W, Zhang F, Luo K and Shi Y. (2002). Structural mechanism of Smad4 recognition by the nuclear oncoprotein Ski: insights on Ski-mediated repression of TFG-beta signaling. *Cell*, 111, 357-67.

Yan YT, Gritsman K, Ding J, et al. (1999). Conserved requirement for EGF-CFC genes in vertebrate left-right axis formation. *Genes Dev* 13: 2527-2537.

Yan, Y.T., Gritsman, K., Ding, J., et al. (1999) Conserved requirement for EGF-CFC genes in vertebrate left-right axis formation. *Genes Dev.* 13, 2527–2537

Yokouchi Y, Vogan KJ, Pearse 2nd RV and Tabin CJ. (1999). Antagonistic signaling by Caronte, a novel Cerberus-related gene, establishes left–right asymmetric gene expression. *Cell*, 98, 573–83.

Yoshioka H,Meno C,Koshiba K, et al. (1998). Pitx2, a bicoid-type homeobox gene, is involved in a lefty-signaling pathway in determination of left-right asymmetry. *Cell* 94: 299-305

Yuan S,Schoenwolf GC. (2000). Islet-1 marks the early heart rudiments and is asymmetrically expressed during early rotation of the foregut in the chick embryo. *Anat Rec* 260: 204-207

Yuan S,Schoenwolf GC.(1999). Reconstitution of the organizer is both sufficient and required to re-establish a fully patterned body plan in avian embryos. *Deve,* 126: 2461-2473

Zawel L, Dai JL, Buckhaults P, Zhou S, Kinzler KW, Vogelstein B and Kern SE. (1998). Human Smad3 and Smad4 are sequence-specific transcription activators. *Molec Cell,* 1, 611-17.

Zhang XM,Ramalho-Santos M,McMahon AP. (2001). Smoothened mutants reveal redundant roles for Shh and Ihh signaling including regulation of L/R symmetry by the mouse node. *Cell* 106: 781-792

Zhou S, Buckhaults P, Zawel L, Bunz F, Riggins G, Le Dai J, Kern SE, Kinzler KW and Vogelstein B. (1998). Targeted deletion of Smad4 shows it is required for transforming growth factor beta and activin signaling

in colorectal cancer cells. *Proc Nat Acad Sci USA,* 95, 2412-16.

Zhu L, Marvin MJ, Gardiner A, et al. (1999). Cerberus regulates left-right asymmetry of the embryonic head

and heart. *Curr Biol* 9: 931-938.

Ziltener P, Mueller C, Haenig B, Scherz MW and Nayler O. (2002). Urotensin II mediates ERK1/2

phosphorylation and proliferation in GPR14-transfected cell lines. J *Recept Signal Trans Res,* 22, 155–68.

Zoccali C, Mallamaci F, Tripepi G, et al. (2006). Urotensin II is an inverse predictor of incident cardiovascular

events in end-stage renal disease. *Kidney Int,* 69, 1253–58.

Appendices

Protocol for the whole-mount *in situ* hybridization on zebrafish embryos

Note: This protocol from:

Dr. Alberto Musa

Max-Planck-Institute for Molecular Genetics

Dept. Prof. H. Lehrach, Vertebrate Genomics

Fabeckstr. 62 - 14195 Berlin – Germany

Synthesis of DIG-labelled RNA probes (DIG-RNA) by *in vitro* transcription.

Note: in order to prevent RNase contamination and contact with harmful chemicals, work must be done using gloves, sterile tubes and solutions.

1. Preparing the DNA template from cDNA clones:

- Linearize 1-1,5 µg of DNA for each probe by digesting with the appropriate restriction enzyme.

- Precipitate the DNA with Ethanol, centrifuge, and wash with RNase free 70% Ethanol.

- Resuspend the DNA in DEPC-water.

- Test an aliquot on agarose gel.

2. Transcription reaction: follow the suggestions of the supplies.

- linearized DNA template	1 µg
- Transcription buffer	2 µL
- DIG-RNA Labeling Mix	2 µL
- RNase inhibitor (40 units/µL)	1 µL
- RNA polymerase (20 units/µL)	2 µL
- DEPC-water to total	20 µL

3. Isolation of the DIG-RNA probes:

- add 0,5M EDTA, pH 8	1 µL
- add 4M LiCl	2,5 µL
- add 100% Ethanol at -70°C	75 µL

- Centrifuge at 18 G for 30 minutes at 4°C.

- Wash with 70% ethanol, dry and resuspend in 20 µL DEPC-water.

- Test 2 µL on agarose gel.

Preparation of the embryos.

1. Sort the embryos at the stages required for the experiment. Staging according to Kimmel et al. (1995).

2. Remove chorions by pronase treatment or manually with Dumont Watchmaker's Forceps no. 5.

3. Fix the embryos in 4% paraformaldehyde (PFA) in 1xPBS overnight at 4°C.

4. Rinse with PBS several times; transfer the embryos into 100% Methanol (MeOH) and store them at -20°C until use.

Whole mount *in situ* hybridization.

1. Rehydrate the embryos by successive washes as follow:

- 75% MeOH / 25% PBS for 5 minutes

- 50% MeOH / 50% PBS for 5 minutes

- 25% MeOH / 75% PBS for 5 minutes

- 100% PBT (PBS/Tween20 0.1%) 4x 5 minutes

Note: after storing in 100% methanol, zebrafish embryos younger than 24hpf do not need permeabilization step.

2. Prehybridize the embryos in Hyb+ for 3 hours at 65°C-70°C.

Note: Based on the differentiations of different probes modify to proper hydrate temperature.

3. Incubate with Hyb+ containing ~100ng/mL of antisense DIG-RNA probe for 5 hours at 65°C-70°C

4. Post-hybridization washes:

- 100% Hyb- at 65°C for 15 minutes

- 75% Hyb- / 25% 2x SSCTw 1x at 65°C for 15 minutes

- 50% Hyb- / 50% 2x SSCTw 1x at 65°C for 15 minutes

- 25% Hyb- / 75% 2x SSCTw 1x at 65°C for 15 minutes

- 2x SSCTw 1x at 65°C for 15 minutes

- 0,2x SSCTw 2x at 65°C for 15 minutes

- 75% 0,2x SSCTw /25% PBTw 1x at RT for 15 minutes

- 50% 0,2x SSCTw /50% PBTw 1x at RT for 15 minutes

- 25% 0,2x SSCTw /75% PBTw 1x at RT for 15 minutes

- PBTw 2x at RT for 15 minutes

- Blocking solution 1x at RT for 3 hours

5. Detection:

- Incubation with 1:5000 anti-DIG antibody in blocking solution at RT for 3 hours.

- Post-antibody washes: 6x 15 minutes with PBTw at RT.

6. Staining:

- Wash 2x 15 minutes with Alkaline phosphatase (AP) solution at RT.

- Incubate embryos in staining solution at RT in the dark.

- Monitor the staining reaction with a stereo microscope.

- Stop the reaction with 4% PFA when the signal is came up.

7. Store the embryos in 30% Glycerol at 4°C.

Recipes (all solutions prepared with DEPC-treated water).

1x Phosphate buffer saline + 0,1% Tween 20 (PBTw)

- 10x PBS (DEPC treated)
- 0,1% Tween 20
- DEPC-water

Hybridization solution (Hyb+):

- 50-65% Formamide
- 5x SSC
- 0,1% Tween 20
- Adjust the pH to 6,0 with citric acid
- 50 µg/mL Heparin
- 1 mg/mL tRNA

Note: change the percentage of formamide according to the desired stringency.

Hybridization wash-solution (Hyb-):

- 50-65% Formamide
- 5x SSC
- 0,1% Tween 20
- Adjust the pH to 6,0 with citric acid

2x Saline-sodium citrate buffer + 0,1% Tween 20 (2xSSCTw):

- 1:10 of 20xSSC
- 0,1% Tween 20
- DEPC-water

0,2x Saline-sodium citrate buffer + 0,1% Tween 20 (0,2xSSCTw):

- 1:100 of 20xSSC
- 0,1% Tween 20
- DEPC-water

Blocking solution:

- 2% goat (or sheep) serum
- 2mg/mL BSA
- in PBTw

Preadsorbed anti-DIG antibody.

Incubate the anti-DIG antibody with homogenate of fixed embryos in blocking solution for several hours at RT.

Alkaline phosphatase (AP) solution:

- 100 mM Tris HCl pH 9,5
- 50 mM $MgCl_2$
- 100 mM NaCl
- 0,1% Tween 20

- DEPC-water

Staining solution:

- 135 µg/mL NBT

- 105 µg/mL BCIP

- in AP solution

Nitro Blue Tetrazolium (NBT) stock (store at −20°C):

- 50 mg of NBT

- in 0,7 mL N,N Dimethylformamide + 0,3 mL H_2O.

5-Bromo4-Chloro3-Indoyl phosphate (BCIP) stock (store at −20°C):

- 50 mg of BCIP

- in 1 mL N,N Dimethylfomamide.